Adsorbate-Induced Ordering Transitions of Nematic Liquid Crystals

By

Jacob T. Hunter

A dissertation submitted in partial fulfillment of

the requirements for the degree of

Doctor of Philosophy

(Chemical Engineering)

at the

UNIVERSITY OF WISCONSIN-MADISON

2014

Date of final oral examination: 2/28/2014

The dissertation is approved by the following members of the Final Oral Committee:

Nicholas L. Abbott, Professor, Chemical and Biological Engineering
George W. Huber, Professor, Chemical and Biological Engineering
Daniel J. Klingenberg, Professor, Chemical and Biological Engineering
Michael D. Graham, Professor, Chemical and Biological Engineering
Hongrui Jiang, Professor, Electrical and Computer Engineering

Adsorbate-Induced Ordering Transitions of Nematic Liquid Crystals

Jacob T. Hunter

Under the Supervision of Professor Nicholas L. Abbott

at the University of Wisconsin-Madison

Abstract

The research described in this thesis is focused on surface-driven anchoring transitions of liquid crystals (LC) that are triggered by the presence of targeted vapor analytes. Thin films of nitrile containing LCs align preferentially at metal salt-decorated surfaces via coordination interactions between the nitrile group of the mesogens and the metal cations. A vapor analyte that coordinates with the metal cations more strongly than the nitrile groups of the LCs will triggers an anchoring transition of the LCs.

The first section of this thesis is focused on an investigation of interfacial physicochemical phenomena underlying adsorbate-induced ordering transitions in nitrile-containing LCs supported on surfaces coated with metal perchlorate salts. The results reveal that the ordering of the LC on the metal salt-decorated surfaces is strongly dependent on the loading of metal salt, with key interfacial physicochemical processes being metal ion-nitrile coordination interactions, dissolution of salt into the LC, and formation of electrical double layers.

The second section of my thesis focuses on processes that control the dynamics of the anchoring transition of the LC to the targeted vapor analyte. By flowing a gas containing

dimethyl methylphosphonate (DMMP) over a film of nematic 5CB supported on a surface decorated with aluminum perchlorate, we quantify the dynamics of the optical response of the LC film as a function of key experimental parameters, including linear flow rate of the gas over the surface of the film and the concentration of the DMMP within the gas. The measurements are interpreted within the framework of a simple model of mass transport to reveal that the rate-limiting process underlying the response of the LC is the mass transport of the DMMP across the concentration boundary layer formed on the vapor side of the LC-vapor interface, and not the mass transport of DMMP across the LC film nor the intrinsic ligand exchange kinetics. Analysis of the relaxation of the system leads to an estimate of the sensitivity of the supported LC film to the concentration of DMMP in the gas phase (approximately 150 ppb for the non-optimized system reported in this thesis).

The third section is focused on optimization of the experimental system in order to speed up the dynamic response of the LC sensor system to a targeted analyte. We accomplish this by studying two parts of the system. First, we report that metal salts composed of mixtures of anions of differing coordination strength can be used to increase the sensitivity and selectivity of adsorbate-induced anchoring transitions of LCs supported on surfaces decorated with the metal salts. Second, we manipulate the dynamic response of the LC by changing the thickness of the LC film. We determine that the elasticity of the LC plays a key role in determining the sensitivity of the LC films to analyte when the LC films approach thicknesses of a few micrometers. The role of elastic strain in the LC is explored further through the addition of a chiral dopant to the LC and formation of cholesteric LC phases.

Acknowledgements

I would like to acknowledge the many people that have helped me throughout my graduate career without whom it would have been impossible to accomplish this dissertation. I would like to thank my advisor, Professor Nicholas L. Abbott, for guiding me in my research. In addition, I would like to thank the many members of my research group (past and present) that have helped me in the day to day tasks required of this process. In addition, they were always there for me to listen to any of my problems whether my problems were professional or personal. I have also had the opportunity to talk and work with many different research groups here at the University of Wisconsin, and I appreciate all of the stimulating discussion had. I also thank the many members of the department's staff that have helped me over the course of the years. Finally and most importantly, I wish to thank my friends and family for always being there for me.

Table of Contents

List of Figures and Tables

Chapter 1: Introduction and Thesis Overview

1.1 Introduction

The research in this thesis provides insight into anchoring transitions of thin films of liquid crystals (LCs) that are triggered by the presence of vapor analytes. In this section, a brief introduction of thermotropic LCs is given. This thesis deals exclusively with nitrile containing LCs such as 4-pentyl-4'cyanobiphenyl (5CB) or 4-octyl-4'cyanobiphenyl (8CB). 5CB exhibits a nematic liquid crystalline phase at temperatures between 24 °C – 34 °C in which the mesogens exhibit orientational order but not long-range positional order, see Figure 1. In the case of 8CB, the mesogens exhibit a smectic liquid crystalline phase at room temperatures (~ 25 °C), a LC phase in which the mesogens possess both orientational and positional order.

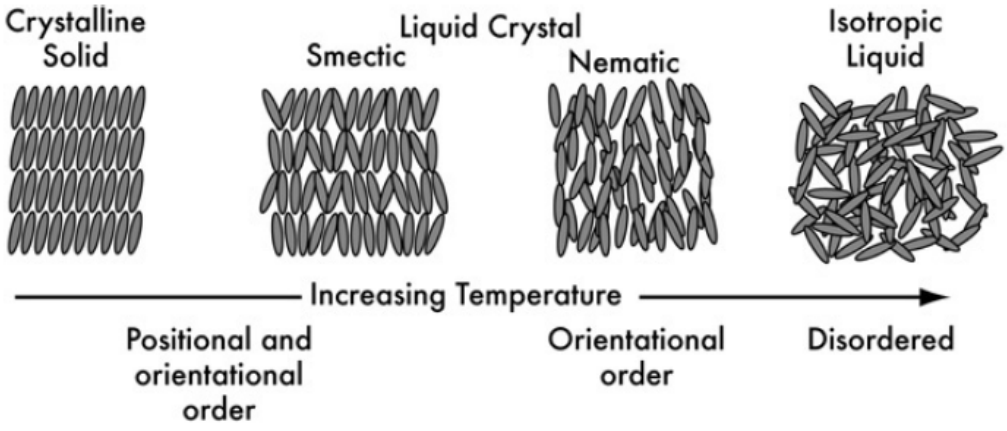

Figure 1.1. Schematic of the molecular organization of the various phases of a thermotropic LC.[1]

LCs are birefringent, meaning that they possess two direction dependent indices of refraction. Therefore depending on the orientation of the LCs, the plane of polarization of light

may rotate as the polarized light is transmitted through the molecule. Based on this phenomenon, polarized light can be used to characterize the orientation of a LC.[1]

1.2 Thesis Overview

Chapters 2-6 were written to be able to be read independently. Chapter 2 is a review of research on LC-based sensors that had been performed prior to this thesis.[2] Chapters 3-6 are independent research manuscripts. A summary of Chapters 3-6 is given below.

In Chapter 3, we report an investigation of interfacial physicochemical phenomena underlying adsorbate-induced ordering transitions in nitrile-containing LCs supported on surfaces coated with metal perchlorate salts. When the mass density of $Al(ClO_4)_3$ deposited onto a surface was low (0.39±0.03 ng/mm^2), we measured 20μm-thick films of nematic 5CB to initially exhibit perpendicular (homeotropic) ordering, consistent with the influence of coordination interactions between the nitrile groups of 5CB and Al^{3+} ions on the surface on the ordering of the LC. Furthermore, exposure of freshly prepared LC films to vapors of an adsorbate that coordinates strongly to Al^{3+} ions (dimethylmethylphosphonate, DMMP) triggered an ordering transition in the LC films, supporting our conclusion that the initial perpendicular orientation of the LC was induced by nitrile-Al^{3+} coordination interactions. Subsequent equilibration of the LC on the surface (hours), however, resulted in a slow, time-dependent ordering transition in the absence of DMMP that corresponded to the tilting of the LC away from the surface normal. Measurements of the solubility of $Al(ClO_4)_3$ in nematic 5CB (saturation value of 1.7 μmol/ml) supported our hypothesis that the slow ordering transition observed in the absence of DMMP was due to the loss of metal ions from the surface into the

LC film (dissolution). In contrast, the solubilization capacity of a 20 μm-thick film of 5CB was determined to be insufficient to dissolve 2.14 ± 0.24 ng/mm^2 of the salt from a surface, and we measured the homeotropic ordering of nematic films of 5CB on these surfaces to persist for days. Equilibration of theses samples, however, was accompanied by a loss of response to DMMP (perpendicular orientation of the LC before and after exposure to DMMP). Finally, by coating surfaces with $Al(ClO_4)_3$ at loading that were intermediate to those reported above (1.13± 0.0.09 ng/mm^2), we observed (i) perpendicular ordering of the LC in the absence of DMMP, and (ii) reversible ordering transitions induced by DMMP, during storage of samples over 4-5 days. These results, when combined, indicate that the ordering of the LC on the metal salt decorated surfaces is strongly dependent on the loading of metal salt, with key interfacial physicochemical processes being metal ion-nitrile coordination interactions, dissolution of salt into the LC, and formation of electrical double layers.[3]

In Chapter 4, we report a study that elucidates key physicochemical phenomena that underlie the dynamics of adsorbate-induced ordering transitions in micrometer-thick films of LCs supported on chemically functionalized surfaces. By flowing a gas containing DMMP over a film of nematic 5CB supported on a surface decorated with aluminum perchlorate, we quantify the dynamics of the optical response (intensity of transmitted light) of the LC film as a function of key experimental parameters, including linear flow rate of the gas over the surface of the film and the concentration of the DMMP within the gas. Building from prior infrared spectroscopic analysis revealing that the optical response of the LC is due to an ordering transition triggered by competitive ligand-exchange reactions at the chemically functionalized

surface (i.e., between the phosphonate and nitrile groups of the DMMP and LC, respectively, with the aluminum perchlorate-decorated surface), we interpret the measurements reported herein within the framework of a simple model of mass transport. The model reveals that the rate-limiting process underlying the response of the LC is the mass transport of the DMMP across the concentration boundary layer formed on the vapor side of the LC-vapor interface, and not the mass transport of DMMP across the LC film nor the intrinsic ligand exchange kinetics. The analysis also reveals that the response of the LC is triggered once the concentration of DMMP within the LC film rises to approximately 0.25 mM. By flowing a stream of gas free of DMMP over a LC film pre-exposed to DMMP, we established that the relaxation of the LC film to the initial state is also largely controlled by mass transport of the DMMP across the vapor side of the LC-vapor interface. Analysis of the relaxation of the system leads to an estimate of the sensitivity of the supported LC film to the concentration of DMMP in the gas phase (approximately 150 ppb for the non-optimized system reported in this paper). These results and others reported in this paper identify key physical phenomena that dictate the dynamics of adsorbate-induced ordering transitions in LC systems.[4]

In Chapter 5, we report that metal salts composed of mixtures of anions of differing coordination strength can be used to increase the sensitivity and selectivity of adsorbate-induced anchoring transitions of LCs supported on surfaces decorated with the metal salts. Specifically, the dynamics of anchoring transitions triggered by the adsorbate DMMP on surfaces of aluminum (III) salts were analyzed within the framework of a model for mass transport to reveal that the sensitivity of a nitrile-containing nematic LC to DMMP increased from 250 parts-per-billion (ppb) to 25 ppb when the composition of the (counter) anion was

changed from 100% perchlorate to 90% nitrate and 10% perchlorate (by mole percent). To provide insight into these observations, Polarization-Modulation Infrared Reflectance-Absorbance Spectroscopy (PM-IRRAS) was used to show that the intensity of the absorption band in the IR spectrum corresponding to the coordinated state of the nitrile group (but not the position of the peak) decreased with increase in mole fraction of the strongly coordinating anion (nitrate) in the anion mixture, thus suggesting that the addition of the strongly coordinating anion decreased the number of coordination interactions (per unit area of the interface) but not the strength of the individual coordination interactions between the metal cation and the LC. We also measured the incorporation of the nitrate anion into the metal salt to decrease the effect of humidity on the dynamic response of the LC to DMMP, a result that is consistent with weaker interactions between the nitrate anion and water as compared to the perchlorate anion and water. Finally, the bidentate anion acetylacetonate was measured to cause a similar increase in sensitivity to DMMP when mixed with perchlorate in a 1:1 ratio (the resulting sensitivity of the system to DMMP was 100 ppb). Overall, these results suggest that tailoring the identity of the anion represents a general and facile approach for tuning the orientational response of LCs supported on metal salts to targeted analytes.[5]

In Chapter 6, we investigate the effect of elastic energies on the dynamics of anchoring transitions of thin films of liquid crystals (LCs) in the presence of vapor analytes. The system studied is comprised of thin films of LCs that are supported on surfaces decorated with metal salts that define the alignment of the LC at that interface via coordination interactions. When the system is exposed to a vapor analyte (such as dimethyl methylphosphonate, DMMP), the coordination interactions at the solid interface between the metal salt and the LC are disrupted

causing a surface induced anchoring transition at the solid surface. This change in alignment of the LC causes an elastic strain in the system to accommodate the planar anchoring at one surface and a homeotropic alignment at the other confining surface (hybrid alignment). We observe that this strain is increased for thin films of LCs, and eventually at small enough thicknesses (< 4 μm) begins to slow the anchoring transition. Next, we study the addition of a chiral dopant to the system as a way of manipulating the elastic energies of the LC system to accelerate the anchoring transition of the LC. By adding a chiral dopant into the LC, we see a helical structure formed in the LC phase. For this system, a surface driven anchoring transition results in a change in the defect structure of the samples when viewed through cross polarizers. Overall, our preliminary research in this area has shown that LC systems with chiral pitches that are less than or equal to the LC film thickness can be advantageous for LC-based sensing.

1.3 References

1. Lockwood, N. A.; Gupta, J. K.; Abbott, N. L. *Surf. Sci. Rep.* **2008,** *63*, 255-293.
2. Hunter, J. T.; Abbott, N. L., Liquid Crystal-Based Chemical Sensors In *Liquid Crystals Beyond Displays: Chemistry, Physics, and Applications*, Li, Q., Ed.; Wiley: Hoboken, New Jersey, **2012**; pp 485-505.
3. Hunter, J. T.; Pal, S. K.; Abbott, N. L. *ACS Appl. Mater. Interfaces* **2010,** *2*, 1857-1865.
4. Hunter, J. T.; Abbott, N. L. *Sens. Actuators, B* **2013,** *183*, 71-80.
5. Hunter, J. T.; Abbott, N. L. *ACS Appl. Mater. Interfaces* **2013**.

Chapter 2: Literature Review

2.1 Background and Motivation

This chapter presents an overview of recent advances in the use of liquid crystals (LCs) for sensing of small organic molecules from vapors (chemical sensing). The fundamental phenomenon underlying the approach to LC-based sensors addressed in this chapter is an adsorbate-driven anchoring transition in a film of LC, a phenomenon that has been known since the pioneering studies in the early 1990's by Pieranski and Jerome.[1-4] Recent studies have sought to realize chemical sensors based on LCs by using combinations of chemically tailored surfaces and LCs in order to engineer highly selective adsorbate-induced ordering transitions in the LCs. We also note that cholesteric LCs have been used for chemical sensing (with a change of pitch occurring upon absorption of an analyte), but approaches to chemical sensing based on cholesteric liquid crystals lie beyond the scope of this chapter.[5-14] Finally, a number of studies with LCs as biological sensors have been reported over the past decade, however we do not attempt to address those advances but rather refer the interested reader to relevant literature.[15-24]

Figure 2.1 depicts two examples of adsorbate-driven ordering transitions that have been utilized as the basis of chemical sensors. In the first example, intermolecular interactions between the chemically functionalized surface and the LC lead to an initial azimuthal orientation of the LC on the surface (Figures 2.1A and 2.1B). Binding of the targeted analyte to the surface disrupts the intermolecular interactions of the surface with the LC, resulting in an

azimuthal ordering transition of the LC to an orientation that is orthogonal to the initial orientation, as dictated by an anisotropic topography engineered into the chemically functionalized surface.

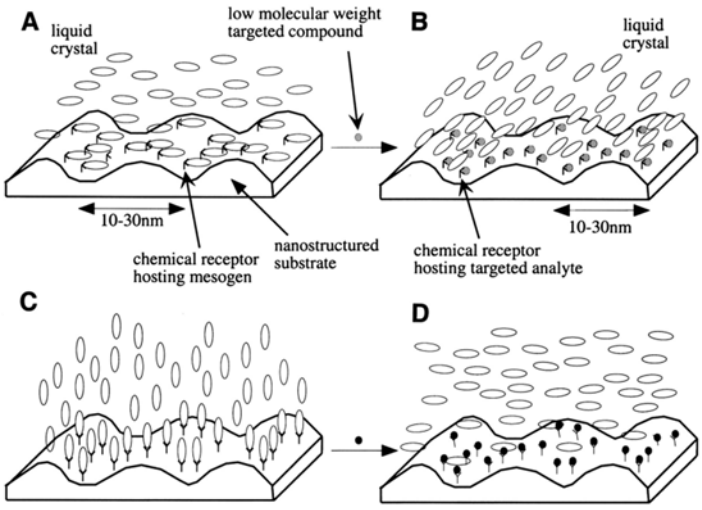

Figure 2.1. Schematic illustration of the competitive interaction between a LC and a low molecular weight targeted compound for a molecular receptor hosted on a surface with nanometer-scale topography. (**A**) Before exposure to a targeted compound, the molecules forming the LC mesogens bind with the molecular receptor and thereby anchor the LC in an azimuthal orientation that is orthogonal to the topography of the surface. (**B**) Binding of the targeted analyte to the surface-immobilized receptors displaces the LC from its interaction with the receptor shown in (A), and the LC orients along the topography. (**C**) A receptor-induced orientation of a LC that is perpendicular to a surface. (**D**) Binding of a targeted analyte to the surface-immobilized receptors displaces the LC from its interaction with the receptor shown in (A), and the LC tilts away from the surface normal. Reprinted with permission from Shah, R.R. and N.L. Abbott, *Principles for measurement of chemical exposure based on recognition-driven anchoring transitions in liquid crystals.* Science, 2001. 293(5533): p. 1296-1299. Copyright 2001 AAAS.

As discussed later in this chapter, this type of azimuthal, adsorbate-induced ordering transition in a LC can lead to the detection of organoamine compounds. As shown in Figure 2.2A, prior to binding of the organoamine, a LC with a nitrile group (e.g. 4'-pentyl-4-biphenyl-carbonitrile, 5CB) will assume a uniform azimuthal orientation on a surface presenting oriented, carboxylic acid groups due to hydrogen bonding between the nitrile groups of the LC and the

carboxylic acids. Upon exposure of the system to organoamines, the stronger acid-based interaction of the amine and carboxylic acid will displace the nitrile group from its hydrogen bonded state on the surface: this loss of hydrogen bonding results in an azimuthal ordering transition of the LC. As noted above, the final azimuthal orientation of the LC is dictated by topography of the surface.[25-28]

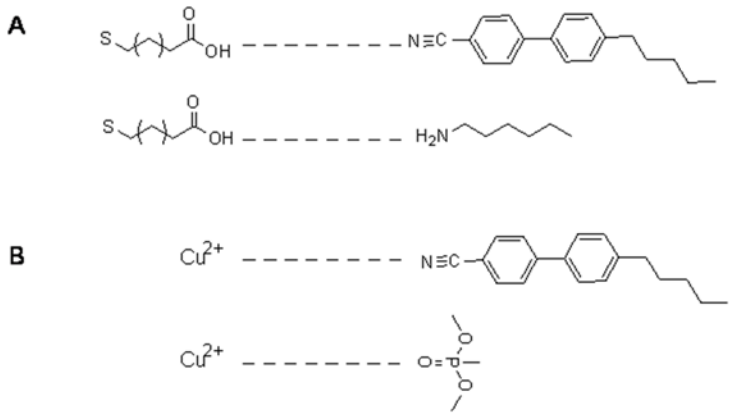

Figure 2.2. Schematic illustration the intermolecular interactions that occur between chemically functionalized surfaces and either mesogens (top) or analytes (bottom) to create chemically-responsive LC systems. See text for details.

The second class of ordering transitions to be discussed in this chapter as the basis of chemical sensors are those that involve a change in the out-of-plane orientation of the LC (Figures 2.1C and 2.1D). In this case, the intermolecular interactions between the chemical functionality presented by the surface and the LC lead to an initial homeotropic orientation of the LC. Upon binding of the adsorbate to the surface, the loss of these intermolecular interactions results in a tilting of the LC away from the homeotropic orientation. As detailed in the next section of this chapter, a number of studies have revealed that surfaces decorated with metal salts that coordinate with the nitrile groups of LCs, can be used to achieve the initial homeotropic orientation of the LC (Figure 2.2B). Upon exposure of the system to an analyte

that coordinates to the metal ions with an affinity that is greater than the nitrile group (e.g., a molecule with a phosphoryl group), the nitrile-metal ion coordination interaction is lost, resulting in an ordering transition of the LC towards a planar orientation.[25, 29-39]

The remainder of the chapter is as follows. In Section 2.1.1, we present design principles for chemically functionalized surfaces that can be used to create LC-based chemical sensors based on adsorbate-driven ordering transitions. In Section 2.1.2, we describe the analytic characteristics of LC sensors for detection of coordinating compounds. Section 2.1.3 addresses principles for LC sensors designed using acid-base interactions.

2.1.1 Design of Chemically Functionalized Surfaces for Use in LC-Based Chemical Sensors

2.1.1A Surfaces Decorated with Metal Salts.

As described in the Introduction, surfaces that are decorated with metal salts represent a promising class of surfaces for chemical sensing because choice of the metal cation of the salt can be used to tune the selectivity of the LC-based sensor. In this section, we describe enabling studies of the orientations of LCs on surfaces decorated with metal salts, and summarize evidence that coordination interactions between the nitrile group of LCs and the metal cation play a central role in determining the orientations of the LCs.

The effect of varying the metal perchlorate salt presented on a surface to thin films of nematic 5CB on the resulting LC orientations of nematic 5CB is shown in Figure 2.3. The figure shows polarized light micrographs (crossed polars) of nematic 5CB, placed into the pores of 20 μm-thick metallic grids supported on metal perchlorate salt-decorated surfaces. Because the

easy axis of the nematic phase of 5CB at the air interface is homeotropic, images that appear dark between crossed polars indicate that the anchoring of the 5CB on the metal salt surface was homeotropic. Thus, it is apparent from Figure 2.3 that the perchlorate salts of Cu^{2+}, Fe^{3+}, Cd^{2+}, Al^{3+}, Zn^{2+}, Eu^{3+}, Ni^{2+}, Co^{2+} and La^{3+} all cause homeotropic anchoring whereas Mn^{2+}, Mg^{2+}, Cs^{+}, Ag^{+} and Na^{+} lead to bright micrographs between cross polars indicating a tilted or planar orientations of the LC at the metal salt decorated surfaces.[38]

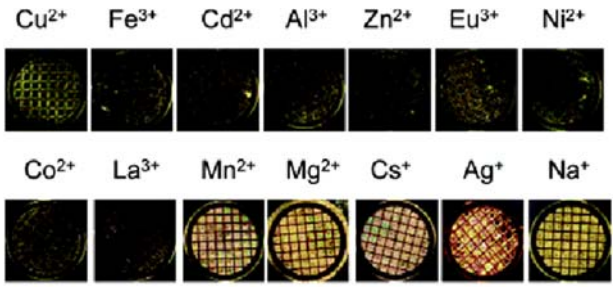

Figure 2.3. Optical images (crossed polars) of gold grids impregnated with 5CB supported on metal perchlorate salts. Each grid is 3 mm in diameter. Reprinted with permission from Yang, K.L., K. Cadwell, and N.L. Abbott, *Mechanistic study of the anchoring behavior of liquid crystals supported on metal salts and their orientational responses to dimethyl methylphosphonate.* Journal of Physical Chemistry B, 2004. **108**(52): p. 20180-20186. Copyright 2004 American Chemical Society.

The results described in Figure 2.4A provide insight into the origins of the cation-dependent orientation of the LCs seen in Figure 2.3. These results reveal that the alignment of 5CB in contact with the metal perchlorate salts is dependent on the electron affinity of the metal cation, where metal cations with a high electron affinity cause homeotropic orientations of the nematic phase of 5CB whereas metal cations with a low electron affinity cause planar or tilted orientations. Because the electron affinity of an ion is a measure of its affinity for electron-donating ligands (e.g., nitrile groups), the correlation between the orientation of the LC and electron affinity of the metal ions suggests that the orientations of the LC result from the

binding of the nitrile groups of the nematic phase of 5CB with the metal ions presented at these surfaces. This proposition is supported by infrared (IR) spectroscopy (Figure 2.4B). Whereas free nitrile groups give rise to a peak in the vibrational spectrum at ~2227cm^{-1}, a new peak is evident in the IR spectrum for surfaces presenting metal ions with high electron affinity. For example, for Cu^{2+} a peak is apparent at ~2287cm^{-1}, consistent with formation of a nitrile-Cu^{2+} complex.[40-42] We note that while the LC used in the IR studies shown in Figure 2.4B and 2.4C is 8CB, it possesses the same nitrile chemical functionality as 5CB.[38]

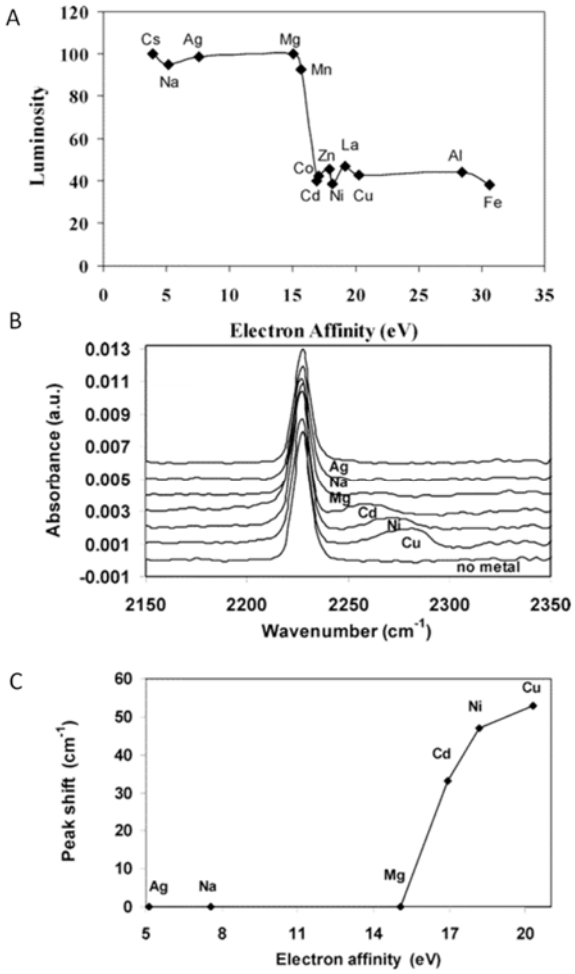

Figure 2.4. Characterization of the ordering of LCs on metal ion-decorated surfaces, and IR spectroscopy of those surfaces. **(A)** Intensity of light (crossed polars) transmitted through 5CB supported on various metal perchlorate salts as a function of the electron affinities of the metal ions.(**B** and **C**) IR spectra of films of 8CB spin coated onto surfaces presenting metal ions. The peak at 2227 cm^{-1} corresponds to the stretch vibration of the nitrile groups of 8CB in bulk. Reprinted with permission from Yang, K.L., K. Cadwell, and N.L. Abbott, *Mechanistic study of the anchoring behavior of liquid crystals supported on metal salts and their orientational responses to dimethyl methylphosphonate.* Journal of Physical Chemistry B, 2004. **108**(52): p. 20180-20186. Copyright 2004 American Chemistry Society.

Overall, these results along with similar results reported in the literature [31, 38] provide strong support for the proposition that metal salts can be used to prepare a class of chemically functionalized surfaces at which LCs can be oriented through metal ion-LC coordination interactions involving the nitrile group of the LC. As discussed below, these coordination

interactions can be disrupted by targeted chemical analytes, thus leading to a class of LC-based sensors for coordinating compounds.

2.1.1B Surfaces Decorated with Carboxylic Acids.

The principles underlying the design of LC-based sensors, as shown in Figures 2.1A and 2.1B, can be applied to surfaces with a wide range of chemical functionality. As a second example, we briefly mention the use of surfaces that present carboxylic acid groups.[25-26, 28] As described in Section 2.1.3 below, such surfaces are useful for detecting basic analytes such as organoamines.

The utility of carboxylic acid-functionalized surfaces for chemical sensing is the capacity of these surfaces to participate in hydrogen bonding with chemical functional groups present on the LC.[27-28] As evidence that hydrogen bonding between the nitrile group of 5CB and a carboxylic acid-functionalized surface can orient a nematic phase, Figure 2.5 shows that conversion of a carboxylic acid into a sodium carboxylate group on a surface can trigger an azimuthal ordering transition in nematic 5CB. The carboxylic acid can serve as a hydrogen bond donor to the nitrile group of the LC whereas the carboxylate group cannot participate in a hydrogen bond with a nitrile group, consistent with a role for hydrogen bonding in the observed ordering transition. We note here that the surfaces presenting the carboxylic acid/carboxylate species in Figure 2.5 also possess an anisotropic topography. Thus, in the absence of hydrogen bonding, the azimuthal orientation of the LC was dominated by the influence of the topography of the surface.[27]

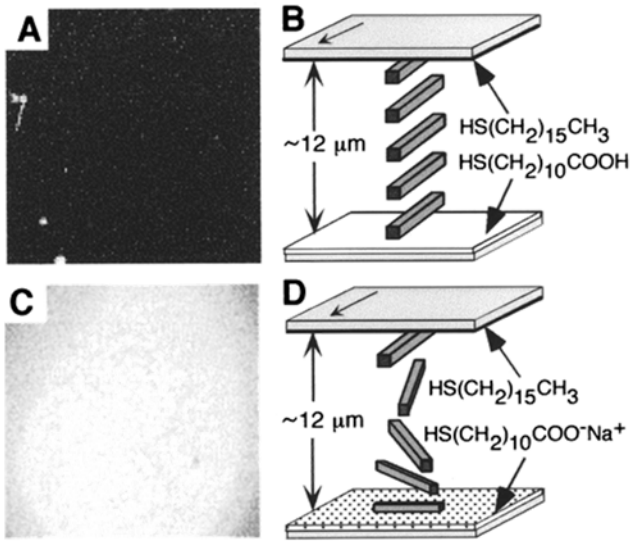

Figure 2.5. **(**A and C) Optical textures (crossed polars) formed by nematic 5CB within optical cells prepared with one surface supporting a self-assembled monolayer (SAM) formed from $H_3C(CH_2)_{15}SH$ and an opposing surface supporting a SAM formed from $HOOC(CH_2)_{10}SH$ that was pretreated at pH 3.2 (A) or 10.6 (C). (B and D) Schematic illustrations of the orientations of the LCs interpreted from the optical textures shown in A and C, respectively. The arrows indicate the direction of deposition of gold onto the substrate. Reprinted with permission from Shah, R.R. and N.L. Abbott, *Using liquid crystals to image reactants and products of acid-base reactions on surfaces with micrometer resolution.* Journal of the American Chemical Society, 1999. **121**(49): p. 11300-11310. Copyright 1999 American Chemical Society.

Additional spectroscopic evidence for hydrogen bonding is found in the IR spectra shown in Figure 2.6. Figure 2.6A shows the IR spectra of the carboxylic acid-terminated surface prior to contact with one of three LCs. Inspection of Figure 2.6A reveals evidence of carbonyl groups within the monolayer in two environments (i.e., two peaks in the IR spectrum). These two peaks correspond to hydrogen bonded and non-hydrogen bonded carbonyl groups, with the hydrogen bonding occurring laterally within the monolayer. Contact of the "A" series LC (Figure 2.6B) with the carboxylic acid-terminated monolayer leads to very little change in the IR spectrum. This indicates that the "A" series LC does not form hydrogen bonds of sufficient strength to disrupt the intra-monolayer hydrogen bonding. In contrast, the IR spectra in (Figure

2.6C and 2.6D) indicate that both 5CB and MBBA do form hydrogen bonds with the carboxylic acid groups of the monolayer and thus disrupt the lateral network of hydrogen bonds between adjacent carboxylic acid groups on the surface.[26] Additional discussion regarding the interpretation of the IR spectra can be found in reference.[26]

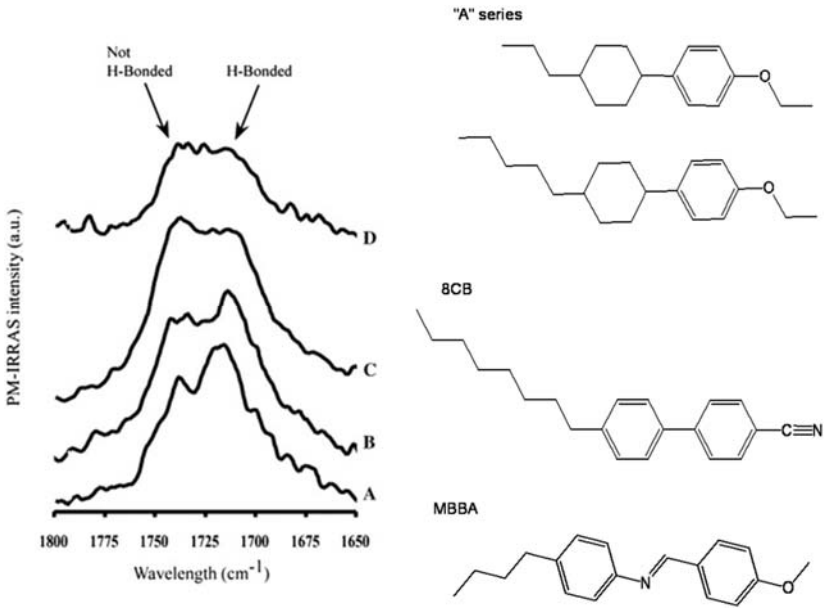

Figure 2.6. IR spectra of carboxylic acid-terminated SAMs before and after contact with liquid crystals. SAMs formed from $HS(CH_2)_{11}COOH$ on gold (A), coated with the liquid crystal ''A'' series (B), 8CB (C) and MBBA (D). Also shown are the molecular structures of the mesogen. Reprinted with permission from Luk, Y.Y., K.L. Yang, K. Cadwell, and N.L. Abbott, *Deciphering the interactions between liquid crystals and chemically functionalized surfaces: Role of hydrogen bonding on orientations of liquid crystals.* Surface Science, 2004. 570(1-2): p. 43-56. Copyright 2004 Elsevier.

2.1.2 Liquid Crystal-Based Sensors for Coordinating Compounds.

The results presented in Section 2.1.1 clearly demonstrate that surfaces presenting metal cations can orient nitrile-containing LCs through metal ion-nitrile coordination interactions. As discussed below, this type of surface presents the opportunity to trigger ordering transitions in LC films through exposure of the system to analytes that coordinate with metal

cations more strongly than the nitrile groups of the LC. Figure 2.7 shows a first example of a LC-based chemical sensor for an organophosphonate compound, dimethylmethylphosphonate (DMMP). DMMP is a common simulant for chemical nerve agents and pesticides, and possesses a phosphoryl group that coordinates strongly to a range of transition metal cations (see Figure 2.2B). As shown in Figure 2.7A-D, prior to exposure to a vapor of DMMP, the film of nematic 5CB assumes a homeotropic orientation on the surface decorated with Cu^{2+} perchlorate, consistent with coordination between the Cu^{2+} ions and the nitrile groups of the LC. Following exposure to a vapor of DMMP, however, the LC film was observed to undergo an orientational transition that was driven by a change in anchoring of the LC at the metal salt-decorated surface. This response is consistent with displacement of the nitrile group of 5CB from its coordination interaction with Cu^{2+}, driven by competitive binding of DMMP (see below for spectroscopic evidence that supports this interpretation).[25]

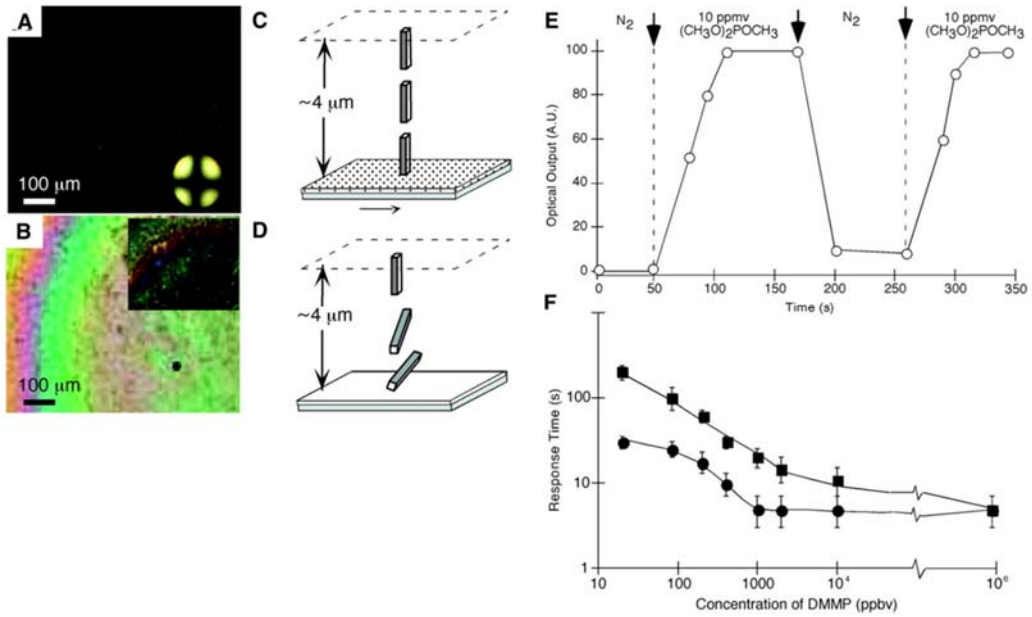

Figure 2.7. Optical textures (crossed polars) formed by a film of nematic 5CB on a surface that was (A) pretreated with 100 mM $Cu(ClO_4)_2$ and (B) pretreated as in (A) and subsequently exposed to a vapor concentration of 900 ppmv $(CH_3O)_2POCH_3$ (viewed at maximum transmission). The inset in (B) shows the optical texture at maximum extinction. (C and D) Schematic illustrations of the orientations of the LCs interpreted from the optical textures shown in (A) and (B), respectively. The arrow in (C) indicates the direction of deposition of gold onto the substrate. (E) Reversibility of the optical brightness of a film of 5CB supported on a SAM formed from $HOOC(CH_2)_{10}SH$ that was pretreated as in (A) and exposed sequentially to 10 ppmv $(CH_3O)_2POCH_3$ and N_2. (F) Response times of films of 5CB (thickness ~4 μm) supported on surfaces presenting Cu^{2+} that were exposed to $(CH_3O)_2POCH_3$ convected to the surface from a nozzle that was placed 2 mm (closed circle) or 3 mm (closed square) above the film of 5CB. The response time is defined as the time at which the onset of reorientation of the LC was visible to the naked eye. Reprinted with permission from Shah, R.R. and N.L. Abbott, *Principles for measurement of chemical exposure based on recognition-driven anchoring transitions in liquid crystals.* Science, 2001. 293(5533): p. 1296-1299. Copyright 2001 AAAS.

Several key characteristics of the DMMP-induced ordering transitions are described in Figures 2.7E and F. Figure 2.7E demonstrates that the DMMP-induced ordering transitions are reversible.[25, 31, 33, 36, 39] Second, Figure 2.7F reveals that the LC responds to concentrations of DMMP that are in the 10's of parts-per-billion range.[25] These ordering transitions are not limited to 5CB as it has been demonstrated, but thin films of 8CB heated to a temperature very

close to the nematic-smectic phase transition, when supported on Cu^{2+}-decorated surfaces, also undergo ordering transitions upon exposure to DMMP (Figure 2.8). In addition, the dynamics of the response of the film of LC is dependent on the concentration of DMMP in the vapor phase that passes above the film of LC. Here we also note that the quantitative response of the LC sensor is strongly dependent on the geometry of the system, and that variations in the thickness of the LC film likely contribute to the scatter in the experimental data shown in Figure 2.8.[39]

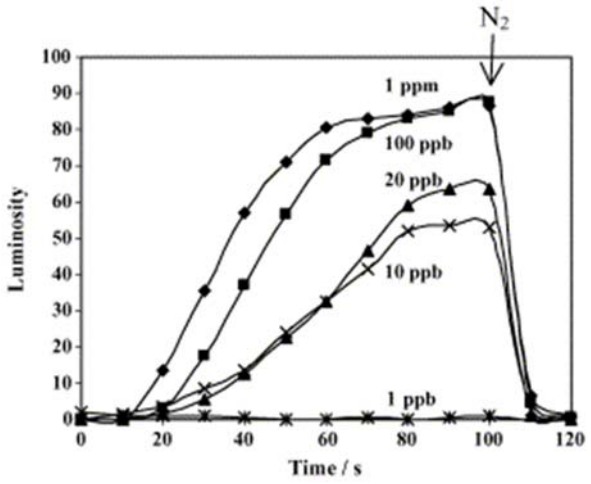

Figure 2.8. Time-dependent change in the intensity of light transmitted through a thin film of 8CB (thickness ~ 900 nm) supported on Cu^{2+}-decorated surfaces following exposure to various concentrations of DMMP. Reprinted with permission from Yang, K.L., K. Cadwell, and N.L. Abbott, *Use of self-assembled monolayers, metal ions and smectic liquid crystals to detect organophosphonates.* Sensors and Actuators B-Chemical, 2005. 104(1): p. 50-56. Copyright 2005 Elsevier.

A key attribute of a chemical sensor is selectivity – detection of the targeted compound but not other compounds found in the sampling environment. Figure 2.9 shows an example of the selective response of LC-based chemical sensors to DMMP as compared to water. Water is commonly problematic in chemical sensing because it is present in many sampling

environments in high yet variable concentrations. Because water does not coordinate with Cu^{2+} with sufficient strength to displace the nitrile group of 8CB from its coordination with Cu^{2+}, the results in Figure 2.9 show that a LC sensor based on 8CB and Cu^{2+}-decorated surfaces does not respond to water present in air at concentrations that correspond to relative humidities of 50% or 75%.[39]

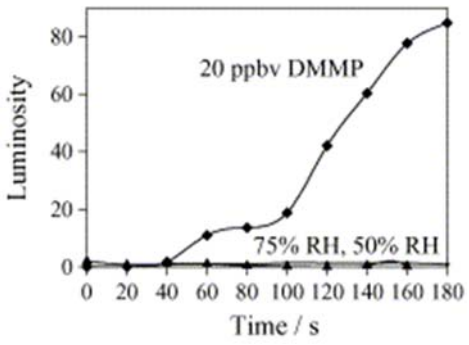

Figure 2.9. Effect of relative humidity (RH) on the visual appearance of a film of 8CB supported on Cu^{2+}-decorated surfaces. No change in luminosity was observed when the sample was exposed to pure N_2 with RH of 50 and 75%, respectively, whereas a 20 ppbv DMMP vaporous stream leads to an observable color change in the 8CB film in 60 s. Reprinted with permission from Yang, K.L., K. Cadwell, and N.L. Abbott, *Use of self-assembled monolayers, metal ions and smectic liquid crystals to detect organophosphonates.* Sensors and Actuators B-Chemical, 2005. 104(1): p. 50-56. Copyright 2005 Elsevier.

The proposition that the ordering transitions shown in Figures 2.7 to 2.9 result from ligand exchange reactions at the metal ion-decorated surfaces is supported by IR spectroscopy.[38] Prior to exposure to DMMP, two nitrile absorption peaks are evident in the IR spectrum (Figure 2.10A, bottom curve). As discussed above, the peak at 2227cm^{-1} corresponds to free nitrile groups and the peak at 2287cm^{-1} corresponds to nitrile groups coordinated with Cu^{2+}. Following exposure to DMMP (Figure 2.10A, middle curve), the peak at 2287cm^{-1}, present prior to exposure, disappears. The loss of this peak is consistent with displacement of the nitrile group of the 8CB from its coordination with the Cu^{2+} due to competitive binding of DMMP with

the Cu^{2+} ion. Finally, following a nitrogen purge of the system the nitrile peak corresponding to the coordinated state of the nitrile group reappears in the IR spectrum (Figure 2.10A, top curve). The reappearance of this peak is consistent with the reversible response of the LC film to DMMP, as shown in Figures 2.7 and 2.8. The connection proposed between the orderings transitions of nitrile containing LCs and IR spectroscopy is further strengthened by the IR spectra shown in Figure 2.10B, obtained using surfaces presenting Ni^{2+} ions. Whereas Ni^{2+}-decorated surfaces cause homeotropic orientations of nitrile-containing LCs (see Figure 2.3), such films of LCs do not undergo ordering transitions upon exposure to DMMP. These observations are consistent with the IR spectra in Figure 2.10B, where exposure of a film of 8CB to DMMP does not result in elimination of the peak corresponding to the coordinated state of the nitrile group. That is, the Ni^{2+}-nitrile coordination complex is not disrupted by DMMP to the extent that is observed with Cu^{2+}-decorated surfaces. Overall, these results and others reported in the literature [31-32, 38, 40-42] support our conclusion that ligand exchange reactions underlie the sensitive and selective ordering transitions of LCs that can be observed on surfaces decorated with metal ions.

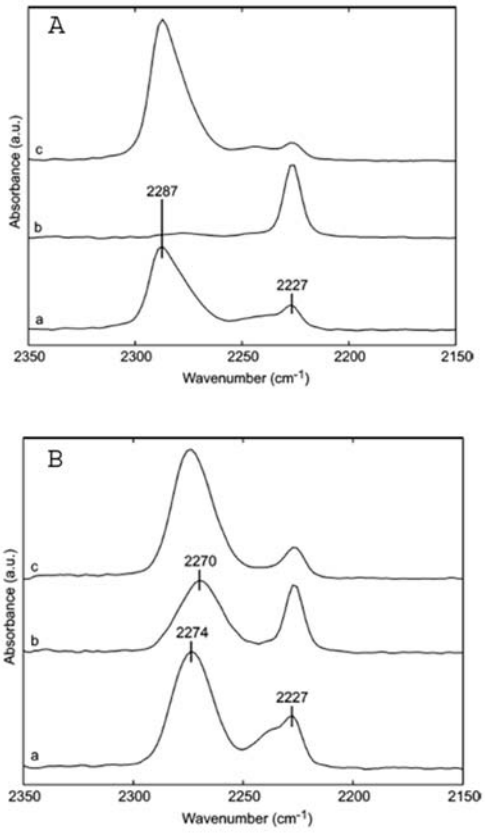

Figure 2.10. Infrared spectroscopy characterizing the response of 8CB supported on surfaces decorated with Cu^{2+} or Ni^{2+} ions to DMMP. (A). IR spectra of a thin film of 8CB on a surface presenting Cu^{2+} perchlorate salts (a) before and (b) during exposure to 10 ppm DMMP and (c) after a 30-min air purge. (B). IR spectra of a thin film of 8CB on a surface supporting Ni^{2+} perchlorate salts (a) before and (b) during exposure to 10 ppm DMMP and (c) after a 30-min air purge. Reprinted with permission from Cadwell, K.D., M.E. Alf, and N.L. Abbott, *Infrared spectroscopy of competitive interactions between liquid crystals, metal salts, and dimethyl methylphosphonate at surfaces.* Journal of Physical Chemistry B, 2006. 110(51): p. 26081-26088. Copyright 2006 American Chemical Society.

We end this section by making several additional observations regarding the promise and opportunity defined by LC-based sensors. First, whereas many of the results presented above were obtained using a model organophosphonate compound, we have also demonstrated that the principles described above can be extended to live nerve agents (which

are also organophosphonates).[25, 31, 38] As shown in Figure 2.11, by using surfaces presenting Al^{3+}, Zn^{2+} and Fe^{3+}, it is possible to use LCs to detect the nerve agents GB, GD, GA and VX.[32]

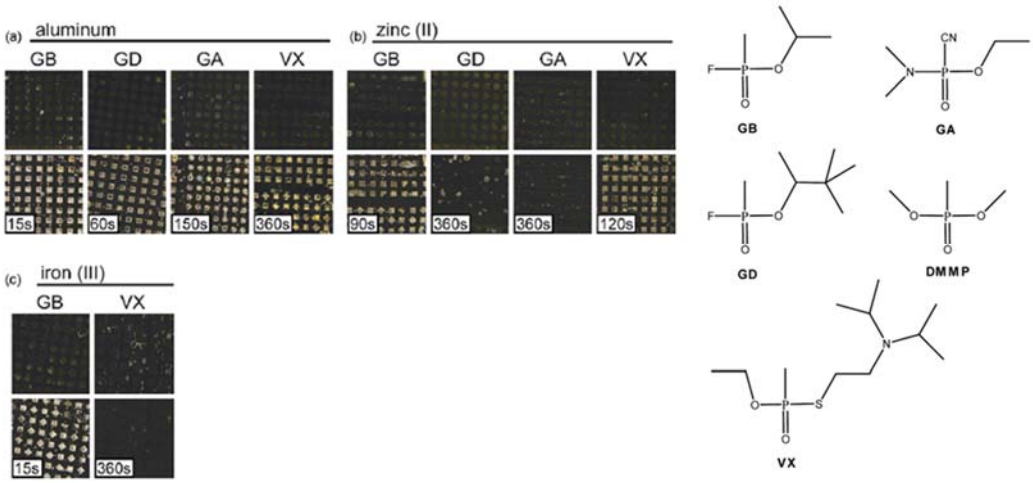

Figure 2.11. Optical images (crossed polars) of the nitrile containg LC E7 supported on perchlorate salts of (a) aluminum(III), (b) zinc(II) and (c) iron(III) before (top row) and after (bottom row) exposure to organophosphorous nerve agents. The duration of agent exposure is indicated. Imaged areas are approximately 7.5mm by 7.5 mm. Reprinted with permission from Cadwell, K.D., N.A. Lockwood, B.A. Nellis, M.E. Alf, C.R. Willis, and N.L. Abbott, *Detection of organophosphorous nerve agents using liquid crystals supported on chemically functionalized surfaces.* Sensors and Actuators B-Chemical, 2007. 128(1): p. 91-98. Copyright 2007 Elsevier.

Second, we comment that there exists a substantially unexplored opportunity to design LCs that are tailored for chemical sensing. The experiments described above were largely based on commercially available LCs that were designed largely with a view to application in LC displays, and there is little reason to believe that they represent optimal designs for LC-based chemical sensors. As a first example of an attempt to tailor the design of a mesogen for chemical sensing, we show in Figure 2.12 results obtained using a mesogen that was synthesized to contain two nitrile groups.[34]

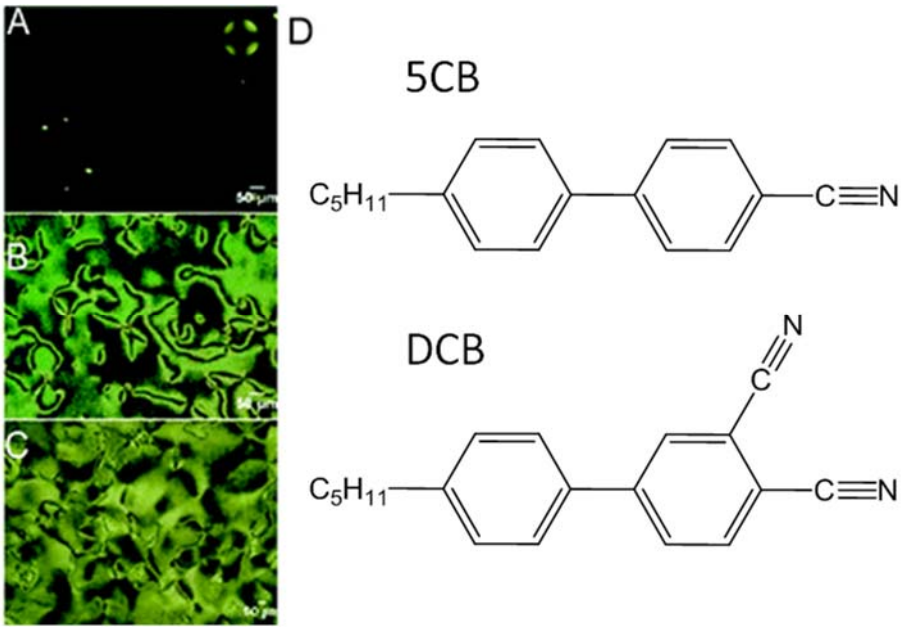

Figure 2.12. (A) Optical micrographs (crossed polars) of a thin film of nematic LC mixture containing 2 wt% DCB (D, lower structure) in 5CB (D, upper structure) confined between SAMs formed from $HOOC(CH_2)_{10}SH$ that were pretreated sequentially with aqueous solution of 0.01 (N) NaOH and 50mM$Cu(ClO_4)_2$, followed by a thorough rinse with ethanol. The inset in A is a conoscopic image indicating homeotropic alignment. (B, C) Optical micrographs (crossed polars) of LCs containing 2 wt% DCB in 5CB confined within optical cells with surfaces prepared from either (B) SAMs formed from $HOOC(CH_2)_{10}SH$ or (C) SAMs formed from $HOOC(CH_2)_{10}SH$ and pretreated with 0.01 (N) NaOH. Reprinted with permission from Pal, S.K., C. Acevedo-Velì lez, J.T. Hunter, and N.L. Abbott, *Effects of Divalent Ligand Interactions on Surface-Induced Ordering of Liquid Crystals.* Chemistry of Materials, 2010. 22(19): p. 5474-5482. Copyright 2010 American Chemical Society.

The incorporation of two coordinating nitrile groups into a mesogen resulted in observations of homeotropic orientations of the LC on surfaces presenting low densities of Cu^{2+} ions (densities that did not cause homeotropic orientation of 5CB)(Figure 2.12). However, the strong coordination of the mesogens to the Cu^{2+}-decorated surface also inhibited ordering transitions triggered by DMMP (that is, DMMP was not able to readily displace the dinitrile-based mesogens from coordination with the Cu^{2+}) (Figure 2.13). This example serves to

illustrate the substantial opportunity that exists to optimize LC-based sensors through the tailoring of the design of mesogens.[34]

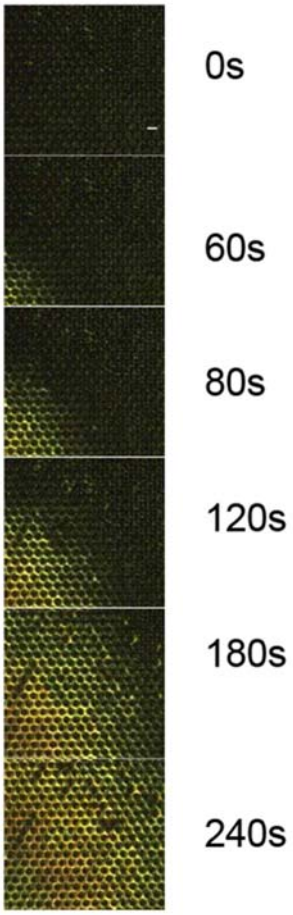

Figure 2.13. Optical images (crossed polars) of a mixture of 5CB containing 2.0 wt% DCB (see Figure 15) showing the time-dependent response of the LCs hosted in micropillar arrays to a vapor of DMMP (Scale bar = 50 μm). Reprinted with permission from Pal, S.K., C. Acevedo-Vel lez, J.T. Hunter, and N.L. Abbott, *Effects of Divalent Ligand Interactions on Surface-Induced Ordering of Liquid Crystals.* Chemistry of Materials, 2010. 22(19): p. 5474-5482. Copyright 2010 American Chemical Society.

2.1.3 Liquid Crystal Sensors Designed to Report Acid-Base Interactions.

To illustrate the generality of LC-based sensors that use chemically functionalized surfaces, we next describe a class of sensors that report acid-base interactions [25-26, 28]. Such sensors can report important classes of compounds such as organoamines, compounds that can be used, for example, to indicate the freshness of foods.[25, 28]

As discussed in the context of Figures 2.5 and 2.6, past studies have provided evidence that hydrogen bonding between carboxylic acid-functionalized surfaces and nitrile-containing LCs can lead to preferred azimuthal orientations of supported LC films.[26-27] The binding of an alkylamine to these surfaces, which results from an acid-base reaction between the amine and carboxylic acid, leads to the disruption of the initial hydrogen bonded state of the LC and thus an azimuthal ordering transition (Figure 2.14). As noted above, in the absence of the hydrogen bonding interactions, the topographical features of the surface define the azimuthal orientation of the LC.[28]

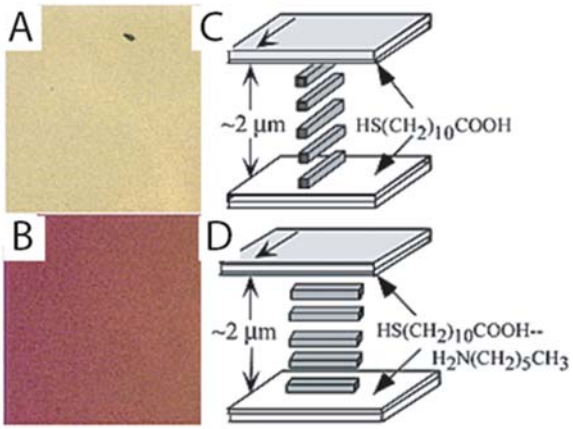

Figure 2.14. (A and B) Interference color of a film of nematic 5CB supported on a SAM formed from $HOOC(CH_2)_{10}SH$ before (A) and after (B) exposure to n-$H_2N(CH_2)_5CH_3$. (C) Schematic illustration of the orientation of the LC in contact with a carboxylic acid monolayer that is consistent with interference colors shown in A. The bold arrow indicates the direction of deposition of gold onto the substrate. (D) Schematic illustration of the orientation of the liquid crystal in contact with the hexylamine-reacted carboxylic acid monolayer that is consistent with the interference colors shown in B. Reprinted with permission from Shah, R.R. and N.L. Abbott, *Orientational transitions of liquid crystals driven by binding of organoamines to carboxylic acids presented at surfaces with nanometer-scale topography.* Langmuir, 2003. 19(2): p. 275-284. Copyright 2003 American Chemical Society.

Exposure of a film of LC confined between two surfaces presenting carboxylic acids groups, when exposed to a vapor of hexylamine, can cause an ordering transition that propagates laterally across the film of LC (Figure 2.15A). If the surface is patterned with stripes of carboxylic acids groups that are separated by methyl-terminated areas, the ordering transition triggered by the hexylamine can lead to patterned orientations of the LC and a diffraction grating (Figures 2.15B and 2.15C).[28]

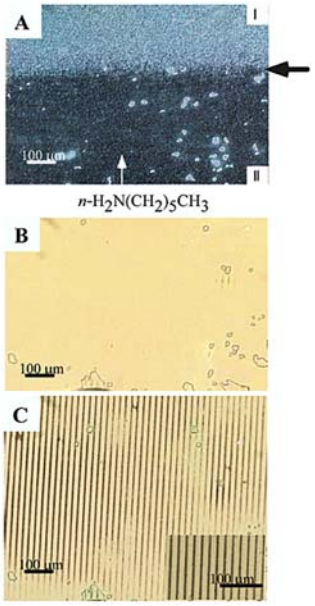

Figure 2.15. Optical images formed by 5CB within optical cells (12 μm) fabricated with surfaces presenting carboxylic acid. The cells were exposed to 750 ppmv *n*-$H_2N(CH_2)_5CH_3$ at the edge shown at the bottom of the image. (A) shows the optical textures of 5CB during diffusion of *n*-$H_2N(CH_2)_5CH_3$ across the cell. In region I, the presentation of carboxylic acid causes a 90° twist distortion in the liquid crystal. In region II, *n*-$H_2N(CH_2)_5CH_3$ bound to the carboxylic acid groups results in a uniform orientation of the liquid crystal. The arrow indicates the limit of the diffusion front of*n*-$H_2N(CH_2)_5CH_3$. (B,C) Optical textures (cross polars) formed by nematic 5CB within optical cells (12 μm) prepared with one surface supporting a SAM formed from $H_3C(CH_2)_{14}SH$ and an opposing surface supporting a SAM patterned using $HOOC(CH_2)_{10}SH$ and $H_3C(CH_2)_{11}SH$ pretreated at pH 3.2 (B) prior to exposure to *n*-$H_2N(CH_2)_5CH_3$ and (C) after exposure for 8 min to 750 ppmv of *n*-$H_2N(CH_2)_5CH_3$. The inset in (C) is a magnified region showing the formation of the patterned region upon exposure to the analyte. Reprinted with permission from Shah, R.R. and N.L. Abbott, *Orientational transitions of liquid crystals driven by binding of organoamines to carboxylic acids presented at surfaces with nanometer-scale topography.* Langmuir, 2003. 19(2): p. 275-284. Copyright 2003 American Chemical Society.

Figure 2.16 illustrates the progression of the ordering transition across the LC sample is consistent with diffusion of the hexylamine laterally across the film. The LC film thus provides a diffusion cell in which transport of the gas across the cell is readily visualized via an ordering transition that is induced in the LC.[28]

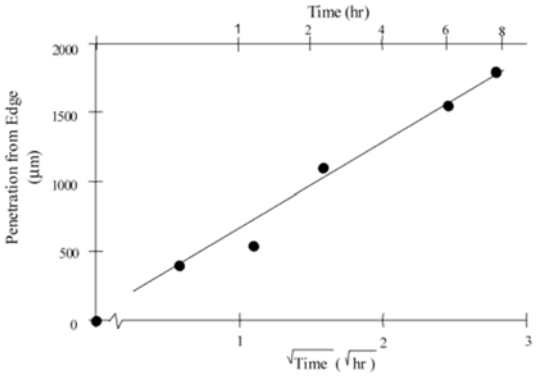

Figure 2.16. Penetration distance (from the edge of a liquid crystal cell) of *n*-$H_2N(CH_2)_5CH_3$ as a function of exposure time and as a function of the square root of exposure time. Reprinted with permission from Shah, R.R. and N.L. Abbott, *Orientational transitions of liquid crystals driven by binding of organoamines to carboxylic acids presented at surfaces with nanometer-scale topography.* Langmuir, 2003. 19(2): p. 275-284. Copyright 2003 American Chemical Society.

2.2 References

1. Pieranski, P.; Jerome, B.; Gabay, M. *Molecular Crystals and Liquid Crystals Incorporating Nonlinear Optics* **1990,** *179*, 285-315.
2. Jerome, B.; Shen, Y. R. *Physical Review E* **1993,** *48*, 4556.
3. Bechhoefer, J.; Duvail, J. L.; Masson, L.; eacute; rme, B.; Hornreich, R. M.; Pieranski, P. *Physical Review Letters* **1990,** *64*, 1911.
4. Bechhoefer, J.; eacute; rme, B.; Pieranski, P. *Physical Review A* **1990,** *41*, 3187.
5. Novak, T. J.; Poziomek, E. J.; Mackay, R. A. *Analytical Letters* **1972,** *5*, 187-192.
6. Poziomek, E. J.; Novak, T. J.; Mackay, R. A. *Molecular Crystals and Liquid Crystals* **1972,** *15*, 283-295.
7. Dickert, F. L.; Haunschild, A.; Hofmann, P.; Mages, G. *Sensors and Actuators B: Chemical* **1992,** *6*, 25-28.
8. Dickert, F. L.; Haunschild, A.; Hofmann, P. *Fresenius' Journal of Analytical Chemistry* **1994,** *350*, 577-581.
9. Rey, A. D. *Molecular Crystals and Liquid Crystals Science and Technology. Section A. Molecular Crystals and Liquid Crystals* **1997,** *293*, 87-109.
10. Winterbottom, D. A.; Narayanaswamy, R.; Raimundo, I. M. *Sensors and Actuators B: Chemical* **2003,** *90*, 52-57.
11. Kirchner, N.; Zedler, L.; Mayerhofer, T. G.; Mohr, G. J. *Chemical Communications* **2006**, 1512-1514.
12. Sutarlie, L.; Qin, H.; Yang, K.-L. *Analyst* **2010,** *135*, 1691-1696.

13. Sutarlie, L.; Lim, J. Y.; Yang, K.-L. *Analytical Chemistry* **2011,** *83*, 5253-5258.

14. Poziomek, E. J.; Novak, T. J.; Mackay, R. A. *Molecular Crystals and Liquid Crystals* **1974,** *27*, 175-185.

15. Bai, Y.; Abbott, N. L. *Langmuir* **2011,** *27*, 5719-5738.

16. Bi, X.; Lai, S. L.; Yang, K.-L. *Analytical Chemistry* **2009,** *81*, 5503-5509.

17. Brake, J. M.; Daschner, M. K.; Luk, Y.-Y.; Abbott, N. L. *Science* **2003,** *302*, 2094-2097.

18. Govindaraju, T.; Bertics, P. J.; Raines, R. T.; Abbott, N. L. *Journal of the American Chemical Society* **2007,** *129*, 11223-11231.

19. Gupta, V. K.; Skaife, J. J.; Dubrovsky, T. B.; Abbott, N. L. *Science* **1998,** *279*, 2077-2080.

20. Jang, C.-H.; Cheng, L.-L.; Olsen, C. W.; Abbott, N. L. *Nano Letters* **2006,** *6*, 1053-1058.

21. Jang, C.-H.; Tingey, M. L.; Korpi, N. L.; Wiepz, G. J.; Schiller, J. H.; Bertics, P. J.; Abbott, N. L. *Journal of the American Chemical Society* **2005,** *127*, 8912-8913.

22. Price, A. D.; Schwartz, D. K. *Journal of the American Chemical Society* **2008,** *130*, 8188-8194.

23. Shiyanovskii, S. V.; Schneider, T.; Smalyukh, I. I.; Ishikawa, T.; Niehaus, G. D.; Doane, K. J.; Woolverton, C. J.; Lavrentovich, O. D. *Physical Review E* **2005,** *71*, 020702.

24. Birchall, L. S.; Ulijn, R. V.; Webb, S. J. *Chemical Communications* **2008**, 2861-2863.

25. Shah, R. R.; Abbott, N. L. *Science* **2001,** *293*, 1296-1299.

26. Luk, Y. Y.; Yang, K. L.; Cadwell, K.; Abbott, N. L. *Surf. Sci.* **2004,** *570*, 43-56.

27. Shah, R. R.; Abbott, N. L. *J. Am. Chem. Soc.* **1999,** *121*, 11300-11310.

28. Shah, R. R.; Abbott, N. L. *Langmuir* **2003,** *19*, 275-284.

29. Bi, X.; Yang, K.-L. *Sensors and Actuators B: Chemical* **2008,** *134*, 432-437.

30. Bungabong, M. L.; Ong, P. B.; Yang, K.-L. *Sens. Actuators, B* **2010,** *148*, 420-426.

31. Cadwell, K. D.; Alf, M. E.; Abbott, N. L. *J. Phys. Chem. B* **2006,** *110*, 26081-26088.

32. Cadwell, K. D.; Lockwood, N. A.; Nellis, B. A.; Alf, M. E.; Willis, C. R.; Abbott, N. L. *Sens. Actuator B-Chem.* **2007,** *128*, 91-98.

33. Hunter, J. T.; Pal, S. K.; Abbott, N. L. *ACS Appl. Mater. Interfaces* **2010,** *2*, 1857-1865.

34. Pal, S. K.; Acevedo-Velez, C.; Hunter, J. T.; Abbott, N. L. *Chem. Mater.* **2010,** *22*, 5474-5482.

35. Sen, A.; Acharya, B. R. *Liquid Crystals* **2011,** *38*, 495-506.

36. Sridharamurthy, S. S.; Cadwell, K. D.; Abbott, N. L.; Jiang, H. *Smart Mater. Struct.* **2008,** *17*, 4.

37. VanTreeck, H. J.; Most, D. R.; Grinwald, B. A.; Kupcho, K. A.; Sen, A.; Bonds, M. D.; Acharya, B. R. *Sensors and Actuators B: Chemical In Press, Corrected Proof*.

38. Yang, K. L.; Cadwell, K.; Abbott, N. L. *J. Phys. Chem. B* **2004,** *108*, 20180-20186.

39. Yang, K. L.; Cadwell, K.; Abbott, N. L. *Sens. Actuator B-Chem.* **2005,** *104*, 50-56.

40. Escalona Platero, E.; Peñarroya Mentruit, M.; Morterra, C. *Langmuir* **1999,** *15*, 5079-5087.

41. Marcus, Y. *Journal of the Chemical Society, Dalton Transactions* **1991**, 2265-2268.

42. Pelmenschikov, A. G.; van Santen, R. A.; Janchen, J.; Meijer, E. *The Journal of Physical Chemistry* **1993,** *97*, 11071-11074.

Chapter 3: Adsorbate-Induced Ordering Transitions of Nematic Liquid Crystals on Surfaces Decorated with Aluminum Perchlorate Salts

3.1 Introduction

Surface-induced orientational ordering of micrometer-thick films of liquid crystals (LCs) has been reported to occur on the surfaces of a wide range of organic and inorganic materials.[1-3] Many of the early studies explored relatively simple surfaces (e.g., mechanically rubbed films of polyimides) and were successful in elucidating the underlying intermolecular interactions responsible for the surface-induced order (van der Waals dispersion interactions for the case of polyimides).[2, 4-7] More recent studies, however, have moved to investigate complex surfaces that present a diverse range of chemical functionality with potential application in liquid crystal-based chemical and biological sensors.[8-27] For these latter types of surfaces, the interfacial interactions underlying observations of the ordering of LCs remain poorly understood but potentially include (i) dipolar interactions associated with electrical double layers formed as a result of fixed charges at surfaces,[10] (ii) hydrogen bonding between chemical groups presented at the interface and mesogens comprising the LC,[9, 17] and (iii) metal ion-ligand coordination interactions between surface-immobilized metal ions and mesogens.[8, 12, 18, 27] The study reported in this paper advances our understanding of surface-induced ordering of nitrile-containing LCs at interfaces presenting metal salts that can coordinate with the nitrile groups of the LCs. These surfaces have been reported previously to offer the basis of sensitive and

selective sensors for low molecular weight organic molecules, such as organophosphonates.[8, 11, 28]

As illustrated in Figure 3.1A and 3.1B, when micrometer-thick films of nitrile-containing LCs (e.g., 5CB (4-cyano-4'-*n*-pentyl-biphenyl), 8CB (4-cyano-4'-*n*-octyl-biphenyl) or E7 (a mixture of 51 wt% 5CB, 25 wt% 4-cyano-4'-*n*-heptyl-biphenyl (7CB), 16 wt% 4-cyano-4'-*n*-oxyoctyl-biphrnyl (8OCB) and 8 wt% 4-cyano-4'-*n*-pentyl-p-terphenyl (5CT)) are contacted with surfaces presenting perchlorate salts of metal cations with high electron affinity (e.g., Cu^{2+} or Al^{3+}), infrared spectroscopic studies have revealed that the LCs adopt a perpendicular (homeotropic) ordering as a consequence of coordination interactions between the nitrile groups of the LCs and the cations of the metal salts.[11] The perchlorate counterion is used because of its weak coordinating properties allowing for the aluminum ion to coordinate to 5CB and DMMP.

Additional studies, also based on IR spectroscopy, determined that the phosphoryl groups of organophosphonate compounds (such as dimethylmethylphosphonate, DMMP) bind these metal cations with sufficient affinity that they can competitively displace the nitrile groups of the LCs from coordinating with the metal ions (Figure 3.1A). This ligand exchange was shown to be accompanied by an ordering transition in the LC that propagates from the metal salt-coated surface across the micrometer-thick LC film, thus giving rise to easily detected optical signals (transmission of polarized light) that indicate the presence of DMMP (Figure 3.1C). These ordering transitions were found to be triggered by parts-per-billion concentrations (ppb) of organophosphonate vapors.[8] By patterning different metal ions on a single surface, it was also shown that the (organophosphonate) chemical warfare agents ethyl dimethylphosphoramidocyanidate (GA, tabun), 1,2,2-trimethylpropyl

methylphosphonofluoridate (GD, soman), and O-ethyl S-(2-diidopropylaminoethyl) methylphosphonothiolate (VX) can be detected and distinguished using LCs.[11, 28]

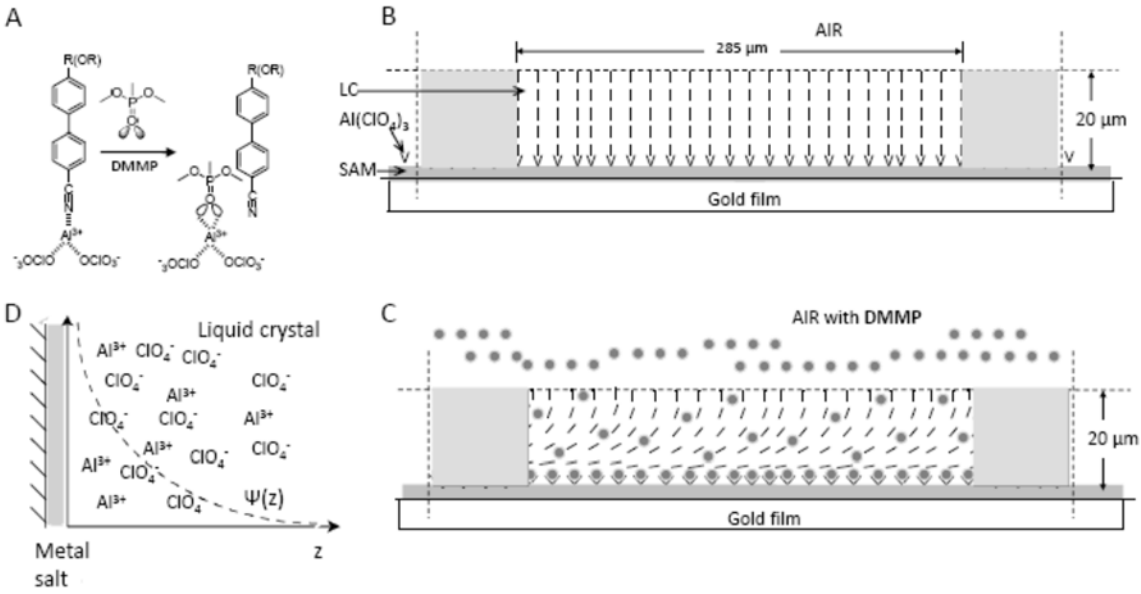

Figure 3.1. Schematic illustration of DMMP-responsive thin films of 5CB hosted within TEM grids supported on metal salt-decorated surfaces. (A) Illustration of competitive coordination interactions between nitrile groups of LC and phosphoryl groups of DMMP with Al^{3+}, (B) Homeotropic anchoring of 5CB at both air and metal salt-decorated interfaces, (C) Exposure of the LC to a vapor of DMMP results in diffusion of DMMP to the Al^{3+}-decorated surface and the triggering of an ordering transition in the LC via displacement of the nitrile groups of the LC from their coordination interactions with the Al^{3+}. (D) Illustration of the formation of an electrical double layer due to the uptake of salt into the LC film from the surface. The electrical potential, ψ(z) is shown in the vicinity of the surface.

Whereas the studies reported above establish the potential utility of surface-induced ordering transitions of LCs as the basis of chemical sensors, a complete picture of the underlying interfacial interactions is lacking, and the influence of key parameters of the system on these ordering transitions is not understood. In this paper, we report an investigation of the effects of the surface density of metal perchlorate salt on the interfacial ordering of nematic phases of 5CB, including the response of the LC films to DMMP. We focus our study on

aluminum perchlorate as a metal salt that was previously identified[12] to have sufficient electron affinity to orient nematic phases of 5CB but has not been characterized in the context of ordering transitions induced by DMMP.

The study reported in this paper also represents a simple but useful advance in the design of an experimental system that enables fundamental insights into surface-induced ordering transitions in LC films. In particular, in micrometer-scale LC systems, the effects of elastic strain of the LC are often in competition with surface-induced ordering.[29-30] This competition between elastic and surface-induced ordering necessitates careful control of the micrometer-scale geometry of the LC system (e.g., LC film thickness) in order to obtain reproducible and quantitative ordering transitions upon exposure of the systems to adsorbates. To this end, recent studies have used microfabricated wells or arrays of micropillars to control the thicknesses of the films of LCs.[8, 11, 26, 28, 31] In preliminary studies performed at the outset of the investigation reported in this paper, we found that the complex topography of microfabricated wells and micropillars prevented precise control over the uniformity and surface density of metal salts deposited by spin or dip coating. To address this issue, we report modification of a procedure described previously by us in which metallic grids are placed onto planar surfaces (as sketched in Figure 3.1B) onto which controlled loadings of metal salts have been deposited by spin coating.[12] This approach allowed us to systematically manipulate and quantify the amount of metal salt on the surface, and thereby unmask the effects of metal salt density on the surface- induced ordering of nematic LC phases (including unexpected time-dependent ordering transitions).

A key finding of the study reported in this paper is that the loading of aluminum perchlorate on a surface used to support a nematic film of 5CB has a substantial and previously unappreciated effect on the surface-induced ordering of the LC film as well as the response to DMMP. In particular, we have found that the loading of metal salt on the surface influences dynamic phenomena that occur at the salt-LC interface over time periods that range from hours to days. Our investigation provides fundamental insights into the molecular origins of these dynamic phenomena, identifying dissolution of metal ions into the LC and formation of interfacial electrical double layers as key physicochemical interfacial events (as illustrated in Figure 3.1D). We also identify conditions and criteria for the design of interfaces that provide stable ordering of LC films for at least 5 days.

3.2 Experimental Methods

3.2.1 Materials

11-Mercaptoundecanoic acid (MUA) and Al(III) perchlorate nonahydrate salts were purchased from Sigma Aldrich (Milwaukee, WI). Nematic 5CB was purchased from EMD Chemicals (Gibbstown, NJ). Titanium (99.999%) and gold (99.999%) were purchased from Advanced Materials (Spring Valley. NY). Methanol and Fischer's Finest glass slides were purchased from Fischer Scientific (Hamton, NH). Absolute ethanol (anhydrous, 200 proof) was purchased from Pharmco-AAPER. All chemicals and solvents were of analytical reagent grade and were used as received without any further purification. All deionized water used in the study possessed a resistivity of 18.2 MΩ-cm.

3.2.2 Methods

3.2.2A Cleaning of glass substrates .

Glass microscope slides were cleaned according to published procedures using 'piranha' solution [70:30 (% v/v) H_2SO_4:H_2O_2 (30%)], as described in detail elsewhere.[32] Briefly, the glass slides were immersed in a piranha bath at 60-80°C for at least 1h, and then rinsed in running deionized water for 2-3 minutes. The slides were then immersed in basic piranha [70:30 (% v/v) KOH (45%): H_2O_2 (30%)] and heated to between 60°C and 80°C for at least 1 h. Finally, the slides were rinsed sequentially in deionised water, ethanol, and methanol, and then dried under a stream of nitrogen. The clean slides were stored in an oven at 110°C. All other glassware was cleaned prior to use.

3.2.2B Deposition of gold films.

Semi-transparent films of gold with thicknesses of 200 Å were deposited onto piranha-cleaned glass slides mounted on a fixed holder within an electron beam evaporator (VEC-3000-C manufactured by Tek-vac Industries, Brentwood, NY). We calculated the angle of incidence of the gold onto the slides to range from 0º to 15º (measured from surface normal). A layer of titanium (thickness 80 Å) was used to promote adhesion between the glass microscope slides and the film of gold. The rates of deposition of gold and titanium were ~0.2 Å/sec. The pressure in the evaporator was maintained at less then 3×10^{-6} torr before and during each deposition. The gold source was periodically cleaned by sequential immersion in aqua regia (70% HNO_3, 30% HCl) and piranha solutions at 50°C (30 min in each solution). The cycle was repeated 3-4 times rinsing between cycles in deionised water.

3.2.2C Formation of chemically functionalized surfaces.

Carboxylic acid-terminated self-assembled monolayers (SAMs) of 11-mercaptoundecanoic acid (MUA) were formed on gold-coated glass slides by immersing the slides overnight in an ethanolic solution containing 2 mM of MUA. The gold films were then rinsed with copious amounts of ethanol and dried under a stream of nitrogen. Metal ions (Al^{3+}) were deposited onto the carboxylic acid-terminated SAMs by spin coating the desired molar concentration (1 mM, 5 mM or 10 mM in ethanol) of Al $(ClO_4)_3 \cdot 9H_2O$ at 3000 rpm for 60s (WS-400A-6NPP/Lite, Laurell Technologies, North Wales, PA).

3.2.2D Ellipsometry.

The optical thickness of the metal salts deposited onto the SAMs were measured by using a Stokes ellipsometer (Model LSE, Gaertner Scientific corporation) at a wavelength of 6328Å (HeNe Laser light source) and an angle of incidence of 70°. Ellipsometric constants of the gold films were determined to be n = 0.20 and k = 3.58. Five spots were measured on each of five samples for each sample type. The apparent optical thickness of each SAM formed from MUA and each layer of metal perchlorate salt was calculated assuming a refractive index of n = 1.5.[33-35]

3.2.2E Formation of thin LC films.

After coating the surface with aluminum perchlorate salt, an 18 μm-thick gold-coated TEM grid (Electron Microscopy Sciences, Hatfield, PA) was fastened to the surface by a thin stainless steel plate (0.44 mm thickness). The stainless steel plate contained a 2 mm diameter hole that was aligned with the TEM grid. The TEM grid was composed of squares with lateral

dimensions of 285 μm and an overall diameter of 3 mm. Both the TEM grid and stainless steel plate were dip-coated with a perfluorocarbon (Nyebar Fluorocarbon Barrier Film, SmartGrease Company, Fairhaven, MA) layer to prevent wicking of the LC from the TEM grid. The grids were filled with LC using a microcapillary tube, taking care to fill the middle squares of the TEM grid only so as to avoid wicking of the LC away from the grid.

3.2.2F Ordering transitions induced by DMMP.

The samples were exposed to 5 ppm DMMP in a home built-flow system. Air of a controlled humidity generated using an air humidifier (LI-610, LI-COR Biosciences, Lincoln, NE**)** was mixed with a 10 ppm DMMP in N_2 (Matheson Tri-Gas Inc, Eagan, MN) in a 1:1 volume ratio so that the humidity of the resulting stream was 30% (relative humidity, RH) and the concentration of DMMP was 5 ppm. The protocol used for exposure of the LC films to DMMP was as follows: (i) the sample was exposed to air (60% RH) for 5 minutes (ii) 5 ppm DMMP (30% RH) was introduced into the flow cell for 2 minutes (iii) then air (60% RH) was passed through the cell for 13 minutes to purge the DMMP from the system. The cycle was repeated to verify the repeatability of the experiment. Optical micrographs through polarizing films were taken every ten seconds and the light intensity of the images was quantified using ImageJ. Control experiments were undertaken to verify that the changes in RH do not affect the ordering of the LC. In these experiments, the air streams (RH 60%) were mixed in a 1:1 volume ratio with dry N_2 to maintain a 30% RH through the entire protocol described above. After exposing each sample to DMMP in a flow cell, the sample was stored in a desiccator maintained at 25ºC and 30% RH.

3.2.2G Measurements of the saturation solubility of salts in LC.

To determine the solubility of metal ions in the LC, excess salts (as solid) were equilibrated with the LC (5CB). The aluminum perchlorate salts were added to 100 µL of 5CB in a small vial. After the desired time of equilibration (days), 50 µL of the LC was withdrawn by pipette and dissolved into 3 ml nitric acid. Care was taken during the withdrawal of the LC from the vial to ensure that no solid particles of the salt were suspended in the LC. The sample was sonicated and vortexed with extensive shaking and tumbling for 10 min to extract all salts into the nitric acid solution. The nitric acid extract was used to measure the ion-concentration by chemical analysis (see below).

3.2.2H Determination of concentration of Al^{3+} dissolved into LC.

The concentration of Al^{3+} dissolved into the LC was measured by elemental analysis using an inductively-coupled plasma emission spectrometer ((ICP-ES, Perkin Elmer optima 3000DV) at a wavelength of 396.153 nm ($\lambda_{Al^{3+}}$ = 396.153 nm)). The detection limit of the instrument was specified to be 0.1 ppb. The argon used was ICP grade. All Al^{3+} solutions were prepared in 2 % nitric acid from stock 70% nitric acid (ACS reagent, trace metal grade). Aluminum standard solutions for ICP-ES calibration were prepared using 1000 ppm aluminum ion stock solution (from High-Purity Standards, cat. No. 10001-1) in 2% nitric acid. At least six serial dilutions of the stock were prepared to obtain standard aluminum solutions between 10 ppm and 1 ppb for the aluminum calibration curve. In addition, the 1 ppm aluminum standard was used for quality control (QC).

Following ignition of the plasma in the ICP-ES, and the instrument equilibrated for 30 minutes. The stock aluminum solutions were analyzed, and the calibration curve was accepted only if the correlation coefficient was >0.999. A duplicate sample was run every 10 samples. To accept the ICP-ES data, duplicate samples could not differ by more than 10 % or 2.2 times the detection limit of the method (0.0001 ppm i.e. 0.1 μg/L). The blank could not exceed 2.2 times the method detection limit. The blank and QC standards had to be within three standard deviations of the historical mean. If they were not, the analysis of the samples and QC standard was repeated. For each sample, all measurements were made in triplicate and averaged.

3.2.2I Measurement of the surface density of salt.

To measure the surface density of the Al^{3+} salts, MUA functionalized gold slides (see above) were spin coated with aluminum perchlorate solutions of known concentration. After deposition, the aluminum perchlorate salt was dissolved into 2 % nitric acid and the mixture was vortexed to extract all salt into the nitric acid solution. The concentration of Al^{3+} was measured by using ICP-ES, as described above. Finally, the surface density of the metal salt was calculated from both the ICP-ES data and knowledge of the area of the surface from which the aluminum perchlorate salts were extracted.

3.3 Results and Discussion

As described in the Introduction, recent investigations of adsorbate-induced ordering transitions in LC films have reported use of microfabricated wells and micropillar arrays to define the thickness of LC films.[11, 26, 31] These approaches, however, do not permit uniform deposition and quantification of the loading of metal salt due to the complex topography of the

surfaces. In the study reported in this paper, we have used planar surfaces onto which metal salts were deposited by spin coating. Films of nematic LCs of prescribed thickness were subsequently formed on these surfaces using metal grids and a procedure modified from that reported previously by us (see Materials and Methods for details).[12] The first experiments described below sought to establish uniformity of coverage as well as control over the surface density (mass/area) of metal salt on each surface. To this end, we employed both ellipsometric measurements and elemental analysis (see Methods for details).

Table 3.1 shows the ellipsometric thickness and surface mass density of aluminum perchlorate deposited onto surfaces by spin coating of ethanolic solutions containing either 1.0 mM, 5.0 mM or 10.0 mM of the salt. Inspection of Table 1 reveals that the ellipsometric thickness of the salt layer varied from ~1.4 nm to 18 nm. These thicknesses correspond to the presence of thin films of between ~3 monolayers to ~38 monolayers of metal salt. The corresponding surface mass densities of metal salt (measured by ICP-ES) were determined to vary from 0.39 ng/mm^2 to 2.14 ng/mm^2. The significance of these values is discussed below, where we establish that the amounts of salt spin-coated from the ethanolic solutions containing 1 mM and 10 mM aluminum perchlorate lie below and above the solubilization capacity of ~20 μm thick films of nematic 5CB, respectively. Importantly, our measurements of ellipsometric thicknesses at various locations on a given sample (and on independently prepared samples) confirmed that our procedures led to deposition of uniform layers of metal salts over the surfaces. Below we report on the impact of the different surface loadings of metal salt (as shown in Table 1) on the ordering of nematic phases of 5CB.

Table 3.1. Ellipsometric thicknesses and surface mass density of aluminum perchlorate on surfaces used in this study.

Concentration of Al^{3+} salt spin coated *(mM)*	Ellipsometric thicknesses *(nm)*	[$] Surface density *($ng/mm^2$)*
1	1.4 ± 0.10	0.39 ± 0.03
5	8.8 ± 0.21	1.13 ± 0.09
10	17.7 ± 0.5	2.14 ± 0.24

[$] Measured using ICP-ES

First, we characterized the orientational ordering of nematic phases of 5CB on the surfaces presenting the lowest density of aluminum perchlorate (0.39±0.03 ng/mm^2) investigated in our study. We sought to determine if 5CB supported on surfaces presenting such a low density of aluminum perchlorate salt would assume a homeotropic ordering (prior studies have not investigated surface loadings of salts as low as those reported here), and if so, whether or not the nematic film would undergo an orientational transition upon exposure to a gas phase containing DMMP. We note that a homeotropic ordering of the LC is desirable because it provides a well-defined initial state of the LC with a distinct optical signature (dark appearance between crossed polarizers) prior to exposure to the DMMP. Finally, we comment that we established through these initial investigations that our experimental procedures provided reproducible responses to DMMP with minimal sample-to-sample variation. In each of our experiments, the intensity of light transmitted through cross polarizing films was measured as the sample was exposed sequentially to (i) air for 5 minutes (ii) a gas phase containing 5 ppm DMMP for 2 minutes and (iii) air for 13 minutes (allowing the film to return to its initial state). This sequence was then repeated to examine the reversible behavior of the system. We note that our experimental set-up led to changes in humidity and DMMP concentration in most of

our experiments (see Materials and Methods for details). In order to establish that the changes in humidity did not influence the results reported in this paper, we performed several control experiments under conditions of constant humidity (compare Figure 3.7 of Supporting Information to Figure 3.2 discussed below).

Figure 3.2A shows that nematic films of 5CB (thickness ~20 μm), when supported on surfaces presenting 0.39 ng/mm^2 of aluminum perchlorate, exhibited a dark optical appearance when viewed between crossed polarizers. Past studies have established that 5CB assumes a homeotropic orientation at its free surface (air-LC interface).[36] The result in Figure 3.2A, when combined with conoscopic images of the sample, led us to conclude that the nematic film of 5CB did assume a homeotropic ordering immediately after contact with this metal salt-decorated surface. In addition, when the supported LC film was exposed to 5 ppm DMMP, a change in the optical appearance of the sample was observed (Figure 3.2A). The initial response was evident within 10 seconds of exposure to DMMP, and the maximum response was achieved after 30 seconds. As reported previously,[8] the bright optical appearance of the LC is caused by a DMMP-induced ordering transition and associated tilting of the orientation of the LC within the film away from the surface normal. Figure 3.2B quantifies the intensity of light transmitted through the LC film upon exposure to the DMMP. Following exposure to the DMMP for 2 minutes, we purged the flow cell with a stream of air. After purging with air, we observed the LC film to return to its initial dark state, although it took approximately 10 minutes for this process to occur. The slow reversal of the response of the LC to DMMP suggests that the dissociation of the DMMP and the Al^{3+} ion may be a rate-limiting process in the relaxation of the system. After returning to the homeotropic state, the sample was again exposed to 5 ppm

DMMP and a similar cycle was observed. The sample-to sample reproducibility of the experimental system is illustrated in Figure 3.2B, where the responses of two LC samples to DMMP are presented.

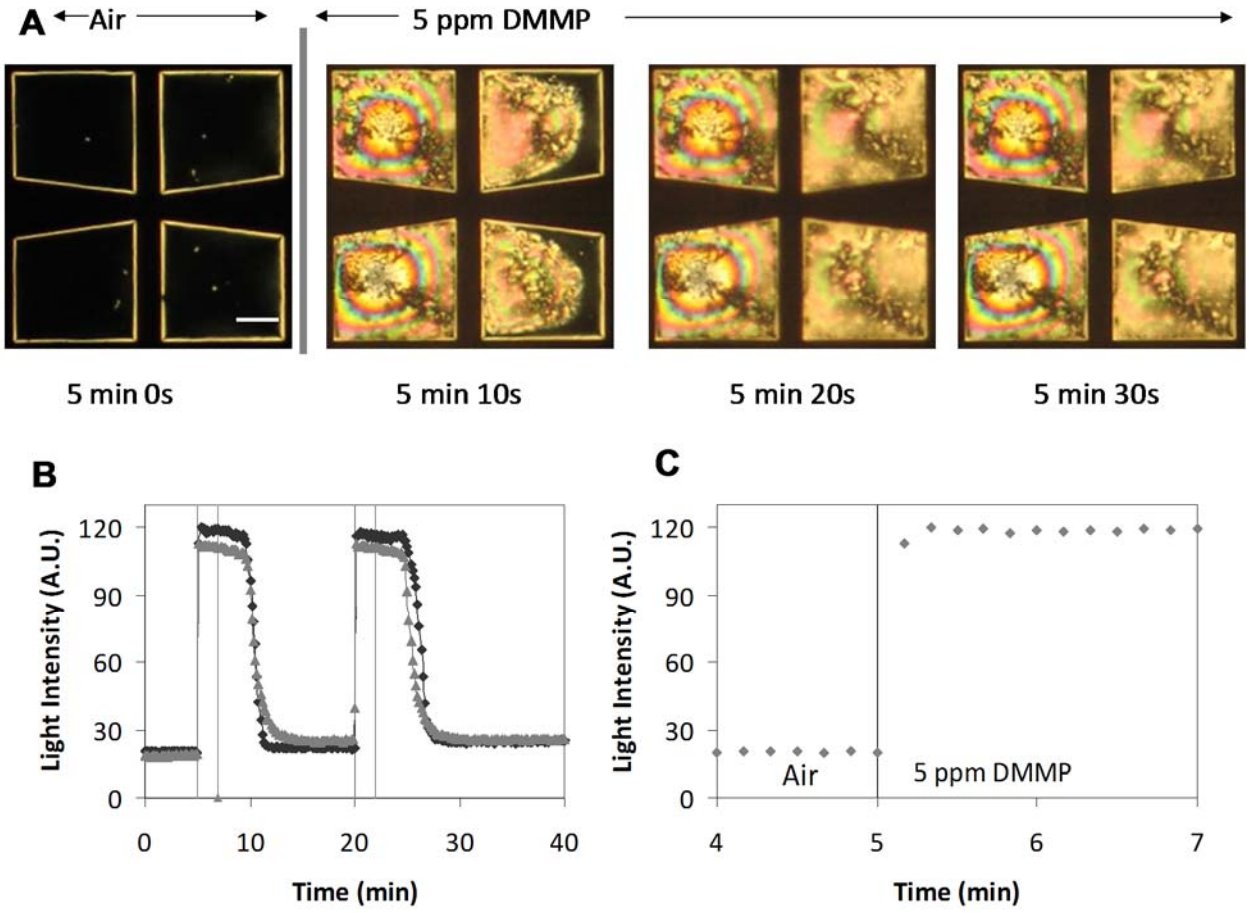

Figure 3.2. Optical response of 5CB supported on surfaces decorated with 0.39 ng/mm^2 Al perchlorate. (A) Optical micrographs (crossed polarizers) showing the change in optical appearance of the LC film upon exposure to DMMP. The direction of gas flow is from left to right in each optical micrograph. The scale bar corresponds to 100 µm. (B) Intensities of light transmitted through films of 5CB as a function of time: from 0 min to 5 min, the sample was exposed to air; from 5 min to 7 min, the sample was exposed to 5 ppm DMMP; from 7 min to 20 min, the sample was exposed to air; from 20 min to 22 min, the sample was exposed to 5 ppm DMMP; and from times over 22 min, the sample was exposed to air. (c) Data from B that shows the response of the LC to 5 ppm DMMP occurs within 10 seconds and reaches a maximum after 30 seconds.

The data characterizing the ordering transition induced by DMMP, as shown in Figure 3.2, was obtained immediately after preparation of the samples (i.e., contact of the LC with the metal salt coated surface). Next, we determined if the ordering of the LC supported on the surface, as well as the ordering transition induced by DMMP, was dependent on the length of time for which the LC was equilibrated on the metal salt coated-surface. After the samples were stored in a controlled humidity environment for a desired length of time, we characterized the state of the LC by measurement of the intensity of light transmitted through the sample (crossed polarizers) before and after exposure to DMMP. As shown in Figure 3.3, immediately after preparation of the sample, and prior to exposure to DMMP, the LC exhibited homeotropic ordering on the aluminum perchlorate-coated surface and the corresponding intensity of light transmitted through the sample was low (18 A.U.). The ordering transition induced by exposure of the freshly prepared sample resulted in an increase in the intensity of light transmitted through the sample to 113 A.U. The change in intensity of light transmitted through the sample (~95 A.U.) was reversed upon purging with air. Following equilibration of the LC film on the aluminum perchlorate-coated surface for 7 hrs, however, we observed the LC to undergo an ordering transition that caused the optical appearance of the LC film to become bright even in the absence of exposure to DMMP (107 A.U., see Figure 3.3). Furthermore, exposure of the sample to DMMP resulted in no measurable change in the ordering of the LC (and thus no significant change in the intensity of light transmitted through the sample). Equilibration of the LC with the surface for an additional 18 hrs did not result in any further changes in the ordering of the sample.

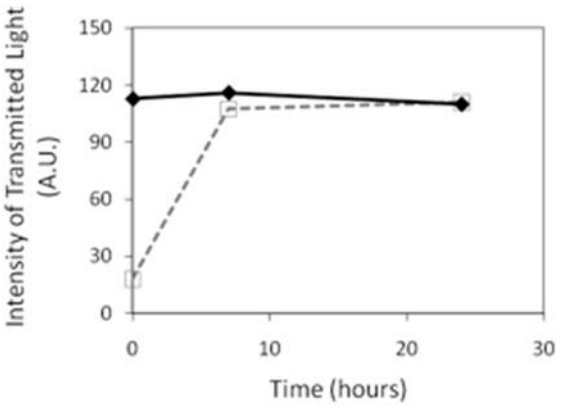

Figure 3.3. Quantification of the optical response of a film of nematic 5CB supported on a surface decorated with 0.39 ng/mm^2 Al perchlorate. The solid data points indicate the response of the LC to exposure to 5ppm DMMP; the open data points show the optical response of the LC prior to exposure to DMMP.

The results described above led us to conclude that the ordering of nematic 5CB within films supported on surfaces decorated with 0.39 ng/mm^2 of aluminum perchlorate does change upon equilibration of the LC film on the salt-coated surface for several hours. In particular, the homeotropic ordering of the LC observed on freshly prepared samples was observed to relax during equilibration to a tilted or planar orientation. Because past studies have established that homeotropic ordering of nematic phases of 5CB on metal salt-coated surfaces can be induced by coordination interactions between the nitrile groups of 5CB and metal salts with high electron affinity,[12, 28] these results suggested to us that coordination interactions between 5CB and Al^{3+} on the surface are lost after a few hours of equilibration of the LC on the surface. This proposition was supported by the absence of the measurable response of the LC to DMMP after 7 hours of equilibration of the LC with the surface (as reported in prior studies,[12] the response to DMMP is caused by a change in the coordination state of the LC on the surface). It occurred to us that several possible interfacial processes may underlie the apparent loss of the

coordination interaction between the LC and surface. We considered it possible, for example, that water from the air may accumulate at the salt-decorated interface of the LC over time, thus leading to a loss of coordination between the nitrile groups of the LC and Al^{3+}. We consider this primarily because of the hygroscopic nature of the metal salts at the interface, and the fact that the presence of water at the interface can factor into the coordination properties of the aluminum ion. However, since the samples were exposed to constant values of R.H. of 30%, the effects of water were minimized. Alternatively, we considered that metal salts deposited at the surface may dissolve into the LC during equilibration of the LC on the surface, resulting in an insufficient, residual, surface density of metal salt at the surface to coordinate to the LC and thus promote homeotropic ordering of the LC.

To test the proposition that the loss of homeotropic ordering of the LC upon equilibration with the metal salt-decorated surface was due to dissolution of the metal salt from the surface into the LC, we equilibrated excess solid, aluminum perchlorate salt with nematic 5CB and measured the concentration of salt that dissolved into the LC as a function of time (see Materials and Methods for experimental details). Figure 3.4 shows the concentration of Al^{3+} dissolved into nematic 5CB as a function of time. Inspection of Figure 3.4 reveals that nematic 5CB slowly dissolves the aluminum perchlorate salt over a period of almost 15 days, finally reaching a saturation concentration of 1.7 μmol/mL. For comparison, the dashed horizontal line (marked as (i)) indicates the concentration of Al^{3+} that would be present in the LC film if all the metal salt on a surface presenting 0.39 ng/mm^2 of aluminum perchlorate dissolved into a 20 micrometer-thick film of 5CB. The result in Figure 3.4 demonstrates that the capacity of the LC film to dissolve the salt does exceed the amount of salt deposited onto the

surface (0.39 ng/mm^2). This result supports our hypothesis that the loss of homeotropic ordering during equilibration of the LC on the surface decorated with 0.39 ng/mm^2 of aluminum perchlorate salt was due to dissolution of the salt into the LC film. We note that the area of contact between the salt crystals and LC is substantially different for the systems leading to the results in Figures 3.3 and 3.4, and thus the slow dynamics evident in Figure 3.4 (days) should not be viewed as inconsistent with the proposition that the phenomena seen in Figure 3.3 (hours) is due to dissolution of salt into the LC. The proposal that dissolution of salt into the LC plays a central role in the time-dependent phenomena observed in these systems is further supported by results shown below based on surfaces that present loadings of aluminum perchlorate that exceed the solubility limit of the 20 μm-thick 5CB films.

Motivated by the evidence reported above that the loss of the homeotropic ordering of the LC film reported in Figure 3.2 and 3.3 was due to dissolution of the metal salt into the LC, next we sought to determine if a surface density of metal salt that exceeded the solubilization capacity of the LC film would maintain the homeotropic ordering of the LC during equilibration of the LC film on the surface. To this end, we characterized the time-dependent ordering of nematic films of 5CB on surfaces onto which aluminum perchlorate was deposited by spin coating of ethanolic solutions of 10 mM of the salt. As reported in Table 3.1, these surfaces were determined to present densities of the salt that corresponded to 2.14±0.24 ng/mm^2. Inspection of Figure 3.4 confirms that this surface mass density of aluminum perchlorate is sufficiently high that it can not be dissolved by the ~20 μm-thick LC film. Immediately following the preparation of LC films supported on surfaces presenting 2.14 ng/mm^2 of aluminum perchlorate, we observed the LC films to (i) exhibit homeotropic ordering prior to exposure to

DMMP, and (ii) exhibit an ordering transition upon exposure to DMMP that was comparable to that shown in Figure 3.2. These observations are reflected in the measured intensities of light transmitted through the supported LC film, as shown in Figure 3.5 (data at t = 0). Inspection of Figure 3.5 also reveals that the initial homeotropic ordering of the LC (observed prior to exposure to DMMP) was preserved during 4 days of equilibration of the LC on the surface. This contrasts to the results obtained with the low surface mass density of metal salt (Figure 3.2), where the initial homeotropic ordering of the LC was lost within 7 hours of equilibration of the LC on the metal salt-decorated surface. When combined, these two results support our hypothesis that dissolution of metal salt into the LC occurs during equilibration of the LC films on the metal salt-decorated surfaces. For the surfaces decorated with the low loading of salt, the dissolution of the metal salt results in the loss of coordination interactions and homeotropic ordering of the LC; for the surfaces presenting high loadings of the metal salt, the LC is saturated with salt prior to complete loss of the metal salt from the surface, and thus the homeotropic ordering is preserved during equilibration of the sample.

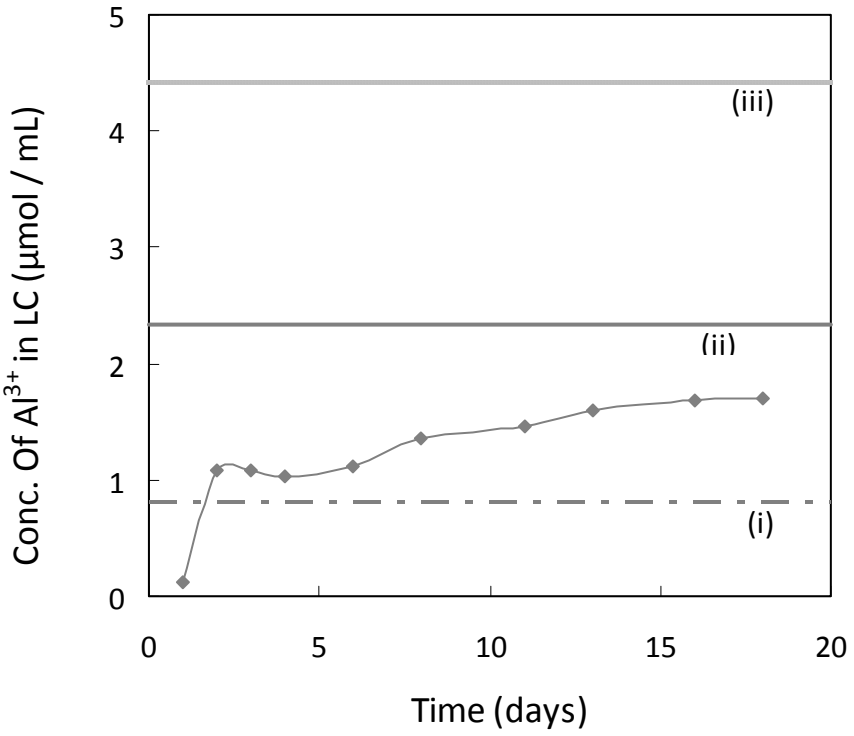

Figure 3.4. The concentration of Al^{3+} dissolved in 5CB as a function of time of contact of the LC with excess Al perchlorate salt as measured by ICP-ES. The horizontal lines indicate the concentration of Al^{3+} that would be present in a 20 µm-thick film of LC if all metal salt on the surface dissolved into the LC; (i) 0.39 ng/mm^2 Al perchlorate (ii) 1.13 ng/mm^2 Al perchlorate (iii) 2.14 ng/mm^2 Al perchlorate.

Although the LC film supported on the high surface loading of aluminum perchlorate exhibited homeotropic ordering over 4 days of equilibration, the results in Figure 3.5 also reveal that the response of the LC film to exposure to DMMP declined during this period of equilibration. The decrease in the intensity of light transmitted through the LC upon exposure to DMMP indicates that the extent to which the LC tilted away from the homeotropic orientation upon exposure to DMMP decreased with equilibration. After approximately 4 days of equilibration of the LC on the surface presenting 2.14±0.24 ng/mm^2 of salt, the LC maintained its homeotropic ordering upon exposure to DMMP (a small change only in the

intensity of light transmitted through the sample upon exposure to DMMP is evident in Figure 3.5). We note here that the absolute intensities of light measured to be transmitted through the samples varied from sample to sample (e.g., homeotropic alignment corresponds to ~20 A.U. in Figure 3.3 and ~ 50 A.U. in Figure 3.5). We note however that the change in intensity upon exposure to DMMP was ~ 100 A.U., independent of the sample. We attribute this variation in absolute intensity to differences in the filling of the TEM grids with LC (see Figure 3.8 of Supporting Information).

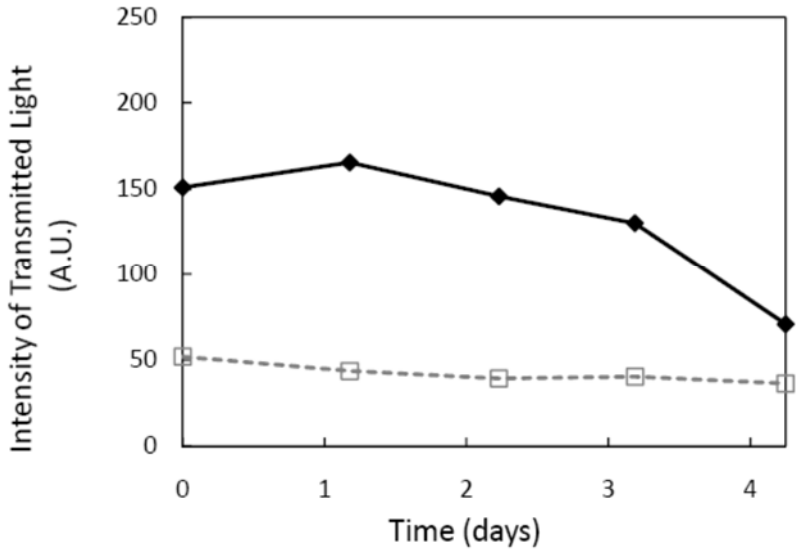

Figure 3.5. Quantification of the optical response of a film of nematic 5CB supported on a surface decorated with 2.14 ng/mm^2 Al perchlorate. The solid data points indicate the response of the LC to exposure to 5 ppm DMMP; the open data points show the optical response of the LC prior to exposure to DMMP.

As noted above, homeotropic ordering of the LC was observed during equilibration of the LC on surfaces decorated with a high loading of metal salts. The absence of a response to DMMP on those surfaces after several days of equilibration, however, suggests that intermolecular interactions between the LCs and surfaces that do not involve coordination of

the metal salts and the LC become dominant at the interface over time, thus maintaining the homeotropic orientation of the LC even when ligand exchange (change in coordination) at the interface is induced by the DMMP. Past studies have established that dissociation of sodium cations from surfaces presenting monolayers of carboxylate salts can lead to the formation of electrical double layers in nematic phases of 5CB.[10] We note that the static dielectric constants of a nematic phase of 5CB are 6 ($\varepsilon_{\perp}$) and 18 ($\varepsilon_{\parallel}$), and thus nematic 5CB can be viewed as relatively polar but anisotropic oil.[37-38] When an electrical double layer is formed at the interface of the LC, the electric field associated with the diffuse part of the double layer can exert a torque on the LC that promotes homeotropic ordering of the LC (for the case of 5CB with a positive dielectric anisotropy, $\varepsilon_{\parallel} > \varepsilon_{\perp}$). We hypothesized that the absence of an ordering transition in the LC film upon exposure to DMMP, as described above, may result from the formation of an electrical double layer at the metal-salt decorated interface as the aluminum perchlorate dissolves into the LC. It is also significant to note that a past study has demonstrated that the influence of electrical double layers on surface-induced orientational ordering of 5CB is most pronounced when high concentrations of salts are present in the LC (because the LC responds to the strength of the electric field associated with the double layer).[10] To test the hypothesis that an electrical double layer can induce homeotropic ordering of nematic 5CB at a surface decorated with a metal perchlorate salt, we formed 20 μm-thick films of 5CB on surfaces decorated with varying surface concentrations of sodium perchlorate. Sodium perchlorate was selected because previous studies using IR techniques have demonstrated that sodium perchlorate salts do not coordinate with the nitrile group of 5CB.[12] We spin-coated sodium perchlorate (10 mM in ethanol) onto a surface and observed the

presence of the salt to induce homeotropic ordering of nematic 5CB, consistent with the proposed formation of an electrical double layer. We note that when the concentration of sodium perchlorate was lowered to 1 mM in ethanol, the nematic films of 5CB adopted a planar orientation, suggesting that at low surface loading of metal perchlorate salt any electrical double layer formed at this interface to 5CB is insufficient to influence the ordering of the LC.

The results described above identify two physicochemical phenomena that lead to time-dependent interfacial ordering of films of nematic 5CB supported on aluminum perchlorate-decorated surfaces. Equilibration of nematic 5CB on surfaces presenting low surface densities of the salt results in extraction of the Al^{3+} from the surface into the LC, thus resulting in loss of the initial homeotropic alignment due to loss of coordination interactions between the 5CB and Al^{3+} on the surface. At high surface densities, dissolution of metal salt into the LC leads to an electrical double layer that promotes the homeotropic alignment, and thus masks any ordering transition that would otherwise result from adsorbate-induced disruption of metal ion-nitrile coordination interactions. We next investigated if these two interfacial phenomena could be avoided by using intermediate surface mass densities of aluminum perchlorate. To this end, as described below, we investigated the ordering of nematic 5CB on surfaces presenting 1.13±0.09 ng/mm^2 of aluminum perchlorate (Table 3.1).

As shown in Figure 3.6, the initial intensity of light transmitted through a film of nematic 5CB supported on a surface presenting 1.13 ng/mm^2 of the aluminum perchlorate was determined to correspond to homeotropic ordering. Following exposure to DMMP, an ordering transition was observed, as indicated in Figure 3.6 by the increase in intensity of light to ~180 A.U. Significantly, and in contrast to the previously described samples, we observed the

homeotropic ordering of the LC in the absence of DMMP to be maintained during equilibration of the LC on the salt-decorated surface for at least 4 days, *and we also measured exposure of the sample to DMMP at any point of time during this interval to result in an ordering transition in the LC*. This result is significant because it indicates that intermediate surface loadings of the aluminum perchlorate salts (i) orient LCs over prolonged periods through coordination interactions but (ii) do not lead to formation of electrical double layers that suppress the response of the LCs to DMMP. We comment that this result is also interesting in light of Figure 3.4, which suggests that the 20 μm-thick LC films do possess the capacity to extract all aluminum salts from surfaces coated with 1.13 ng/mm^2 of the salt. We speculate that interactions between the Al^{3+} ions and the carboxylate-terminated monolayer beneath the aluminum perchlorate may maintain a necessary threshold surface concentration of Al^{3+} to orient the LC through coordination interactions. We also note that in comparison to the surfaces decorated with 0.39 ng/mm^2 of the aluminum perchlorate salt, the driving force for extraction of the salts from the surface into the LC film is lower for the surfaces decorated with 1.13 ng/mm^2 of the salt (due to the higher concentration of salt in the LC). Our results also indicate that the metal salts that dissolve into the LC from surfaces with 0.39 ng/mm^2 $Al(ClO_4)_3$ do not lead to electrical double layers with electric fields that are sufficient in intensity to promote the homeotropic ordering of the LC in the absence of coordination interactions.

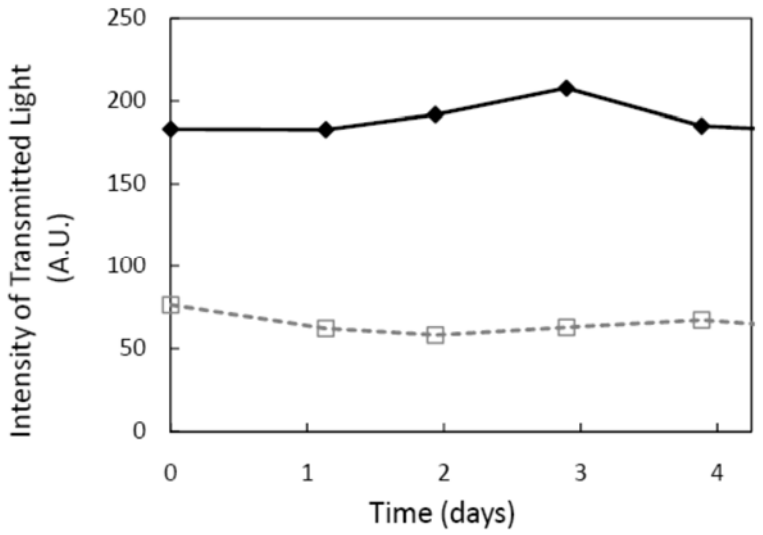

Figure 3.6. Quantification of the optical response of a film of nematic 5CB supported on a surface decorated with 1.13 ng/mm^2 Al perchlorate. The solid data points indicate the response of the LC to exposure to 5ppm DMMP; the open data points show the optical response of the LC prior to exposure to DMMP.

To provide additional insight into the above physical picture, we pre-saturated 5CB with aluminum perchlorate prior to formation of a film of the 5CB on a surface decorated with 0.39 ng/mm^2 of the salt (lowest loading of salt used in our study). Whereas surfaces with this density of aluminum perchlorate did not cause homeotropic ordering of pure 5CB for more than a few hours in the absence of DMMP (see Figure 3.3), when the 5CB pre-equilibrated with metal salt was placed onto the same type of surface, homeotropic ordering was observed to be preserved 20-30 days of equilibration (see Figure 3.9 of Supporting Information). In these cases, however, DMMP did not trigger an ordering transition in the LC (Figure 3.10 of Supporting Information), a result that is consistent with our proposal that electrical double layers formed by dissolution of high concentrations of aluminum perchlorate salt can prevent ordering transitions induced by surface-based ligand exchange reactions involving the LC.

3.4 Conclusions

The study reported in this paper provides two important insights into physicochemical processes that occur at interfaces of films of LCs that are decorated with metal salts. The first insight is that the capacity of the nematic LC films to dissolve metal salts can be sufficiently high so as to deplete the interfaces of the LC of coordinating metal ions. This process of dissolution can lead to ordering transitions in the LC by virtue of the loss of these sites of coordination from surfaces. This phenomenon is encountered with surfaces that are decorated with aluminum perchlorate densities of ~0.39 ng/mm^2, and it is characterized by loss of homeotropic ordering of the nematic 5CB within a few hours of equilibration of the LC with the metal salt-decorated surface. The second insight is that electrical double layers can form at the metal salt-decorated interfaces and that these electrical double layers can lead to interactions with the LC that can compete with the effects of metal ion-nitrile coordination interactions on the LC. In particular, if the concentration of metal salt in the LC is high (> 2.14±0.24 ng/mm^2), the electrical double layers can suppress ordering transitions in the LC induced by adsorbates such as DMMP (i.e., changes in surface coordination of the LC). In addition to identifying the roles of these fundamental physicochemical phenomena, we also established that experimental conditions exist where neither the effects of dissolution of the salts into the LC nor formation of an electrical double layer (i) perturb the homeotropic orientation in the absence of DMMP or (ii) diminish the response of the LC to DMMP during experiments conducted over 4 days. Indeed, for surfaces presenting 1.13 ng/mm^2 of $Al(ClO_4)_3$, we observed some samples to respond to DMMP for ~4 weeks following sample preparation. Over these periods of time, however, we

observed increased variability in our measurements, likely due to processes other than formation of electrical double layers or dissolution of metal salts taking place in these systems. In future studies, we will seek to identify these processes. In summary, the results presented in this paper provide importance guidance for the design of interfaces of LC for use in chemical sensing.

3.5 Acknowledgement

The Authors thank Mr. John Cannon for technical assistance. The study was funded by the Army Research Office through grants W911NF-07-1-0446 and W911NF-06-1-0314 as well as by the National Science Foundation through grants DMR-0520527 and DMR-0602570.

3.6 Supporting Information

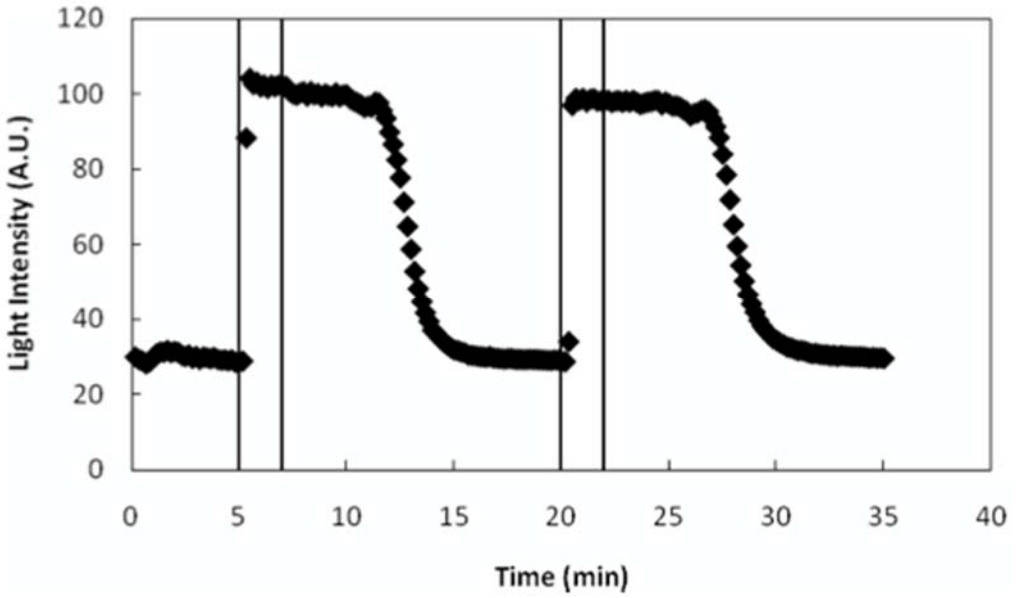

Figure 3.7. Optical response of 5CB supported on surfaces decorated with 0.39 ng/mm^2 Al perchlorate. In this example, the humidity is constant (30%) throughout the entire flow regime. The sample was exposed to air from 0 min to 5 min; from 5 min to 7 min, the sample was exposed to 5 ppm DMMP; from 7 min to 20 min, the sample was exposed to air; from 20 min to 22 min, the sample was exposed to 5 ppm DMMP; and for times over 22 min the sample was exposed to air.

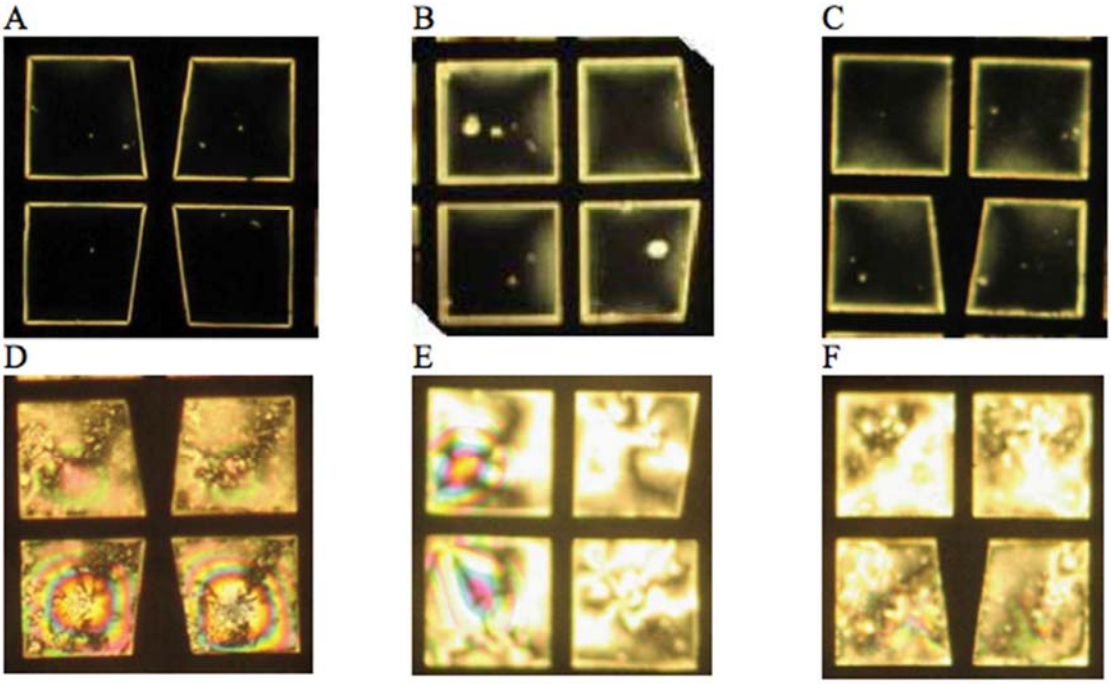

Figure 3.8. Optical micrographs (crossed polars) of three films of 5CB contacted with Al perchlorate salt of varying metal salt loadings. The micrograph images a film of 5CB contacted with (A) 0.39 ng/mm^2 Al perchlorate in air, (B) 1.13 ng/mm^2 Al perchlorate in air, and (C) 2.14 ng/mm^2 Al perchlorate in air. Likewise, the micrographs represents a film of 5CB contacted with (D) 0.39 ng/mm^2 Al perchlorate in 5 ppm DMMP, (E) 1.13 ng/mm^2 Al perchlorate in 5 ppm DMMP, and (F) 2.14 ng/mm^2 Al perchlorate in 5 ppm DMMP.

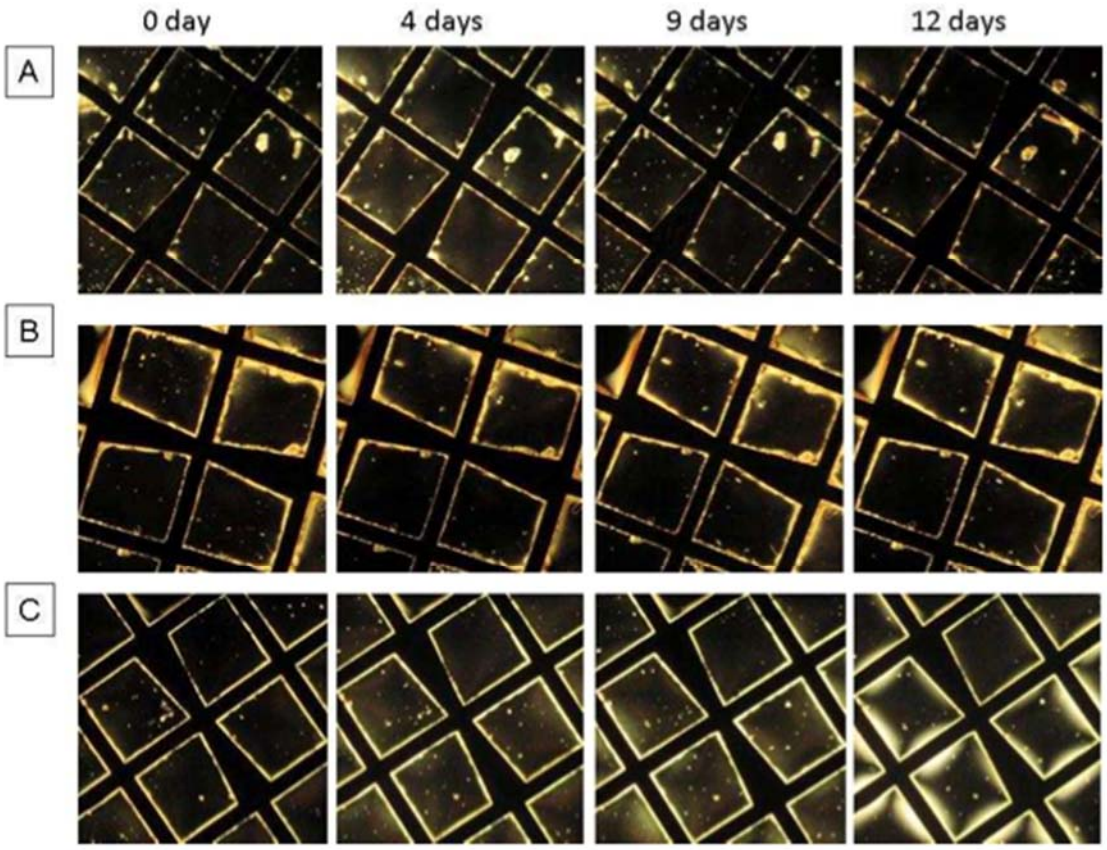

Figure 3.9. Optical images (crossed polars) of TEM grids impregnated with 5CB, presaturated with aluminum perchlorate salt, as a function of time (days) supported on surfaces decorated with (A) 0.39 (B) 0.62 (C) 1.13 ng/mm^2 of aluminum perchlorate salts.

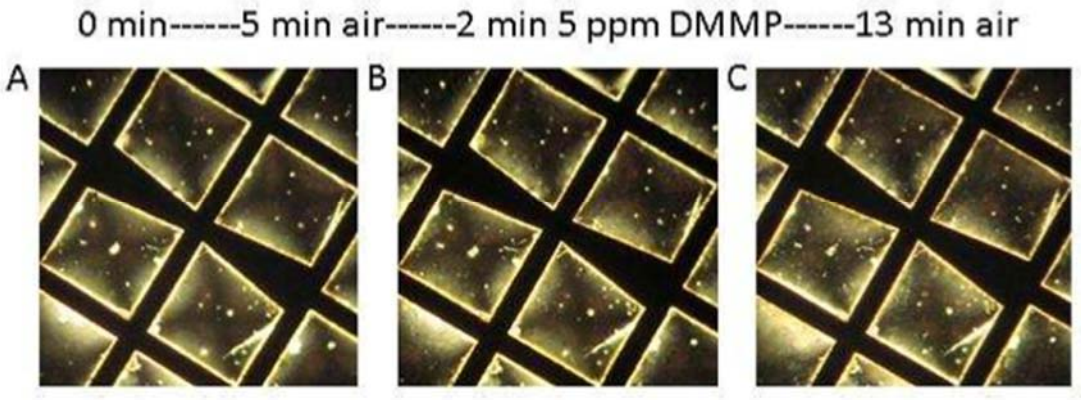

Figure 3.10. Optical images (crossed polars) of TEM grids impregnated with 5CB, presaturated with aluminum perchlorate salts, supported on surfaces decorated with 1.13 ng /mm^2 aluminum perchlorate salts (A) before (B) after exposure to 5 ppm DMMP for 2 min (C) After passing air for 13 min. Similar results were obtained when LC films were supported on surfaces presenting 0.39 and 0.62 ng/mm^2 aluminum perchlorate.

3.7 References

1. Collings, P. J. *Liquid Crystals: Nature's Delicate Phase of Matter*. Princeton University Press: Princeton, NJ, **1990**.
2. Jerome, B. *Reports on Progress in Physics* **1991,** *54*, 391-451.
3. Woltman, S. J.; Jay, G. D.; Crawford, G. P. *Nat. Mater.* **2007,** *6*, 929-938.
4. Barberi, R.; Durand, G. *Phys. Rev. A* **1990,** *41*, 2207.
5. Barbero, G.; Durand, G. *J. Phys. II France* **1991,** *1*, 651-658.
6. Lu, X.; Lu, Q.; Zhu, Z. *Liq. Cryst.* **2003,** *30*, 985-990.
7. Ondris-Crawford, R. J.; Crawford, G. P.; Doane, J. W.; Zumer, S.; Vilfan, M.; Vilfan, I. *Phys. Rev. E* **1993,** *48*, 1998.
8. Shah, R. R.; Abbott, N. L. *Science* **2001,** *293*, 1296-1299.
9. Shah, R. R.; Abbott, N. L. *J. Am. Chem. Soc.* **1999,** *121*, 11300-11310.
10. Shah, R. R.; Abbott, N. L. *J. Phys. Chem. B* **2001,** *105*, 4936-4950.
11. Cadwell, K. D.; Alf, M. E.; Abbott, N. L. *The Journal of Physical Chemistry B* **2006,** *110*, 26081-26088.
12. Yang, K. L.; Cadwell, K.; Abbott, N. L. *J. Phys. Chem. B* **2004,** *108*, 20180-20186.
13. Brake, J. M.; Daschner, M. K.; Luk, Y. Y.; Abbott, N. L. *Science* **2003,** *302*, 2094-2097.
14. Lockwood, N. A.; Gupta, J. K.; Abbott, N. L. *Surf. Sci. Rep.* **2008,** *63*, 255-293.
15. Pal, S. K.; Agarwal, A.; Abbott, N. L. *Small* **2009,** *5*, 2589-2596.
16. Price, A. D.; Schwartz, D. K. *J. Am. Chem. Soc.* **2008,** *130*, 8188-8194.
17. Luk, Y. Y.; Yang, K. L.; Cadwell, K.; Abbott, N. L. *Surf. Sci.* **2004,** *570*, 43-56.

18. Yang, K. L.; Cadwell, K.; Abbott, N. L. *Adv. Mater. (Weinheim, Ger.)* **2003,** *15*, 1819-1823.

19. Shah, R. R.; Abbott, N. L. *Langmuir* **2003,** *19*, 275-284.

20. Bi, X. Y.; Hartono, D.; Yang, K. L. *Advanced Functional Materials* **2009,** *19*, 3760-3765.

21. Bi, X. Y.; Lai, S. L.; Yang, K. L. *Analytical Chemistry* **2009,** *81*, 5503-5509.

22. Hartono, D.; Lai, S. L.; Yang, K. L.; Yung, L. Y. L. *Biosens. Bioelectron.* **2009,** *24*, 2289-2293.

23. Hoogboom, J.; Clerx, J.; Otten, M. B. J.; Rowan, A. E.; Rasing, T.; Nolte, R. J. M. *Chem. Commun.* **2003**, 2856-2857.

24. Hoogboom, J.; Velonia, K.; Rasing, T.; Rowan, A. E.; Nolte, R. J. M. *Chem. Commun.* **2006**, 434-435.

25. Lai, S. L.; Hartono, D.; Yang, K. L. *Appl. Phys. Lett.* **2009,** *95*, 3.

26. Sridharamurthy, S. S.; Cadwell, K. D.; Abbott, N. L.; Jiang, H. *Smart Mater. Struct.* **2008,** *17*, 4.

27. Yang, K. L.; Cadwell, K.; Abbott, N. L. *Sens. Actuator B-Chem.* **2005,** *104*, 50-56.

28. Cadwell, K. D.; Lockwood, N. A.; Nellis, B. A.; Alf, M. E.; Willis, C. R.; Abbott, N. L. *Sensors and Actuators B: Chemical* **2007,** *128*, 91-98.

29. Gupta, J. K.; Meli, M.-V.; Teren, S.; Abbott, N. L. *Phys. Rev. Lett.* **2008,** *100*, 048301.

30. Petrov, M.; Tsonev, L. *Liq. Cryst.* **2002,** *29*, 743-754.

31. Daming, C.; Sridharamurthy, S. S.; Hunter, J. T.; Joon-Seo, P.; Abbott, N. L.; Hongrui, J. *Journal of Microelectromechanical Systems,* **2009,** *18*, 973-982.

32. Skaife, J. J.; Abbott, N. L. *Chem. Mater.* **1999,** *11*, 612-623.

33. Allara, D. L.; Nuzzo, R. G. *Langmuir* **1985,** *1*, 45-52.

34. Patnaik, P. *Handbook of Inorganic Chemicals*. McGraw-Hill: New York, **2003**.

35. Washburn, E. W., Ed. *International Critical Tables of Numerical Data, Physics, Chemistry and Technology (1st Electronic Edition)*. Knovel: Norwich, NY, **2003**; Vol. 2006.

36. Nazarenko, V.; Nych, A. *Phys. Rev. E* **1999,** *60*, R3495-R3497.

37. Bogi, A.; Faetti, S. *Liq. Cryst.* **2001,** *28*, 729-739.

38. Wiederrecht, G. P.; Svec, W. A.; Wasielewski, M. R. *J. Am. Chem. Soc.* **1997,** *119*, 6199-6200.

Chapter 4: Dynamics of the Chemo-Optical Response of Supported Films of Nematic Liquid Crystals.

4.1 Introduction

The development of new materials and processes for the sensing of targeted chemical compounds in the vapor phase has the potential to be broadly useful in a range of contexts, including homeland security (toxic industrial chemicals),[1-2] occupational health (e.g., exposure or farm workers or children to organophosphonates)[3] or medicine (e.g., analysis of ketones in the breath of a diabetic).[4] While substantial effort has been invested in development of new principles for chemical sensing over the past several decades, there remains an unmet need for simple and compact sensors for use in contexts such as point-of-care diagnostics, passive devices (e.g., badges) or autonomous vehicles. In many of these situations, the relevant concentrations of the species in the gas phase are in the parts-per-million (ppm) or parts-per-billion (ppb) range. For example, sarin (GB) is an organophosphonate nerve agent that is lethal to 50% of an exposed population at a dose of 12.2- 16.2 ppm·min (exposure via inhalation).[5]

Several recent studies have reported that micrometer thick films of liquid crystals (LCs) can provide the basis of passive, chemo-responsive material systems that respond to vapor analytes with sensitivities in the ppm to ppb range.[6-13] Specifically, it has been shown that LCs comprised of mesogens such as 4-cyano-4'-pentylbiphenyl (5CB) will form coordination complexes (via the nitrile group of the mesogen) at metal salt-decorated surfaces when the cation of the metal salt possesses a sufficiently high electron affinity.[12, 14-22] The formation of

the coordination complexes, which has been confirmed by examining the vibration spectra of the nitrile group using infrared (IR) spectroscopy, leads to the anchoring of the LC film in an orientation that is perpendicular to the surface. In the presence of targeted phosphonate containing molecules, such as dimethyl methylphosphonate (DMMP), competitive binding of the phosphoryl (P=O) group of the target molecules for the metal ions has shown to displace the nitrile group of the mesogen from the coordination complex at the metal salt-decorated surface, thus triggering an orientational ordering transition within the LC film. Because the LC films are optically and electrically anisotropic,[23-24] the ordering transitions are readily transduced by using a range of optical and electrical (e.g., capacitance-based) methods.[25-27] In contrast to past investigations, which have focused on the identification of the interfacial interactions responsible for the ordering of the LC films,[6, 8, 14-15] elucidation of the rate-limiting physical processes that dictate the *dynamics* of the LC ordering transitions has not been reported. The study reported in this paper was performed to address this gap in knowledge, and thereby provide guidance to the design of LC as chemo-optical materials for use in chemical sensors.

In this paper, we report experimental measurements of the time-dependent response of LC films supported on chemically functionalized surfaces. The measurements were performed under carefully controlled conditions that allowed us to quantify the effects of key experimental parameters on the dynamics of the LC ordering transitions (e.g., linear velocity of the gas over the LC film and concentration of DMMP in the gas). These measurements of the dynamics of the response of the LC films are compared to simple models that describe key rate processes that occur during ordering transitions involving supported LC films. A focus is

directed to the role of mass transport, including diffusion of the DMMP from the vapor phase to the metal-salt decorated interface of the solid and the LC. The remainder of this paper is divided into two main sections: (i) characterization and analysis of the response of LC films to exposure to a vapor containing DMMP, and (ii) characterization and analysis of the relaxation of LC films when, subsequent to exposure to the DMMP, a stream of gas free of DMMP is passed across the LC films. In addition to identifying the processes that dictate the dynamics of the response of the LC films, our analysis also reveals information regarding the limits of sensitivity of the LC films to DMMP.

4.2 Experimental Methods

4.2.1 Materials

11-Mercaptoundecanoic acid (MUA) and Al^{3+} perchlorate nonahydrate salts were purchased from Sigma Aldrich (Milwaukee, WI). 5CB was purchased from EMD Chemicals (Gibbstown, NJ). Titanium (99.999%) and gold (99.999%) were purchased from Advanced Materials (Spring Valley, NY). Methanol and Fischer's Finest glass slides were purchased from Fischer Scientific (Pittsburgh, PA). Absolute ethanol (anhydrous, 200 proof) was purchased from Pharmco-AAPER (Brookfield, CT). All chemicals and solvents were of analytical reagent grade and were used as received without any further purification. All deionized water used in the study possessed a resistivity of at least 18.2 MΩ cm.

4.2.2 Methods

4.2.2A Cleaning of Glass Substrates.

Glass microscope slides were cleaned according to published procedures using acidic "piranha" solution [70:30 (% v/v) H_2SO_4:H_2O_2 (30%)] [19]. Briefly, the glass slides were immersed in an acidic piranha bath at 60-80 °C for at least 1 h, and then rinsed in running deionized water for 2-3 min. The slides were then immersed in basic piranha [70:30 (% v/v) KOH: H_2O_2] and heated to between 60 and 80 °C for at least 1 h. Finally, the slides were rinsed sequentially in deionized water, ethanol, and methanol, and then dried under a stream of nitrogen. The clean slides were stored in an oven at 110 °C. All other glassware was rinsed with distilled water and ethanol and dried under a gaseous stream of nitrogen.

4.2.2B Deposition of thin layers of gold.

Semi-transparent films of gold with thicknesses of 200 Å were deposited onto piranha-cleaned glass slides (see above) mounted on a fixed holder within an electron beam evaporator (VEC-3000-C manufactured by Tekvac Industries, Brentwood, NY). The angle of incidence of the gold was calculated to range from 0° to 15° on the slides (measured from surface normal). A layer of titanium (thickness 80 Å) was used to promote adhesion between the glass microscope slides and the films of gold. The rates of deposition of gold and titanium were 0.2 Å/s. The pressure in the evaporator was maintained at less than 3×10^{-6} Torr before and during each deposition. The gold source was periodically cleaned by sequential immersion in aqua regia (70% HNO_3, 30% HCl) and piranha solutions at 50 °C (30 min in each solution); see above for compositions. The cycle was repeated 3-4 times, rinsing the source between cycles in deionized water.

4.2.2C Preparation of functionalized gold surfaces.

Carboxylic-acid-terminated self-assembled monolayers (SAMs) of 11-mercaptoundecanoic acid (MUA) were formed on gold-coated glass slides by immersing the slides overnight in an ethanolic solution containing 2 mM of MUA. The gold films were then rinsed with an excess of ethanol and dried under a stream of nitrogen. Metal ions (Al^{3+}) were deposited immediately onto the carboxylic-acid-terminated SAMs by spin coating a 5 mM ethanolic solution of $Al(ClO_4)_3 \cdot 9H_2O$ at 3000 rpm for 60s (WS-400A-6NPP/Lite, Laurell Technologies, North Wales, PA).

4.2.2D Formation of Micrometer-Thick Films of LC.

After coating the surfaces with aluminum perchlorate salt, as described above, an 18 μm-thick gold-coated transmission electron microscopy (TEM) grid (Electron Microscopy Sciences, Hatfield, PA) was fastened to the salt-coated surface using a thin stainless steel plate (0.44 mm thickness). The stainless steel plate contained a 2-mm diameter hole that was aligned with the center of the TEM grid. The TEM grid defined square pores with lateral dimensions of 285 μm. The grid had an overall diameter of 3 mm. Both the TEM grid and stainless steel plate were dip-coated with a perfluorocarbon film (Nyebar Fluorocarbon Barrier Film, SmartGrease Company, Fairhaven, MA) to minimize wicking of the 5CB from the TEM grid. The grids were filled with LC using a microcapillary tube at room temperature, taking care to fill only the middle squares of the TEM grid, so as to avoid wicking of the 5CB between the TEM grid and steel plate.

4.2.2E Exposure to DMMP.

The sample, prepared as described above, was exposed to a stream of air containing DMMP within a flow cell that was constructed to direct the flow of air across the LC samples while permitting simultaneous observation of the samples through a polarized light microscope (CH40, Olympus, Melville, NY), as shown in Figure 4.1. The stream of air containing DMMP was generated using a cylinder containing a certified 10 ppm DMMP in nitrogen (Matheson Tri-Gas Inc, Eagan, MN) that was diluted by air at a specified relative humidity, RH. The RH of the air was controlled using a portable dew point generator (LI-610, LI-COR Biosciences, Lincoln, NE). The temperature of the gas fed to the flow cell was maintained at room temperature (25 ^{o}C) and the RH was controlled to 30%. The flow system was plumbed using 1/16'' stainless steel Swagelok tubing (Badger Fluid System Technologies Milwaukee, WI). The flow rate of the gas through the exposure system was controlled using a series of rotameters (Aalborg Instruments & Controls, Inc, Orangeburg, NY). The volumetric flow rate of the 10 ppm DMMP stream from the cylinder was controlled between 0 to 150 mL/min, while the volumetric flow rate of the diluent air stream was controlled between 0 to 1000 mL/min. The concentration of DMMP used in the study reported in this paper ranged from 0.5 ppm to 1.25 ppm, while the volumetric flow rate of the gas stream passed over the samples ranged from 100 mL/min to 1000 mL/min.

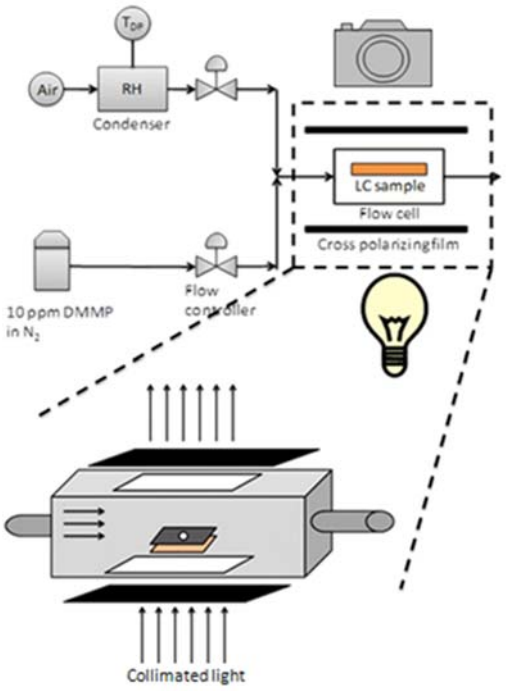

Figure 4.1. Schematic illustration of the flow cell used to expose a supported LC film to a gas stream at specified flow rate, concentration of DMMP, and relative humidity (RH). The sample was imaged using a polarized light microscope.

The time for the DMMP to travel from the gas cylinder to the flow cell was calculated from knowledge of the volumetric flow rate of the gas and the volume of the tubing in the flow system upstream of the sample. The length of the tubing running from the DMMP gas cylinder to the mixing point (where the stream was diluted with air, as needed) was approximately 120 cm, and after leaving the mixing point, the length of the tubing running to the flow cell was approximately 5 cm. When the volumetric flow rate of gas to the flow cell was 1000 mL/min, the time for DMMP to flow from the source cylinder (10 ppm) to the flow cell and mix with air to a concentration of 1 ppm was calculated to be 7 seconds.

The flow cell was fabricated by machining a rectangular prism of aluminum metal. Glass windows allowed transmission of polarized light through the flow cell. The intensity of light

that was transmitted through the LC sample in the flow cell was quantified using an Olympus camera (Olympus C2040Zoom, Melville, NY). The total volume of the flow cell was 10.5 cm^3 (6cm x 3.5cm x 0.5cm), giving rise to a residence time of ~0.6 sec when the flow rate was 1000 mL/min. The Reynolds number was calculated to be 51 for airflow within the flow cell at 1000 mL/min that is well below the turbulent regime.

4.3 Results

4.3.1 Qualitative Observations Regarding the Optical Response of Supported LC Film to DMMP.

We first describe the experimental set-up and the qualitative optical response of a supported LC film to DMMP. Prior to exposure to DMMP, the orientation of the LC at the Al perchlorate-coated surface was homeotropic. Because the orientation of the LC at the LC-vapor interface was also homeotropic, when viewed between crossed polars in transmission mode, the initial appearance of the LC film was dark (see Figure 2A, 0 s). Following the introduction of a gas stream containing 1 ppm DMMP into the head space above the LC film, the intensity of light transmitted through the LC increased as a function of increasing time of exposure (Figure 4.2A, 0-360 sec). The optical response of the LC shown in Figure 4.2A is consistent with past studies that have shown that DMMP causes nematic 5CB supported on Al perchlorate-coated surfaces to change to a planar alignment.[14, 20] Figure 4.2B shows a plot of the average intensity of light transmitted through the LC sample as the system was exposed to 1 ppm DMMP vapor. The normalized intensity of transmitted light increases from the initial intensity (normalized to a value of 0) to the maximum intensity (normalized to a value of 1)

over a period of approximately 200s. In the experiment shown in Figure 4.2, the flow of DMMP into the head space above the LC film was stopped at t=420 seconds, and replaced by a stream of air that was free of DMMP. Inspection of both Figure 4.2A and B reveals that, upon removal of the DMMP from the system, the intensity of the light transmitted through the sample returned to the initial value.

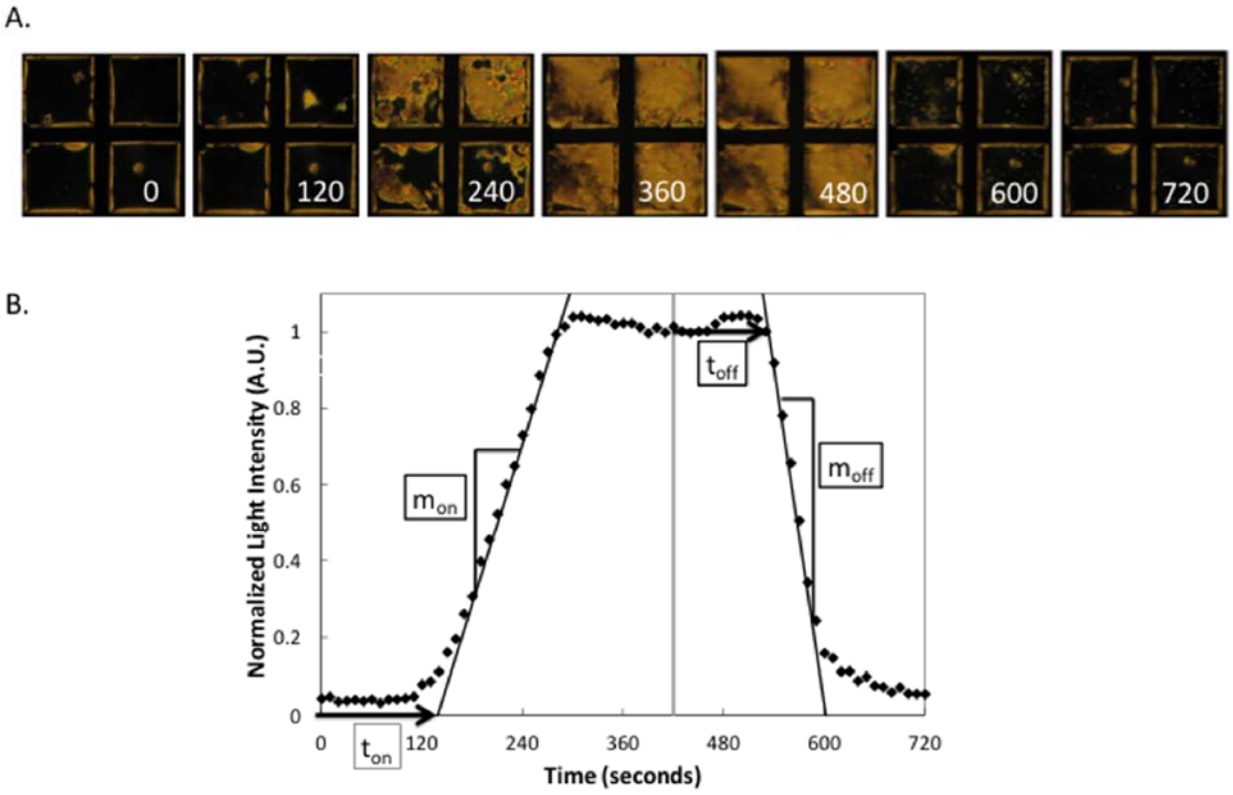

Figure 4.2. (A) Polarized light micrographs of representative LC film supported on an Al perchlorate-coated surface. The sample was exposed to a gas stream containing 1 ppm DMMP flowing at a rate of 1000 mL/min from 0 to 420 seconds. At 420 seconds, the gas stream containing DMMP was replaced by a gas stream free of DMMP flowing at a rate of 1000 mL/min. (B) The normalized light intensity of the sample shown in (A). A typical optical response of the LC film to DMMP was characterized by the four parameters shown in boxes in (B). The lateral dimension of each square in the micrographs is 285 µm.

In the sections below, we report on two key issues related to the initial response of the LC to DMMP and the way that we quantify the response to DMMP, as seen in Figure 4.2. First,

we investigated the factors that determine the time at which the initial change in the intensity of light transmitted through the LC was evident (t_{on}, see Figure 4.2B). Second, we report an investigation of the processes that control the rate of increase of the intensity of light transmitted through the LC following the onset of the response (m_{on}, also see Figure 4.2B). These factors were calculated by fitting the initial change in light intensity to a linear line and calculating the time at which the line crosses 0 light intensity (t_{on}) and the slope of the line (m_{on}). Similarly, with respect to the response of the system following cessation of exposure to DMMP, we sought to understand the factors that determine the time that elapses before the intensity of light transmitted through the LC film begins to decrease (t_{off}), and the subsequent rate of decrease in the intensity of transmitted light to the initial dark state (m_{off}). Both t_{off} and m_{off} are defined in Figure 2B and are calculated in a similar to the response rate by fitting the initial decrease in light intensity to a linear line and calculating the time in which the line cross a light intensity of 1 and the slope of the line.

4.3.2 Quantification of Initial Response of the LC Films to DMMP

This section of the paper seeks to provide insight into the factors that dictate the time between when flow of gas containing the DMMP over the LC was initiated and when the LC films exhibited a measurable optical response (i.e., t_{on} in Figure 4.2B). The factors that dictate the time of response are studied by varying (i) the flow rate of DMMP gas passing over the LC sample from 100 to 1000 mL/min and (ii) the concentration of DMMP within the vapor phase. In order to isolate the role of the vapor flow rate, the concentration of DMMP within the gas stream was held constant at 1 ppm for the studies shown in Figure 4.3a. Likewise, the role of

the concentration of DMMP on the time of response was studied at a constant flow rate of 1000 mL/min for the studies shown in Figure 4.3b. Inspection of the experimental results shown in Figure 4.3 (data points) reveals that the value of t_{on} decreases with increasing flow rate of gas over the surface of the LC film (Figure 4.3a); and also the value of t_{on} decreases with increasing concentrations of DMMP in the gas phase (Figure 4.3b). We seek to explain these results focused on the mass transport of DMMP from the vapor phase to the Al perchlorate decorated surface. Other factors can play a role in the time of response of the sample including the kinetics of the ligand exchange reaction at the solid interface and the time required for the LC film to change orientation at the interface. The approximations of the model are further explored in the Discussion section (Section IV).

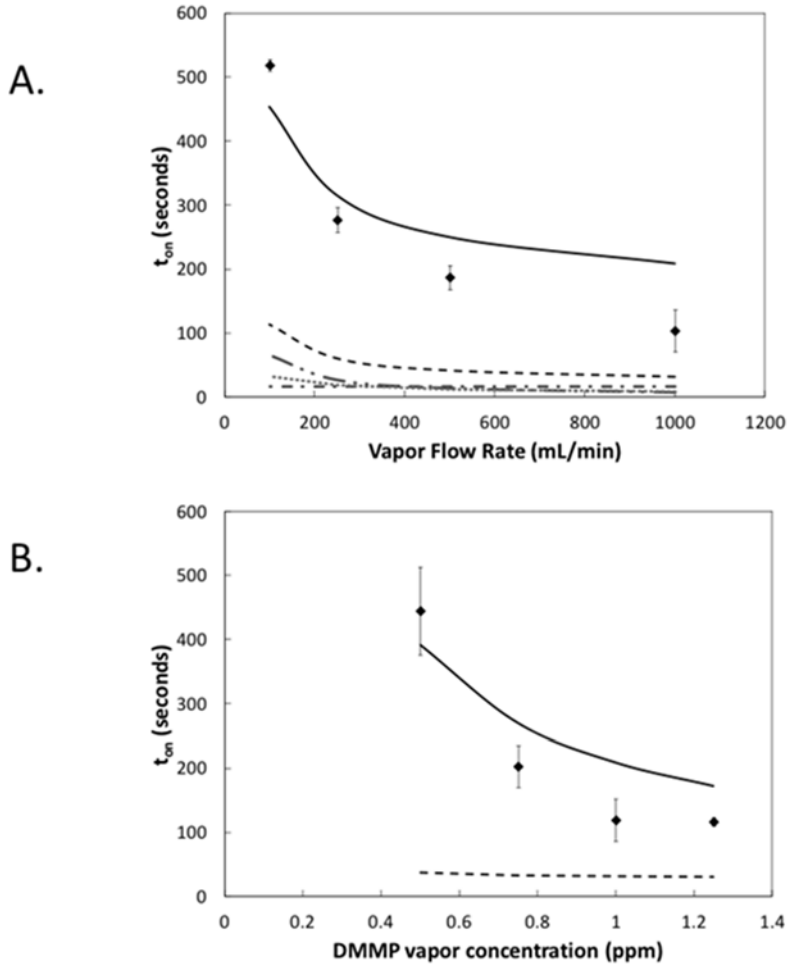

Figure 4.3. The experimental measurements of t_{on} as a function of the (A) gas flow rate and (B) the concentration of the DMMP concentration in the gas stream. In (A) a concentration of 1 ppm of DMMP was used for all samples, and in (B) the overall gas flow rate was 1000 mL/min. In A and B, the model predicted value of $t_{transport}$ is shown by the dashed black line, and the sum of t_{conc} and $t_{entrance}$ is shown by the solid black line.

We begin our analysis by testing the proposition that the decrease in t_{on} with increase in flow rate is related to mass transport of the DMMP from the vapor phase to the solid interface between the metal salt and LC. To this end, we developed a simple model to estimate the time required for the diffusion of DMMP from the vapor phase to the chemically functionalized surface based on the total diffusion length. The total diffusion length is calculated by the addition of two lengths (i) the diffusion length in the vapor phase based on the development of

a concentration boundary layer and (ii) the diffusion length in the LC phase based on the thickness of the LC film and is shown in Figure 4.4. In order to accomplish this task, past studies were consulted to model the boundary layers as detailed in the Supporting Information. The flow cell described above is used to create a defined, repeatable boundary layer in the vapor phase above the LC film that can be used in the models presented to calculate the diffusion length within the vapor phase.

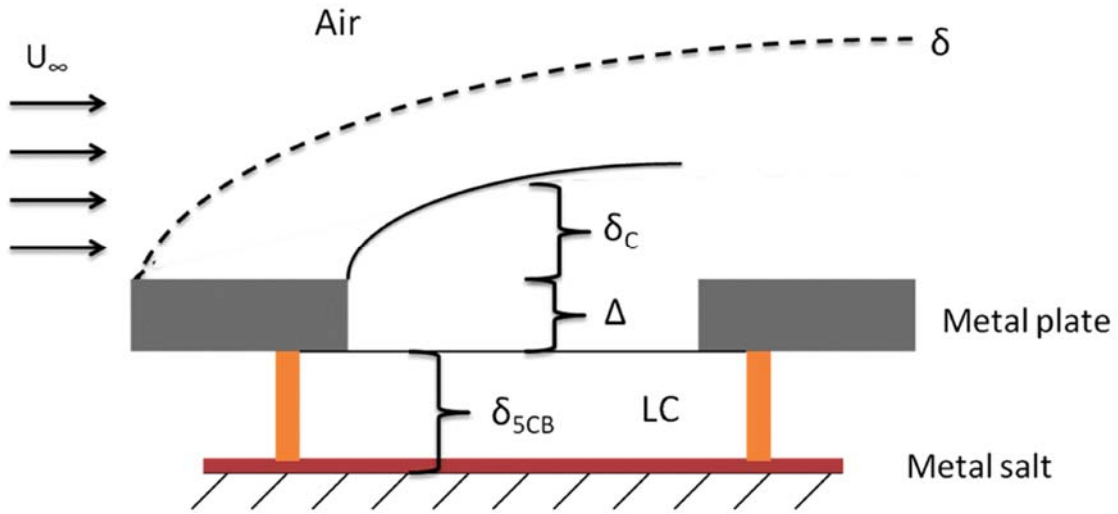

Figure 4.4. A schematic illustration of the boundary layer thicknesses (hydrodynamic and concentration) that determine mass transfer of DMMP to the metal-salt decorated surface that supports the film of LC. The hydrodynamic boundary layer thickness is indicated by δ and the concentration boundary layer by δ_C. See text for additional details.

The characteristic time required for diffusion of DMMP from the vapor phase to the solid interface between the LC and metal salt ($t_{transport}$) is estimated to be comprised of three contributions, namely

$$t_{transport} = t_{entrance} + \frac{\delta_V^2}{2 \cdot D_{Air}} + \frac{\delta_{5CB}^2}{2 \cdot D_{5CB}} \qquad (1)$$

where $t_{entrance}$ is the time required for the DMMP to pass through the volume of the tubing that connects the cylinder containing 10 ppm DMMP to the flow cell, and the second and third terms characterize the diffusion times for transport of DMMP across the concentration boundary layer on the gas side (δ_V) and LC side (δ_{5CB}) of the LC-gas interface, respectively. D_{Air} is the diffusion coefficient of DMMP in air (estimated to be 0.05 cm^2/s), and D_{5CB} is the diffusion coefficient of DMMP in the 5CB film (estimated to be 10^{-7} cm^2/s). A specific example of each of the components of Equation 1 is shown in the Supplemental Information.

Inspection of Figure 4.3 shows that, while the values calculated for $t_{transport}$ decrease with increases in the vapor flow rate (black dashed line), they are much smaller than the experimentally measured values of t_{on}. We also note that $t_{transport}$, as estimated by equation 1, is independent of the concentration of DMMP in the vapor phase. In contrast, we measured the experimental values of t_{on} to exhibit a significant decrease with increase in DMMP concentration (Figure 4.3B). Overall, the comparison of the experimental data provided in Figure 4.3 to the characteristic transport times calculated from equation 1 led us to conclude that t_{on} is not determined solely by the time taken for DMMP to diffuse from the bulk of the gas stream to the interface between the LC and metal salt.

In light of the result above, we next explored the alternative proposition that the underlying cause of t_{on} is the need for a threshold concentration of DMMP to accumulate within the LC film in order for mass-action to drive the ligand exchange reaction and thus the optical response of the LC film. In order to do this, we developed a simple model in order to describe the flux of DMMP to the LC and the subsequent accumulation of DMMP within the LC

film. We define this characteristic accumulation time as t_{conc}, and outline below a simple model for this physical situation.

Our model for t_{conc} is based on the evaluation of the flux of DMMP from the vapor phase into the LC film. To begin, the individual mass fluxes of DMMP through the air and LC film (diagrammed in Figure 4.5A) were calculated. The mass transfer coefficient for the vapor phase, k_G, was evaluated as

$$k_G = \frac{D_{Air}}{\delta_V} \qquad (2)$$

and used to calculate the flux of DMMP across the concentration boundary layer on the gas side (N_{Air}) based on k_G and the difference in the concentration across the boundary layer as

$$N_{Air} = k_G\left(C_{\infty,Air} - C_{i,Air}\right) \qquad (3)$$

where $C_{\infty,Air}$ is the concentration of DMMP in the vapor phase and $C_{i,Air}$ is the concentration of DMMP at the vapor side of the air-LC interface. Similarly, the mass transport coefficient for the LC side of the interface, k_L, was evaluated as

$$k_L = \frac{D_{5CB}}{\delta_{5CB}} \qquad (4)$$

and used to calculate the flux of DMMP across the LC side (N_{5CB}) of the interface as

$$N_{5CB} = k_L\left(C_{i,5CB} - C_{surf,5CB}\right) \qquad (5)$$

where $C_{i,5CB}$ is the concentration of DMMP in the 5CB at the air-LC interface and $C_{surf,5CB}$ is the DMMP concentration in the LC at the interface between the LC and Al perchlorate-coated surface. Because the time of diffusion is smaller than the experimental times that are observed as seen by the times associated with equation 1 underestimating the time of

response, we assume that there is an accumulation of DMMP within the 5CB film. In order to simplify this process, we assume that no concentration gradient of DMMP is formed within the 5CB film and that the concentration of the DMMP in the 5CB film is set as C_{5CB}. In the simple model calculation below, we assume that the kinetics of binding of DMMP by the Al perchlorate to be fast and irreversible.

Next, and as illustrated in Figure 4.5A, we equated the initial flux of DMMP on the air side of the LC interface to the initial flux of DMMP through the film of LC to the metal salt-coated surface, leading to

$$N = N_{Air} = N_{5CB} \qquad (6)$$

In order to solve equation 4.6 to obtain the overall flux (N) for specified values of $C_{\infty,Air}$, it is necessary to relate the concentration of DMMP on the vapor side ($C_{i,Air}$) and LC side ($C_{i,5CB}$) of the vapor-LC interface using the Henry's law coefficient, H, namely

$$C_{i,Air} = H \cdot C_{i,5CB} \qquad (7)$$

Although the value of H for the partitioning of DMMP from air into LC is not known, we note that previous studies have reported the value of H for DMMP at the air-water interface to be 5.3×10^{-5} and that Henry's law coefficients generally fall within the same order of magnitude for water and toluene.[28-29] Thus we initially used the Henry's law coefficient for partitioning of DMMP into nematic 5CB as 5.3×10^{-5} (additional results presented below provide support for this value). In order to calculate the overall flux using known variables, the air flux from equation 3 and the 5CB flux from equation 5 were equated and the interfacial concentrations were substituted using equation 7. From this relationship, the interfacial concentration is

calculated in terms of known variables, H, k_G, k_L, and the concentrations of DMMP in air and 5CB. The interfacial concentration is then substituted into Equation 5 and the overall flux of DMMP into the LC film, N, (due to equation 6) can be calculated as

$$N = \frac{\partial n_{DMMP}}{A \cdot \partial t} = \frac{1}{\frac{1}{k_G} + \frac{H}{k_L}} \cdot \left(C_{\infty,Air} - H \cdot C_{5CB}\right) = K_G \cdot \left(C_{\infty,Air} - \frac{H \cdot n_{DMMP}}{A \cdot \delta_{5CB}} \right) \quad (8)$$

where K_G is the overall mass transfer coefficient, n_{DMMP} is the number of moles of DMMP, A is the cross sectional area of the sample, δ_{5CB} is the thickness of the LC film, and C_{5CB} is the concentration of DMMP that accumulates within the LC film. For a LC sample that is 18 µm thick and a gas flow rate passing parallel to the sample at 1000 mL/min, the value of k_G is calculated as 0.3 cm/s from equation 2 and the value of k_L is calculated from equation 4 as 5.5×10^{-5} cm/s. By using the Henry's law coefficient described above, K_G is calculated from equation 8 as 0.24 cm/s. For this example, $1/k_G$ is equal to 3.2 s cm^{-1} while H/k_L is equal to 0.9 s cm^{-1}. This result indicates that the mass transfer process is rate-limited by the transfer process on the air side of the LC-air interface. This implies that the flow rate of the DMMP gas over the sample is a key parameter in the overall mass transfer processes, a result that is consistent with the data in Figure 4.3.

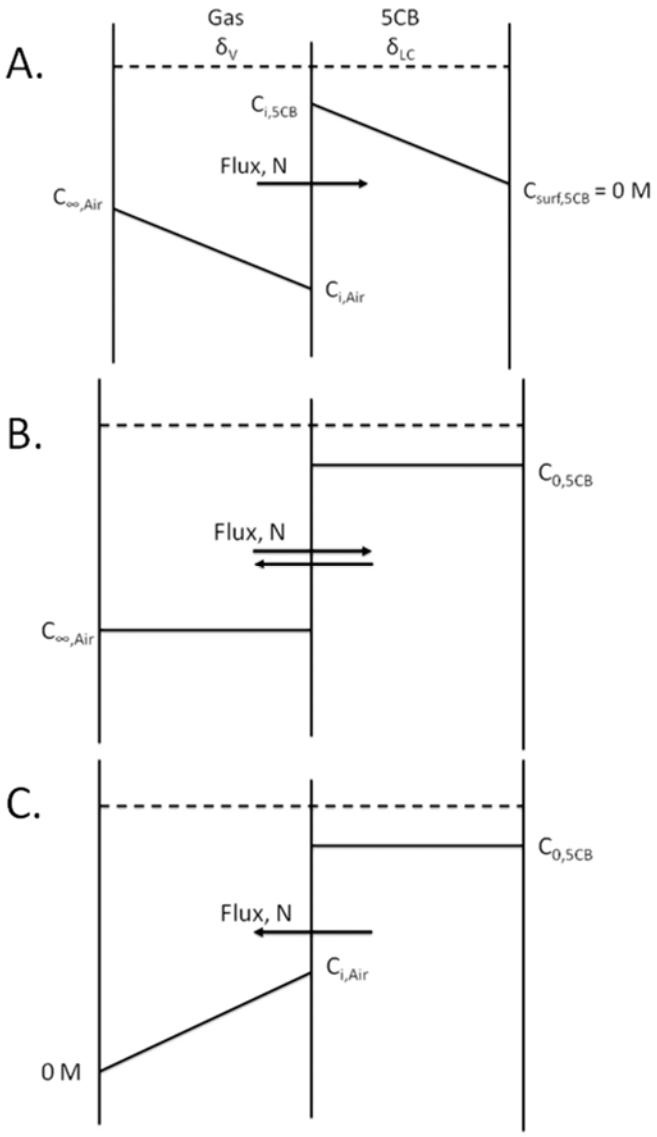

Figure 4.5. Schematic illustration of the concentration profiles of DMMP within the vapor phase and LC during different stages of the process of transport of DMMP to the surface sensor. The schematic in (A) depicts a concentration gradient in the gas stream with a thickness of δ_V, in which the concentration of the DMMP decreases from the bulk concentration $C_{\infty,Air}$ to the interfacial concentration $C_{i,Air}$. Likewise, in the LC phase, the concentration decreases from the interfacial concentration to the concentration at the metal-salt-functionalized surface. The schematic illustration in (B) depicts the concentrations in the air and the LC after equilibrium is reached between the gas stream and the LC. After removing the DMMP from the gas stream, the DMMP is transported out of the LC film via the gradients in concentration shown in (C).

In order to relate the time of response to the experimental conditions within the flow cell, we integrated equation 8 in order to account for the accumulation of DMMP within the LC film (C_{5CB}). This result is shown in Equation 9

$$t_{conc} = \frac{\delta_{5CB}}{H \cdot K_G} \cdot \ln\left(\frac{C_{\infty,Air}}{C_{\infty,Air} - H \cdot C_{on}^*}\right) \quad (9)$$

where C_{on}* is the concentration of DMMP within the LC film that must accumulate in order to drive the ligand-exchange reaction to an extent that an optical response is seen. We fit equation 9 to both sets of experimental data shown in Figure 4.3 using a single value of C_{on}* as a fitting parameter. As shown in Figure 4.3, the dependence of t_{on} on the velocity of the gas stream and the concentration of DMMP in the gas stream, as measured experimentally, are well described by the sum of $t_{entrance}$ and t_{conc} (solid black line in Figure 4.3). The best-fit value of C_{on}* was found to be 0.25 mM.

The analysis described above lead to the prediction that a concentration of approximately 0.25 mM of DMMP accumulates in the LC film supported on the Al^{3+} salt to trigger an optical response in the LC film. We note, however, that this prediction is based on a simplified mass transport model and uses many approximations such as an assumed value of H, the Henry's law constant for partitioning of DMMP from air into the LC film. Thus, we sought to obtain verification of this prediction for C_{on}* as a means of assessing the validity of the valued assumed for H (see above for additional discussion). To obtain this validation, we dissolved liquid DMMP at a known concentration within 5CB, and then confined the mixture of DMMP and 5CB between two surfaces decorated with aluminum perchlorate salts. At DMMP concentrations lower than 1 mM in these experiments, we measured the orientation of the LC

to be homeotropic. In contrast, at concentrations of DMMP above approximately 1 mM, we observed the LC to adopt planar/tilted orientations at the Al^{3+} coated surfaces. This independent estimate of the concentration of DMMP in the LC that is required to trigger the anchoring transition (1mM) is close to that obtained from our above-presented analysis of the dynamic response of the LC to exposure to the DMMP-containing gas stream (0.25 mM). While this experiment does provide support for the value of H used in our model of C_{on}*, we note also that the concentration of 1 mM is an upper bound as the volatility of DMMP resulted in the loss of some DMMP from the mixture of LC and DMMP in the above-described experiment. In particular, the magnitude of t_{conc} was estimated from the initial mass transport coefficient of DMMP to the surface even though, in practice, the mass transfer coefficient is changing with time as DMMP is accumulated within the LC film. The accumulation of DMMP within the LC will decrease the flux over time and ultimately eliminate the flux, as shown in Figure 5B. The key conclusion that emerges from the above analysis, however, is that the initial response of the sensor appears to be largely determined by the period of time required for the DMMP to accumulate to a threshold concentration within the LC.

A second characteristic of the optical response of the LC films that we aimed to understand was the rate of rise of the optical intensity of the LC sensor following the initial delay time, t_{on}. The increase in intensity of light transmitted through the LC film, measured as a function of time (m_{on}), is plotted in Figure 4.6 as a function of both the gas flow rate and the DMMP concentration in the gas stream. The evaluation of m_{on} is described previously and is dependent on the slope of the initial light intensity as soon as an optical response is seen. The slope used is related to the initial change in the light intensity of the sample and is subject to a

greater amount of error based on the evaluation method. However, the calculation of the initial slope gives an indication on the initial dynamics of the change in optical intensity of the sample. As the gas flow rate increases at a constant concentration of 1 ppm, we measured m_{on} to decrease, although the decrease was masked to some extent by variability between samples characterized under the same flow rate (Figure 4.6A). Despite this scatter, we note the significant difference between the values of m_{on} measured at the highest and lowest flow rates in Figure 4.6A. We note also that the experimental data shown in Figure 4.6 was obtained using 3 independent samples for each data point. Additional experiments with similar LC based sensors (data not shown) showed trends and scatter comparable to the data in Figure 4.6A. A more pronounced trend in m_{on} is evident in the results of experiments performed with increasing concentrations of DMMP within the gas stream, with the values of m_{on} increasing by a factor of three with concentration of DMMP (Figure 4.6B).

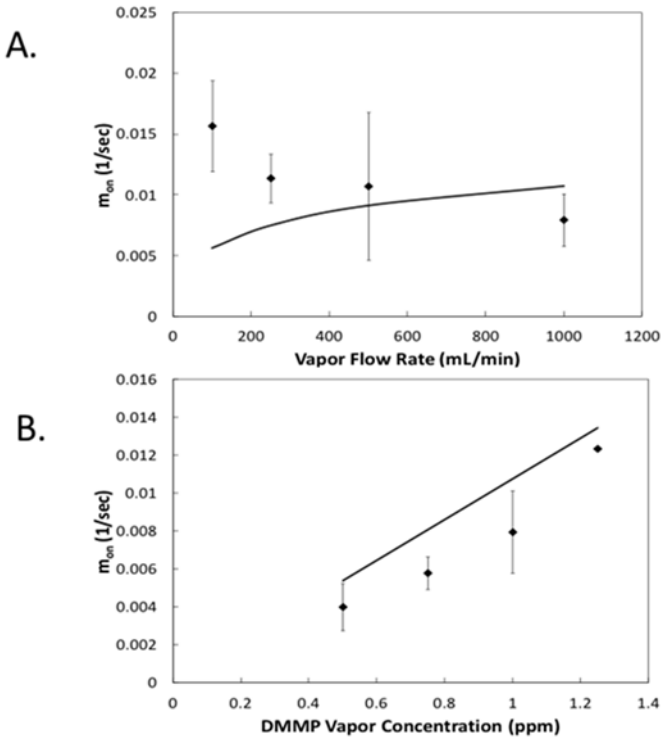

Figure 4.6. The optical response of the LC film, m_{on}, measured as a function of (A) the gas flow rate and (B) the DMMP concentration in the gas phase. The solid line is a model predicted value of $m_{on,model}$. In (A) a concentration of DMMP of 1 ppm was used for all samples, and in (B) the gas flow rate remained constant at 1000 mL/min.

To provide insight into the origin of the trends measured in m_{on}, we tested the hypothesis that m_{on} is proportional to the flux of DMMP to the Al^{3+}-decorated surface. This hypothesis was based on the proposition that the rate of rise of the optical response of the LC is proportional to the rate of rise in concentration of DMMP within the LC film (as determined by the flux of DMMP to the surface). This hypothesis leads to the prediction that m_{on} can be evaluated as

$$m_{\text{on}} = \alpha \cdot K_G \cdot C_{\infty,Air} \quad (10)$$

where α is a proportionality constant. Equation 10 was fit to the experimental values of m_{on} measured as a function of velocity and concentration of DMMP, as shown in Figure 4.6 (A and

B), to find the value of α (27.6 cm^2/ mole) that provided the best fit of m_{on} to the experimental results. We comment that only the initial change in the optical appearance is fit to a linear line and in this time we do not expect the flux to change significantly. Inspection of Figure 4.6 reveals two key points. First, inspection of Figure 4.6B reveals that equation 10 provides a qualitatively correct prediction of the effect of DMMP concentration on the rate of rise of the optical response of the LC film. We interpret this result to indicate that an increase in concentration of DMMP in the gas stream flowing over the film of LC leads to an increase in the rate of accumulation of DMMP within the LC film, and thus an increase in the rate of the optical response of the LC film. Second, inspection of Figure 4.6A reveals that equation 10 provides a prediction for the effect of gas flow rate on the rate of response of the LC film that is opposite qualitatively to that observed in the experiments (at least, at the low flow rates). Despite the fact that the effect of the vapor flow rate results shown in Figure 4.3 suggest that our model correctly predicts the effect of flow rate on t_{on}, we do not yet fully understand why equation 10 does not correctly describe the effect of vapor flow rate on the rate of response of the LC film. We note, however, that t_{on} varies with flow rate, and thus the LC films characterized in Figure 4.6A were exposed to the DMMP streams for different periods of time prior to measurement of the rate of response of the LC film. This result hints that there may be kinetic processes associated, for example, with the rate of the ligand exchange reaction, that are influencing the rate of response of the LC film. This point requires additional investigation, which will be reported in a future study. We also note, however, that from the point of view of sensor design, the data in Figure 4.6A suggests that the rate of response of the LC is not strongly dependent on gas flow rate, provided that the flow rate is above 200 mL/min.

4.3.3 Relaxation of the LC film to the initial state following cessation of exposure to DMMP

We next address the dynamics of the relaxation of the LC films back to their initial state (homeotropic), following cessation of exposure of the DMMP-loaded LC films to a stream of air free of DMMP. As shown in Figure 4.2A, the flow of the gas stream containing DMMP to the system was replaced at t=420 seconds by a stream of air (at the same flow rate) that was free of DMMP. We define the time that elapses between the introduction of the DMMP-free stream of air and the initial decrease in the optical response of the LC film as t_{off} (see Figure 4.2B). In addition, after the initial decrease in the intensity of light transmitted through the LC film, we characterize the rate of decrease by fitting the change in the linear optical response to a linear line with a slope of m_{off} (see Figure 4.2B). Below we report experiments that characterize the influence of the gas flow rate and DMMP concentration used to load the LC film on the parameters t_{off} and m_{off} in a similar manner to the discussion in Section 4.2. Specifically, we sought to test the hypothesis that t_{off} is the time required for the concentration of DMMP within the LC film to fall below the threshold value required to initiate the relaxation of the LC towards the homeotropic state.

Figure 4.7 shows the experimentally measured dependence of t_{off} on gas flow rate (Figure 4.7A) and concentration of DMMP in the gas stream used to load the LC film (Figure 4.7B). Qualitatively, we measured t_{off} to decrease as the airflow rate increased, and to be independent of the DMMP concentration used to load the LC film (within the error of the experiment). To provide insight into the dependence of t_{off} on vapor flow rate and DMMP

concentration, we developed a simple mass transport model to test the hypothesis that the concentration of DMMP in the LC film drops to a threshold value in the LC film at t_{off}. The physical situation is depicted in Figure 4.5C, in which the flux of DMMP out of the LC film is governed by mass transport across the vapor side of the boundary layer. As indicated in Figure 4.5C, and consistent with the analysis reported above, we assume that there are no concentration gradients formed within the LC phase during the process of mass transfer of DMMP out of the film; that is, the rate-limiting concentration gradient within the system is present within the gas phase. The concentration of DMMP in the LC film (just prior to introduction of the gas stream that is free of DMMP), $C_{5CB,0}$, is calculated as the product of the concentration of the DMMP in the gas stream used to load the LC film with DMMP and the Henry's law coefficient. That is, at the end of the exposure of the LC film to the stream of gas containing DMMP, we assume that equilibrium has been established between the DMMP in the LC film and the gas stream (Figure 4.5B). In support of this proposition, we varied the time of exposure of the LC film to the gas stream containing DMMP, and measured the time required for the onset of the relaxation of the LC film following cessation of exposure to DMMP. As the duration of exposure to the gas stream containing DMMP increased beyond 420 s, the time required for the onset of the relaxation of the LC film became independent of the exposure time. This result is consistent with an equilibrium distribution of DMMP between the DMMP in the vapor phase and within the LC sample being reached after 420 s of exposure of the LC film to the DMMP stream.

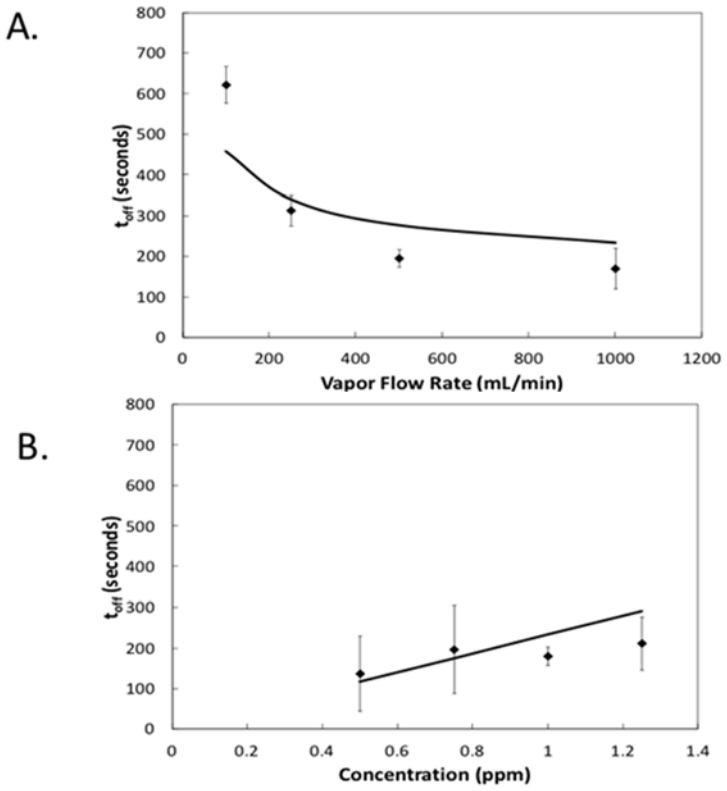

Figure 4.7. Experimental measurements of t_{off}, as a function of (A) the flow rate of the air passing over the sample (LC film loaded with DMMP concentration of 1 ppm) and (B) concentration of DMMP in the gas phase used to load the LC film (at a constant gas flow rate of 1000 mL/ min). The solid lines are the values of t_{off} predicted by equation 16.

As noted above, the rate of mass transfer of the DMMP out of the LC film is set by a concentration gradient that develops in the gas phase. The corresponding mass transfer coefficient k_G is given by equation 6. We also note that as the LC film is depleted of DMMP, the concentration of DMMP on the air side of the LC interface, $C_{i,Air}$, decreases according to Henry's law, thus decreasing the magnitude of the concentration gradient across the gas side of the interface. The flux of the DMMP leaving the LC film, N, can be calculated as

$$N = \frac{\partial n_{DMMP}}{A \cdot \partial t} = k_G \cdot \left(C_{i,Air} - 0\right) = k_G \cdot \left(\frac{n_{DMMP}}{A \cdot \delta_{5CB}} - 0\right) \quad (11)$$

Integration of equation 11 from the initial amount of DMMP to the final amount of DMMP (under constant volume, $C_{i,Air,0}$ to C_{off}* respectively) yields

$$\ln\left(\frac{C^*_{off}}{C_{i,Air,0}}\right) = \frac{k_G}{\delta_{LC}} \cdot t_{off} \qquad (12)$$

where C_{off}* is the threshold value of DMMP at the air interface below which the LC relaxes towards a homeotropic alignment. We fit equation 12 to the experimental data in Figure 4.7 to obtain a best fit value of C_{off}* of 0.15 ppm of DMMP. Inspection of Figure 4.7 reveals that this value of C_{off}* does provide good agreement between the experimental values of t_{off} and the model-predicted values of t_{off}. We emphasize that C_{off}* is an estimate of the concentration of DMMP in the gas phase near the surface of the LC film at which the orientation of the LC sample begins to transition to the homeotropic alignment. In other words, the best fit value of C_{off}* suggests the minimum value of DMMP that is required within the gas phase to maintain a planar alignment of the LC at the Al^{3+}-decorated interface is 0.15 ppm. The model described by equation 12 also suggests a slight increase in t_{off} with increase in DMMP vapor concentration. This trend is not evident in the experimental data as it lies at the limits of the error bars of the experimental measurements (see Figure 7B).

Next, we turned our attention to m_{off}, and report the dependence of m_{off} on the vapor flow rate and concentration of DMMP. Inspection of equation 12 leads to the prediction that when the intensity of light transmitted through the LC film begins to decrease, the concentration of the DMMP in the LC film is the same for all samples. For this reason, the value of m_{off} is predicted to be independent of the DMMP concentration used to load the LC film and dependent only on the value of the gas flow rate. Inspection of the experimental data in Figure

4.8 shows the model-predicted decrease in m_{off} to lie largely within the error of the measurements. Consistent with the model prediction, however, we note that m_{off} measured at a flow rate of 100 mL/min is significantly less than that measured at 500 mL/min. Also consistent with the model, the values of t_{off} measured as a function of DMMP concentration were invariant with concentration of DMMP (Figure 4.8B).

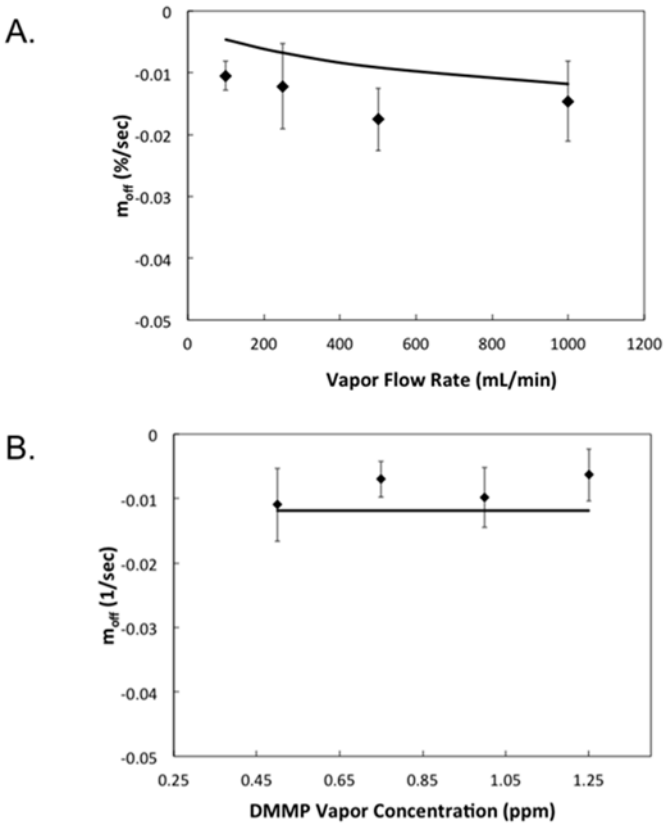

Figure 4.8. Experimental measurements of m_{off}, as a function as a function of (A) the flow rate of the air passing over the sample (LC film loaded with DMMP concentration of 1 ppm) and (B) concentration of DMMP in the gas phase used to load the LC film (at a constant gas flow rate of 1000 mL/ min). The solid lines are the model-predicted values of m_{off}.

4.4 Discussion

We point out that the model described within this paper contains several approximations that are described below. Despite this, the mass transport model presented in

this study illustrates the qualitative behavior of the experimental system as both the flow rate of the vapor and concentration of DMMP in the vapor changes. The model gives insight into the sensitivity of the LC sensor system that is independent of the conditions of exposing the LC sensor to the vapor analyte. We focused our discussion on the mass transport properties of the DMMP to the interface and assume that both the kinetics of the ligand exchange reaction and the kinetics of the LC transition will be fast when compared to the time scales that are seen for the LC sensor system. This assumption is consistent with past studies.[30] In addition, there are assumptions associated with the flow of air within the flow cell. We assume that the air is developed, thus allowing us to assume the flow of air occurs in one direction across the LC sample. The entrance length for the flow cell under the highest flow rate conditions is calculated to be 2.6 cm. This distance is shorter than the distance the LC film is placed from the entrance of the flow cell. We assume that the mass transport of DMMP from the vapor phase to the solid surface is a one dimensional mass transport problem. The samples that were analyzed were studied in the central regions in order to minimize any edge effects of the LC sample. In analyzing the optical micrographs in Figure 4.2A, we do not see a change in the pattern of the optical appearance as a function of the lateral dimensions of the sample. In analyzing the samples, there is not a significant difference in the appearance of the changes in optical intensity of the sample in the different regions of the LC sample. Furthermore, the presence of back flow or the development of a pressure within the flow cell was assumed to be negligible due to the fact that the outlet of the flow cell is large. The patterns of airflow can be modeled more precisely using complex models, but that goes beyond the scope of this study.

A key result that emerges from the experiments reported in this paper is that mass transport of the DMMP from the gas to the gas-LC film interface dominates the dynamics of the response of the LC film (t_{on} and m_{on}). This is evidenced by the results shown in Figure 4.3 and Figure 4.6B. In contrast, mass transport across the LC film, from the gas interface of the LC to the metal-salt-decorated surface of the solid is fast compared to the dynamics of the response of the system.

The above-summarized insight into the rate-limiting processes underlying the dynamics of the response of the LC films provides important guidance to the design of LC sensors. Our results suggest that to optimize the optical response of the system, the thickness of the concentration boundary layer of the DMMP in the gas passing over the LC sample should be minimized in order to increase the mass transfer coefficient from the gas phase. This can be accomplished by a number of approaches, including by maximizing the flow rate of the gas stream parallel to the LC interface or by changing the geometry of the device to impinge gas at normal incidence onto the surface of the LC (as was done in some past reports of LC-based sensing of DMMP).[8] In the limiting case in which the resistance to transport of gas across the gas-side concentration boundary layer is minimized, the overall flux of DMMP to the metal-salt decorated interface will become controlled by mass transport of the DMMP on the LC side of the air-LC interface. In this case, for a 10 μm-thick LC film, the overall mass transfer coefficient would be 0.9 s cm^{-1} that leads to a 4-fold decrease in t_{on}, as reported in Figure 4.3.

A second key result of our analysis is that the thickness (or volume) of the LC film is a key variable in the design of LC-based sensors because the concentration of DMMP within the

LC film must build to a threshold value before an optical response of the sample is observed. This is evident in equation 9, where t_{conc} is proportional to the thickness of the LC film, δ_{LC}. Therefore, we predict that at high flow rates, where the effect of $t_{entrance}$ is minimal, the response time will be faster for thinner films of LC. Specifically, we predict that for a LC film with a thickness of 3 μm, the response of the LC film will be 6-fold faster than a 18 μm thick LC film (15 seconds at 3 μm, as compared to 100 seconds for an 18 μm film, with a flow of 1000 mL/min). Furthermore, if we were to maximize K_G (four times larger based on minimization of resistance to transfer in the gas phase) in addition to using a 3 μm-thick LC film, we predict a response time on the order of about 5 seconds would be achieved. Here we note that past studies have reported optical responses in LC systems within 10 seconds, when LC samples with a thickness of 4 μm were exposed to a 1 ppm DMMP vapor stream that was incident on the LC sample at near normal incidence.[8]

Finally, we comment that the results presented in this paper provide a methodology based on analysis of the dynamic response of the LC film that permits assessment of the sensitivity of LC films to gas phase analytes. While the sensitivity of the LC film will depend strongly on the identity of the metal salts used to orientate the LCs, the amount of metal salt deposited onto the solid surface, the chemical functionality of the LC and other factors that have been reported elsewhere,[8, 11, 13-15] for the experimental conditions used in the current study, we estimate the sensitivity of the LC film to DMMP to be in the range of 150-250 ppb. We note that while the methodology reported in this paper permits assessment of the sensitivity of the LC films, we emphasize that we did not seek to create an experimental LC system that provided maximal sensitivity to DMMP. Indeed, in past studies, using Cu^{2+} salts

deposited under conditions that differed from those reported in this paper, we have observed LC films of 5CB[8] and 8CB[15] to respond to concentrations of DMMP in the low ppb range.

4.5 Conclusions

The study reported in this paper provides experimental measurements of the dynamics of the response of LC-based sensor for gas-phase analytes, as a function of the concentration of the analyte in the gas phase and gas flow rate. These measurements are compared to models of mass transport of analytes from the gas phase into the LC film to provide fundamental insights into the physical processes that govern the dynamic response of the LC films. The most important conclusions to emerge from the study are that (i) the rate-limiting process governing the response of the LC sensor is mass transfer across the concentration boundary layer formed on the gas side of the LC interface, and (ii) the response of the LC to the gas phase analyte is controlled by accumulation of the analyte in the LC film, thus leading to the prediction that the dynamics of the response will be a strong function of the LC film thickness. Specifically, for the system described in this paper, we determined that a threshold concentration of approximately 0.25 mM of DMMP was required to trigger a response in the LC film. This concentration corresponds to an air-side concentration of DMMP of approximately 250 ppb. We emphasize that the sensors used in the study reported in this paper were not optimized to provide maximal sensitivity. The measurements and analysis reported in this paper, however, do provide a convenient methodology for determining the sensitivity of LC based sensors, a methodology that could be exploited for future sensor optimization. Overall, the results presented in this paper provide useful guidance to the design of LC-based sensors.

4.6 Acknowledgements

The authors thank Mr. John Cannon for help fabricating the metal plates and the flow cell. The study was funded primarily by the National Science Foundation (DMR-1121288, Materials Research Science and Engineering Center), with additional partial support from the Army Research Office (W911NF-11-1-0251 and W911NF-10-1-0181), DOE DE-SC0004025 and the National Institute of Health grant CA108467 and CA105730.

4.7 Supporting Information

4.7.1 Calculation of diffusion length thicknesses

The calculation of the diffusion length in the vapor phase is discussed below. As shown in Figure 4 in the main text, the DMMP vapor flows parallel to the LC sample within the flow cell. The flow of the vapor across the stainless steel plate that fastens the TEM grid to the solid surface (length of 12.7mm) leads to the development of a hydrodynamic boundary layer with a thickness δ that can be evaluated for laminar flows as

$$\delta = \sqrt{\frac{12 \cdot \mu \cdot x}{\rho \cdot U_{\infty}}} \qquad \text{(S.1)}$$

where μ is the viscosity of air, ρ is the density of air, x is the horizontal distance across the metal plate, and U_{∞} is the velocity of the vapor stream.[31] For a vapor flow rate of 1000 mL/min and a value of x of 12.7 mm (corresponding to the distance from the edge of the plate to the central point over the LC film), δ is calculated from equation S.1 to be 6 mm. At a flow rate of 100 mL/min, the value of δ increases to 18 mm. As the stream of DMMP vapor passes across the LC surface (starting at x = 11.7mm, the location of the outer edge of the LC), the DMMP in the

vapor is absorbed by the LC, and a concentration boundary layer of thickness δ_c will develop inside the hydrodynamic boundary layer (as shown in Figure 4). We note that the horizontal distance across which the gas stream flows to reach the center of the LC sample is 1 mm (the diameter of the removed inset within the stainless steel plate is 2mm), and we calculate the thickness of the concentration boundary layer at the center of the LC sample, δ_C, as[32]

$$\delta_C = 3.0\left(\frac{x}{U_\infty}\right)^{1/2}\left(1-\left(\frac{x_0}{x}\right)^{3/4}\right)^{1/3}\left(\nu_G\right)^{1/6}\left(D_{Air}\right)^{1/3} \qquad \text{(S.2)}$$

where x_o is the horizontal distance over which the concentration boundary layer has developed (1mm), x is defined in equation S.1, ν_G is the kinematic viscosity of air and D_{Air} is the diffusion coefficient of DMMP in air (estimated in past studies to be 0.05 cm^2/s[33]). Equation S.2 shows that δ_c varies as $U_\infty^{-1/2}$, thus highlighting the importance of U_∞ in the thickness of the concentration boundary layer. For a vapor flow rate of 1000 mL/min, δ_C is calculated from equation S.2 to be 1.1 mm at the center of the LC sample (at the same location, the hydrodynamic boundary layer is 6 mm in thickness). At a flow rate of 100 mL/min, the value of δ_C increases to 3.5 mm. The above analysis is accurate for a planar, solid surface over which both hydrodynamic and concentration boundary layers develop. Inspection of Figure 4 reveals that the geometry of our experiment is more complex, as the DMMP must also diffuse across a stagnant layer with a thickness corresponding to that of the metal plate (0.44 mm) to reach the LC surface. We take this additional diffusion length into account in an approximate manner, by considering the total concentration boundary layer thickness δ_v to be the sum of δ_C and the thickness of the metal plate (Δ).

4.7.2 Specific example from Equation 1

The thickness of the diffusion length in air is described by the simplified concentration boundary layer analysis, and the diffusion coefficient of DMMP in air is 0.05 cm^2/s. Therefore, the time required for the DMMP to diffuse across the boundary layer when the air is flowing at 1000 mL/min is calculated to be 2 seconds. The time of diffusion increases to 13 seconds when the flow rate of the gas is decreased by an order of magnitude (100 mL/min). Likewise, the time required for DMMP to diffuse across the LC film is calculated. The thickness of the diffusion length in the LC phase, δ_{5CB} is defined by the thickness of the LC film. The thickness of the LC film is estimated to be equal to the thickness of the TEM grid (18 µm) that supports the LC film. The diffusion coefficient of DMMP through the LC, D_{5CB}, is estimated from past studies as 10^{-7} cm^2/s.[34] The diffusion time for DMMP across the LC film is 16 s and remains constant for all of the studies done within this study. Values of $t_{transport}$ calculated using equation 3 are shown in Figure 3.

4.7.3 Error associated with the slope of response

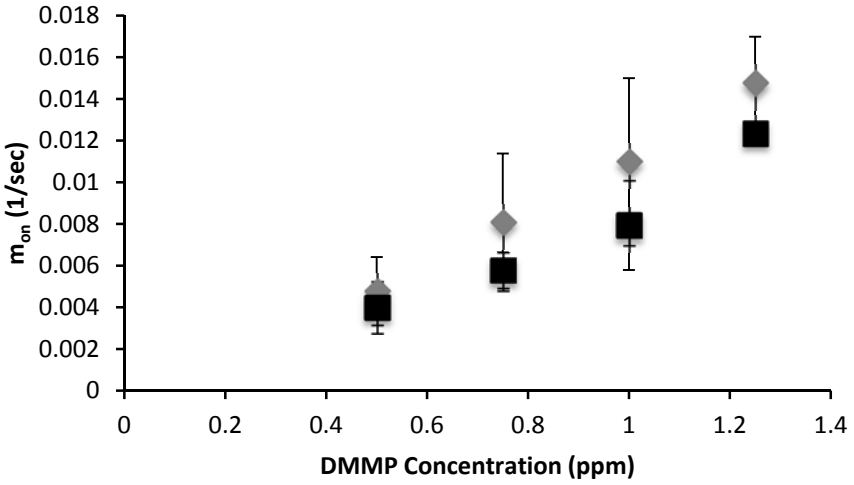

Figure 4.9. The slope of response for two independent batches of experiments demonstrating the effect of the DMMP concentration on the slope of response. We see similar trends evidence for the different batches of experiments and in general the slopes of the samples fall within the error of each experiment.

4.8 References

1. Wang, J.; Yang, L.; Boriskina, S.; Yan, B.; Reinhard, B. M. *Anal. Chem.* **2011,** *83*, 2243-2249.
2. Sylvia, J. M.; Janni, J. A.; Klein, J. D.; Spencer, K. M. *Anal. Chem.* **2000,** *72*, 5834-5840.
3. Ashley, K. *J. Hazard. Mater.* **2003,** *102*, 1-12.
4. Righettoni, M.; Tricoli, A.; Pratsinis, S. E. *Anal. Chem.* **2010,** *82*, 3581-3587.
5. Stewart, C. E. *Weapons of mass casualties and terrorism response handbook*. Jones & Bartlett Learning: Sudbury, MA, **2006**.
6. Bai, Y. Q.; Abbott, N. L. *Langmuir* **2011,** *27*, 5719-5738.
7. Sen, A.; Acharya, B. R. *Liq. Cryst.* **2011,** *38*, 495-506.
8. Shah, R. R.; Abbott, N. L. *Science* **2001,** *293*, 1296-1299.
9. Shah, R. R.; Abbott, N. L. *Langmuir* **2003,** *19*, 275-284.
10. Bi, X. Y.; Yang, K. L. *Sensors and Actuators B-Chemical* **2008,** *134*, 432-437.
11. Bungabong, M. L.; Ong, P. B.; Yang, K.-L. *Sens. Actuators, B* **2010,** *148*, 420-426.
12. Cadwell, K. D.; Lockwood, N. A.; Nellis, B. A.; Alf, M. E.; Willis, C. R.; Abbott, N. L. *Sensors and Actuators B-Chemical* **2007,** *128*, 91-98.
13. Wang, P.-H.; Yu, J.-H.; Zhao, Y.-B.; Li, Z.-J.; Li, G.-Q. *Sensors and Actuators B: Chemical* **2011**.
14. Yang, K. L.; Cadwell, K.; Abbott, N. L. *J. Phys. Chem. B* **2004,** *108*, 20180-20186.
15. Yang, K. L.; Cadwell, K.; Abbott, N. L. *Sensors and Actuators B-Chemical* **2005,** *104*, 50-56.
16. VanTreeck, H. J.; Most, D. R.; Grinwald, B. A.; Kupcho, K. A.; Sen, A.; Bonds, M. D.; Acharya, B. R. *Sens. Actuators, B* **2010,** *In Press, Corrected Proof*.

17. Sridharamurthy, S. S.; Cadwell, K. D.; Abbott, N. L.; Jiang, H. *Smart Materials & Structures* **2008,** *17*, 4.

18. Cadwell, K. D.; Alf, M. E.; Abbott, N. L. *J. Phys. Chem. B* **2006,** *110*, 26081-26088.

19. Yang, K. L.; Cadwell, K.; Abbott, N. L. *Adv. Mater. (Weinheim, Ger.)* **2003,** *15*, 1819-1823.

20. Hunter, J. T.; Pal, S. K.; Abbott, N. L. *ACS Appl. Mater. Interfaces* **2010,** *2*, 1857-1865.

21. Pal, S. K.; Acevedo-Velez, C.; Hunter, J. T.; Abbott, N. L. *Chem. Mater.* **2010,** *22*, 5474-5482.

22. Cheng, D. M.; Sridharamurthy, S. S.; Hunter, J. T.; Park, J. S.; Abbott, N. L.; Jiang, H. R. *J. Microelectromech. Syst.* **2009,** *18*, 973-982.

23. P.-G. de Gennes, J. P. *The Physics of Liquid Crystals*. 2nd ed.; Oxford University Press: New York, **1993**.

24. Stephen, M. J.; Straley, J. P. *Reviews of Modern Physics* **1974,** *46*, 617-704.

25. Hassanzadeh, A.; Lindquist, R. G. *IEEE Sens. J.* **2012,** *12*, 1536-1544.

26. Zou, Y.; Namkung, J.; Lin, Y. B.; Lindquist, R. *Appl. Opt.* **2010,** *49*, 1865-1869.

27. Namkung, J.; Zou, Y.; Abu-Abed, A.; Lindquist, R. G. *IEEE Sens. J.* **2010,** *10*, 1479-1485.

28. Bartelt-Hunt, S. L.; Knappe, D. R. U.; Barlaz, M. A. *Critical Reviews in Environmental Science and Technology* **2008,** *38*, 112-136.

29. Jauregui-Haza, U. J.; Pardillo-Fontdevila, E. J.; Wilhelm, A. M.; Delmas, H. *Latin American Applied Research* **2004,** *34*, 71-74.

30. Atkins, P.; Overton, T.; Rourke, J.; Weller, M.; Armstrong, F. *Shriver and Atkins' Inorganic Chemistry*. OUP Oxford: **2009**.

31. Bird, R. B.; Stewart, W. E.; Lightfoot, E. N. *Transport Phenomena*. Wiley: **2007**.

32. Krenn, J.; Baesch, S.; Schmidt-Hansberg, B.; Baunach, M.; Scharfer, P.; Schabel, W. *Chem. Eng. Process.* **2011,** *50*, 503-508.

33. Fuller, E. N.; Schettler, P. D.; Giddings, J. C. *Industrial & Engineering Chemistry* **1966,** *58*, 18-27.

34. Daniel, R. S.; Alexis, L. T.; Wesley, C. C. *The Journal of Chemical Physics* **2001,** *114*, 3842-3847.

Chapter 5: Adsorbate-Induced Anchoring Transitions of Liquid Crystals on Surfaces Presenting Metal Salts with Mixed Anions

5.1 Introduction

Nematic liquid crystals (LCs) are liquids that possess long-range orientational order. At a solid interface, the orientational ordering of the LC reflects intermolecular interactions between the mesogens and the solid.[1-5] For example, strong coordination interactions between transition metal cations deposited on a surface (e.g., Cu^{2+} or Al^{3+}) and nitrile-containing mesogens (i.e. 4-cyano-4'-pentylbiphenyl, 5CB) result in the homeotropic ordering (orientation parallel to surface normal) of the LC. Past studies have shown that the alignment of the LC is dependent on both the strength and number of coordination interactions between the LC and the metal salt (i.e., electron affinity of the cation in the salt).[1, 6-14]

Past studies have also shown that adsorbates introduced in the vapor phase above the LC film can competitively disrupt coordination interactions between the metal ions and the LC mesogens.[1, 6, 15] This process occurs if the adsorbate coordinates more strongly with the metal ion as compared to the mesogen. Disruption of these coordination interactions by an adsorbate triggers a change in the ordering of the LC at the solid surface to a planar alignment (perpendicular to surface normal).[1, 6, 8-9, 14-18] For example, the analyte dimethyl methylphosphonate (DMMP), when introduced as a vapor over the LC, triggers an ordering transition in a micrometer-thick film of nematic 5CB supported on a surface decorated with aluminum (III) perchlorate salts.[12, 15] As detailed elsewhere, DMMP is widely used as a simulant

of nerve agents including sarin. Detection of these types of analytes in the low parts-per-million (ppm) concentrations is important because the lethal concentration time for 50% of humans by inhalation of sarin is around 10-15 ppm min.[19]

The majority of the above described past studies have focused on high electron affinity cations, such as aluminum (III), nickel (II), and copper (II). The cations were deposited on surfaces as salts of weakly coordinating anions, such as perchlorate.[6] We emphasize here that the choice of anion is important because the anion, in addition to the electron affinity of the metal cation, impacts the nature of the coordination interactions between the LC and metal cation.[20] For example, metal salts composed of anions that coordinate more strongly than perchlorate (such as nitrate, chloride, or acetate) do not give rise to the homeotropic ordering seen on surfaces with metal perchlorates (planar anchoring is observed). Conversely, other weakly coordinating anions, including hexafluorophosphate (PF_6^-) and tetrafluoroborate (BF_4^-), have been observed to generate a homeotropic alignment of the LC when paired with a high electron affinity cation.[20]

In general, the strength of a coordination complex formed between an anion and cation can be correlated with the basicity constant of the anion, a parameter that measures the chemical equilibrium of hydrogen between the anion and the hydrogen ion. A large basicity constant indicates an equilibrium that lies towards the complex with the hydrogen ion, which suggests strong coordination.[21-28] Figure 5.1 shows that past observations of the effects of cation and anion type on the anchoring of nematic 5CB are well correlated by using metal ion electron affinity and anion basicity.[6, 29] In this paper, we build from these prior observations to

explore how mixtures of anions influence the anchoring of LCs and adsorbate-triggered anchoring transitions of LCs.

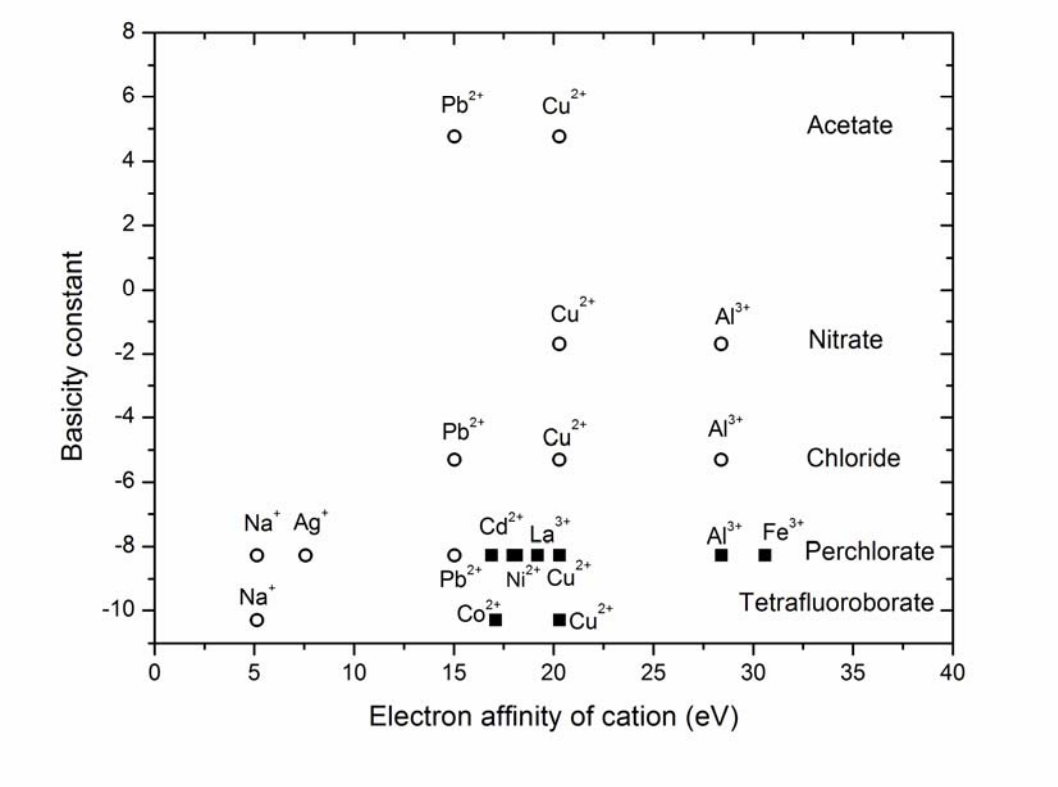

Figure 5.1. Alignment of LC films supported on metal salt-decorated surfaces taken from various past studies.[6, 29] The solid square data points (■) represent homeotropic alignment of the LC and the open circle data points (O) represent a planar or tilted alignment of the LC.

The study reported herein is focused on aluminum (III) and copper (II) salts with mixed anions. These two cations were selected because they induce a homeotropic alignment of nematic 5CB when paired with weakly coordinating anions such as perchlorate. In addition, the coordination interactions formed between the perchlorate salts of these cations and 5CB are disrupted by the presence of DMMP.[6] The strongly coordinating anions used in the present study are nitrate, chloride, and acetylacetonate, all of which possess basicity constant values

that are larger than perchlorate (see Figure 5.1). The anion acetylacetonate was selected because it is a bidentate ligand.

This study reported below is divided into three main sections. The first section demonstrates that the alignment of a nitrile containing LC on a metal salt surface can be manipulated using a mixture of weakly and strongly coordinating anions. The second section shows that the anion composition of the metal salt supporting the LC film also impacts the sensitivity of the LC film to the vapor analyte DMMP. Insight into the origin of this effect is provided via the use of infrared spectroscopy. The third section reports an investigation of the impact of the anion composition on the effects of humidity (i.e., the extent to which the response of the system to DMMP is impacted by changes in humidity). Overall, the results of this study suggest that control of anion composition (using mixed anions) provides a facile method to tailor the interactions between a coordinating metal cation and a LC, and thus manipulate the anchoring of the LC and the orientational response of the LC to a vapor phase analyte.

5.2 Experimental Methods

5.2.1 Materials

11-Mercaptoundecanoic acid (MUA), aluminum (III) perchlorate nonahydrate, aluminum (III) nitrate nonahydrate, copper (II) perchlorate hexahydrate, and copper (II) chloride dehydrate salts were purchased from Sigma Aldrich (Milwaukee, WI). Aluminum (III) acetylacetonate was purchased from Alfa-Aesar (Ward Hill, MA). 5CB was purchased from EMD Chemicals (Gibbstown, NJ). Titanium (99.999%) and gold (99.999%) were purchased from

Advanced Materials (Spring Valley, NY). Methanol and Fischer's Finest glass slides were purchased from Fischer Scientific (Pittsburgh, PA). Absolute ethanol (anhydrous, 200 proof) was purchased from Pharmco-AAPER (Brookfield, CT). All chemicals and solvents were of analytical reagent grade and were used as received without any further purification. All deionized water used in the study possessed a resistivity of at least 18.2 MΩ cm.

5.2.2 Methods

5.2.2A Cleaning of Glass Substrates.

Glass microscope slides were cleaned using acidic "piranha" solution 70:30 (% v/v) [H_2SO_4:H_2O_2]. Briefly, the glass slides were immersed in an acidic piranha bath at 60-80 °C for at least 1 h, and then rinsed in running deionized water for 2-3 min. The slides were then immersed in basic piranha 70:30 (% v/v) [KOH: H_2O_2] and heated to between 60 and 80 °C for at least 1 h. Finally, the slides were rinsed sequentially in deionized water, ethanol, and methanol, and then dried under a stream of nitrogen. The clean slides were stored in an oven at 110 °C. All other glassware was rinsed with distilled water and ethanol and dried under a gaseous stream of nitrogen.

5.2.2B Deposition of thin layers of gold.

Semi-transparent films of gold with thicknesses of 200 Å were deposited onto piranha-cleaned glass slides (see above) mounted on a fixed holder within an electron beam evaporator (VEC-3000-C manufactured by Tekvac Industries, Brentwood, NY). The angle of incidence of the gold ranged from 0° to 15° on the slides (measured from surface normal). A layer of titanium

(thickness 80 Å) was used to promote adhesion between the glass microscope slides and the films of gold. The rates of deposition of gold and titanium were 0.2 Å/s. The pressure in the evaporator was maintained at less than 3×10^{-6} Torr before and during each deposition. The gold source was periodically cleaned by sequential immersion in aqua regia (70% HNO_3, 30% HCl) and piranha solutions at 50 °C (30 min in each solution); see above for compositions. The cycle was repeated 3-4 times, rinsing the source between cycles in deionized water.

5.2.2C Preparation of functionalized gold surfaces.

Carboxylic-acid-terminated self-assembled monolayers (SAMs) of 11-mercaptoundecanoic acid (MUA) were formed on gold-coated glass slides by immersing the slides overnight in an ethanolic solution containing 2 mM of MUA. The gold films were then rinsed with an excess of ethanol and dried under a stream of nitrogen. Mixtures of the metal salt were formed in an ethanolic solution in which the concentration of the metal cation remained constant at 5 mM. The metal salts were then deposited immediately onto the carboxylic-acid-terminated SAMs by spin coating the ethanolic salt solution at 3000 rpm for 60s (WS-400A-6NPP/Lite, Laurell Technologies, North Wales, PA).

5.2.2D Formation of Micrometer-Thick Films of LC.

After coating the surfaces with metal salt, as described above, an 18 µm-thick gold-coated transmission electron microscopy (TEM) grid (Electron Microscopy Sciences, Hatfield, PA) was fastened to the salt-coated surface using a thin stainless steel plate (0.44 mm thickness). The stainless steel plate contained a 2-mm diameter hole that was aligned with the center of the TEM grid. The TEM grid contained square pores with lateral dimensions of 285

μm. The grid had an overall diameter of 3 mm. Both the TEM grid and stainless steel plate were dip-coated with a perfluorocarbon film (Nyebar Fluorocarbon Barrier Film, SmartGrease Company, Fairhaven, MA) to minimize wicking of the 5CB from the TEM grid. The grids were filled with LC using a microcapillary pipet at room temperature, taking care to fill only the middle squares of the TEM grid, so as to avoid wicking of the 5CB between the TEM grid and steel plate.

5.2.2E Exposure to DMMP.

The sample, prepared as described above, was exposed to a stream of air containing DMMP within a flow cell that was constructed to direct the flow of air across the LC samples while permitting simultaneous observation of the samples through a polarized light microscope (CH40, Olympus, Melville, NY). The stream of gas containing DMMP was generated using a certified cylinder containing 10 ppm DMMP in nitrogen (Matheson Tri-Gas Inc, Eagan, MN). The gas of DMMP was diluted by air at a specified relative humidity (RH). The RH of the air was controlled using a portable dew point generator (LI-610, LI-COR Biosciences, Lincoln, NE). The temperature of the gas fed to the flow cell was maintained at room temperature (25 °C) and the RH was controlled to 30% unless indicated otherwise. The flow system was plumbed using 1/16'' stainless steel Swagelok tubing (Badger Fluid System Technologies Milwaukee, WI). The flow rate of the gas through the exposure system was controlled using a series of rotameters (Aalborg Instruments & Controls, Inc., Orangeburg, NY). The volumetric flow rate of the 10 ppm DMMP stream from the cylinder was controlled and ranged between 0 to 150 mL/min, while the volumetric flow rate of the diluent air stream was controlled to range between 0 to 1000

mL/min. The concentration of DMMP used in the study reported in this paper ranged from 0.1 ppm to 1.25 ppm, while the overall volumetric flow rate of the gas stream passed over the samples remained constant at 1000 mL/min.

The flow cell was fabricated by machining a rectangular prism of aluminum metal. Glass windows allowed transmission of polarized light through the flow cell. The intensity of light that was transmitted through the LC sample in the flow cell was recorded using an Olympus camera (Olympus C2040Zoom, Melville, NY). The total volume of the flow cell was 10.5 cm^3 (6 cm x 3.5 cm x 0.5 cm), giving rise to a gas residence time of ~0.6 sec when the flow rate was 1000 mL/min. The Reynolds number was calculated to be 51 for airflow within the flow cell at 1000 mL/min. This value corresponds to laminar flow.

5.2.2F Analysis of the polarized light images during exposure to DMMP.

The images of the LC films viewed through cross-polars were analyzed by quantifying the increase in the average intensity of light transmitted through LC films hosted in four central squares of the TEM grid. The increase in intensity of light transmitted through the LC (quantified relative to the initial state of the LC) was normalized such that the initial intensity value corresponded to a value of 0% and the final state of the LC after exposure to DMMP corresponded to a value of 100%. The time of response (t_{on}) of each LC sample was obtained by fitting the initial change in the normalized intensity of light transmitted through the sample to a straight line and calculating the time at which this line crossed 0%. Additional details can be found in a previous study.[15]

5.2.2G Measurement of the birefringence of films of 5CB:

The birefringence of thin films of 5CB was measured for thin films confined between two metal salt decorated surfaces. These surfaces were decorated with salts with anions that varied in composition. The sandwich cells were separated by an approximately 18 μm thick Mylar spacer. The exact thickness of the sandwich cells was measured by using interferometry. The sandwich cells were then filled with 5CB and the retardance of the cells was measured using a compensator. From these values, the apparent birefringence of the samples was calculated and the value of the tilt angle of the 5CB was determined using the known birefringence of 5CB.[30]

5.2.2H Fourier Transform Polarization-Modulation IR Reflectance- Absorbance Spectroscopy (PM-IRRAS).

Substrates decorated with metal salts were prepared with the following modifications to the procedures described above. For PM-IRRAS, we deposited 1000 Å of gold onto silicon wafers (using 100 Å of titanium as an adhesion promoter) in order to obtain a reflective surface. In addition, we used a thin film of 4-*n*-octyl-4'-cyanobiphenyl (8CB) deposited onto the surface by spin coating a 1% (by weight) solution of 8CB in toluene at 3000 rpm for 1 minute. The IR spectra of 8CB on surfaces were obtained using a Nicolet Magna-IR 860 FT-IR spectrometer with a photoelastic modulator (PEM-90, Hinds Instruments, Hillsboro, OR), a synchronous sampling demodulator (SSD-100, GWC Technologies, Madison, WI), and a liquid-N_2-cooled mercury cadmium telluride (MCT) detector. All spectra were recorded at an incident angle of 83° with the modulation centered at 2200 cm^{-1}. All spectral data reported within this article were recorded within 500 cm^{-1} of the modulation center.

5.3 Results

5.3.1 Effect of anion composition of metal salts on the anchoring of nematic films of 5CB

Our first set of measurements was designed to examine the influence of the anion of aluminum (III) salts on the alignment of supported films of 5CB. As noted in the Introduction, past studies have established that the electron affinity of the cation and basicity constant of the anion impact the alignment of supported films of 5CB. We also comment that the aluminum salts used in our experiments were purchased as hydrates (see Materials and Methods) and, as reported in previous studies,[31-33] the first coordination shell of the cation will be partially or completely occupied by water. The coordination interactions of the nitrile group and the aluminum (III), which are evident in the orientational behavior of the nitrile-containing LCs on surfaces of aluminum (III), largely reflect interactions that occur in the second and third coordination spheres of the cation.[1, 6, 8-9, 11-12, 15] In support of this interpretation, IR spectra of aluminum (III) perchlorate dissolved in deuterated acetonitrile in the presence of water show a small peak related to the first coordination sphere of aluminum (III) and a larger peak assigned to the second coordination shell.[31] Our first set of results, as shown in Figure 5.2, expands upon these prior studies by investigating the anchoring of 5CB at the surface of aluminum (III) salts with mixed anions. For these studies, we confined a film of 5CB between two surfaces decorated with the metal salts. As described in the Methods section, we determined the distance between the two surfaces to be ~18 μm by using interferometry prior to filling the cavity defined by the two surfaces with 5CB. After filling, we measured the retardance of the

film of 5CB and calculated the average birefringence as the ratio of the retardance of the 5CB film to the thickness of the film of LC. Finally, the birefringence was used to calculate the average tilt angle at the interface, as shown in Figure 5.2a.[30]

The anion combinations that we studied were mixtures of a weakly coordinating anion (perchlorate) and a more strongly coordinating anion (either nitrate or acetylacetonate). Figure 5.2a reveals that the tilt angle of a nematic film of 5CB at the aluminum (III) nitrate-coated surface is close to 90° from surface normal (within uncertainty in the measurement). We note that we attribute the measurements of an apparent tilt angle that is slightly greater than 90° to uncertainty in the measurement (and to correspond to planar anchoring of the LC). As the mole fraction of perchlorate in the salt increased to almost 10%, the tilt angle of the LC at the interface remained close to a value of 90°. However, at a critical composition of the anion (around 10% perchlorate, 90% nitrate by mole percent), we measured a discontinuous change in the alignment of the LC at the interface. For samples anchored on surfaces with salts containing more than 10% perchlorate, we measured the LC to adopt a homeotropic alignment (tilt angle of zero). This critical composition is shown in Figure 5.2a as the vertical solid black line. We also comment that when the compositions of the anions were close to the critical concentration we observed some variation of the anchoring of the LC across the sample, likely reflecting local variation in composition of the anions.

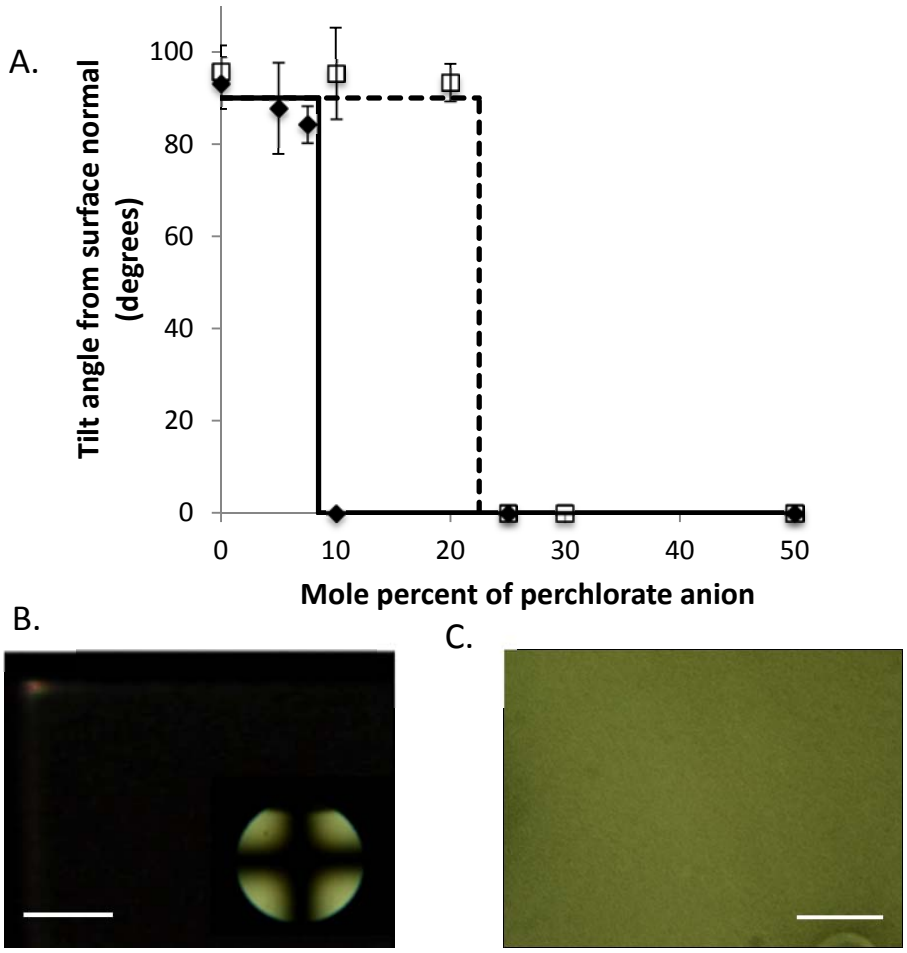

Figure 5.2. (A) Tilt angle from surface normal for films of nematic 5CB anchored on surfaces decorated with aluminum (III) salts comprised of mixed anions (perchlorate/ nitrate, solid points; perchlorate/acetylacetonate, open squares). Polarized light micrographs of 5CB films anchored on surfaces that are coated with aluminum (III) salts with either (B) perchlorate or (C) nitrate anions. The conoscopic image in lower right of (B) confirms a uniform homeotropic alignment of the LC film. The scale bars represent 1 mm.

Polarized light micrographs of the LC films in contact with surfaces composed of 100% perchlorate and 100% nitrate are shown in Figure 5.2b and 2c, respectively. These optical micrographs are consistent with the tilt angles shown in Figure 5.2a. Figure 5.2b (100% perchlorate) shows a dark image when viewed through cross polarizers that is indicative of homeotropic alignment of the LC. This behavior is further confirmed by the cross-hair pattern

obtained by using conoscopy (inset in Figure 5.2b). In contrast, as shown in Figure 5.2c, the 5CB films supported on metal salt films containing 100% of the strongly coordinating nitrate anion exhibited a bright appearance (consistent with planar anchoring of the LC). This general behavior was also observed for other metal salts such as mixtures of copper (II) perchlorate and copper (II) chloride (this system exhibited a critical composition that was similar to the aluminum (III) perchlorate/ nitrate system; data shown in supporting information).

Next, we characterized the mixed anion system comprised of perchlorate and acetylacetonate. The anion acetylacetonate was used because it is a bidentate anion (i.e., interacts with the cation at two independent coordination sites). Figure 5.2a shows that the acetylacetonate/perchlorate system exhibited a behavior similar to the nitrate/perchlorate system. However, a key difference is the observation of a critical composition that is almost double that of perchlorate (around 25% perchlorate, 75% acetylacetonate by mole percent) as compared to the nitrate-perchlorate system. This increase in the critical composition of the perchlorate anion is consistent with the idea that each individual acetylacetonate molecule interacts with the aluminum (III) cation at two different coordination sites. In brief, if we assume that the aluminum (III) cation is able to participate in six coordination interactions and the salt is electro-neutral, then each cation with three unidentate cations will have three coordination sites available for interaction with species such as the nitrile group of the LC. However, in the case of a bidentate anion, the anion occupies two coordination sites. This simple model leads to the conclusion, for example, that an aluminum (III) cation with one acetylacetonate and two perchlorate anions will have only two coordination sites available to interact with the other species. Our observation that a larger amount of perchlorate is needed

in order to achieve homeotropic alignment of 5CB when using acetylacetonate is thus consistent with the bidentate nature of acetylacetonate ion occupying sites of potential coordination with the LC.

The results in Figure 5.2 demonstrate that the anchoring of the LC supported on the thin film of metal salt is dependent on the anion of the metal salt film. In general the anchoring of the LC at the metal salt interface is dependent on both the number of interactions and the strength of the individual interactions between the metal salt and LC. Two possible physical scenarios may, therefore, explain the observations shown in Figure 5.2. First, changes in the anion of the salt may influence the number of coordination interactions between the salt surface and the LC. Specifically, the more strongly coordinating anion may prevent the cation from participating in coordination interactions with the LC leading to fewer interactions (per unit area) between the metal salt and LC. Alternatively, the introduction of a strongly coordinating anion may decrease the strength of the individual interactions between the LC and the metal salt. This decrease in the strength of the individual interactions would not change the number of interactions at the interface. In this second scenario, there would exist a minimum strength of interactions between the metal salt and LC that is needed to cause the homeotropic alignment of the LC.

To distinguish between these two scenarios, we characterized the interactions between the nitrile group and the metal salt with mixed anions using PM-IRRAS. To obtain these results, it was necessary to make two changes to the experimental system. First, 5CB was replaced by the nitrile containing smectic 8CB to obtain stable thin films of the LC less than 1000 nm thick, as required for the PM-IRRAS measurements.[8] Second, the aluminum (III) salts were exchanged

for copper (II) salts of mixed anions (perchlorate and chloride) because the coordination interactions between copper perchlorate and 8CB have been well studied in the past,[8] and because the nitrile absorption peak in the IR spectrum is very weak when using aluminum (III).[31] As noted above, in the presence of water, past studies[8, 31] have demonstrated the copper (II)-nitrile complex to give rise to a stronger absorption band than the aluminum (III)-nitrile complex because water largely occupies the first coordination sphere of aluminum (III) and thus the nitrile group coordinates through the second and third coordination spheres of aluminum (III). For this reason, we focused our IR studies on characterization of the effects of anion composition on the copper (II) system. Here we emphasize that we described experiments earlier in this paper in which the anchoring behavior of nematic 5CB as a function of the surface composition of anions was shown to be similar for copper (II) salts and aluminum (III) salts (the change in tilt occurs at approximately 10% perchlorate/ 90% chloride when using copper (II)).

We measured IR spectra centered around the vibration of the nitrile group of 8CB in contact with copper (II) salts to characterize the intensity of the nitrile vibration frequencies in both the free and coordinated vibrational states. Figure 5.3 shows that, for 8CB in contact with 100% copper perchlorate, a free nitrile peak is observed at 2227 cm^{-1} and a coordinated nitrile peak is observed around 2281 cm^{-1}, consistent with past studies.[6, 8] The coordinated peak is attributed to 8CB interacting with the copper (II) perchlorate salts. When a strongly coordinating anion was introduced into the salt, the intensity of the peak due to the coordination interaction between the LC and copper cation decreased while the free nitrile peak increased. This result indicates that a smaller number of coordination interactions are formed between the metal salt surface and the 8CB as the fraction of non-coordinating anion in

the salt was increased. We quantified this change by calculating the ratio of the intensity of the coordinated nitrile peak to the sum of the intensity of the peaks corresponding to coordinated and free nitrile groups (Figure 5.3b). At low percentages of the perchlorate anion (compositions that did not lead to a homeotropic alignment of the LC), the coordinated nitrile peak was no longer measurable. We also note that the position of the maximum in the intensity of the coordinated nitrile peak was measured to be located at 2279 cm^{-1} to 2281 cm^{-1}. The location of the free nitrile peak remains constant at 2227 cm^{-1}. A previous study has shown that the location of the peak corresponding to a coordinated nitrile shifts to longer wave numbers with increase in the electron affinity of the metal (i.e., stronger coordination[6]). Because there is very little shift in the position of the coordinated nitrile peak in the measurements in Figure 5.3 and a significant decrease in the intensity of the coordinated nitrile peak (as evidenced by the ratio of the coordinated nitrile peak to the total intensity shown in Figure 3b), the IR analysis supports the hypothesis that there is a decrease in the number of coordination interactions between the nitrile moiety and the metal salt as the composition of the anions changes from being perchlorate rich to nitrate rich.

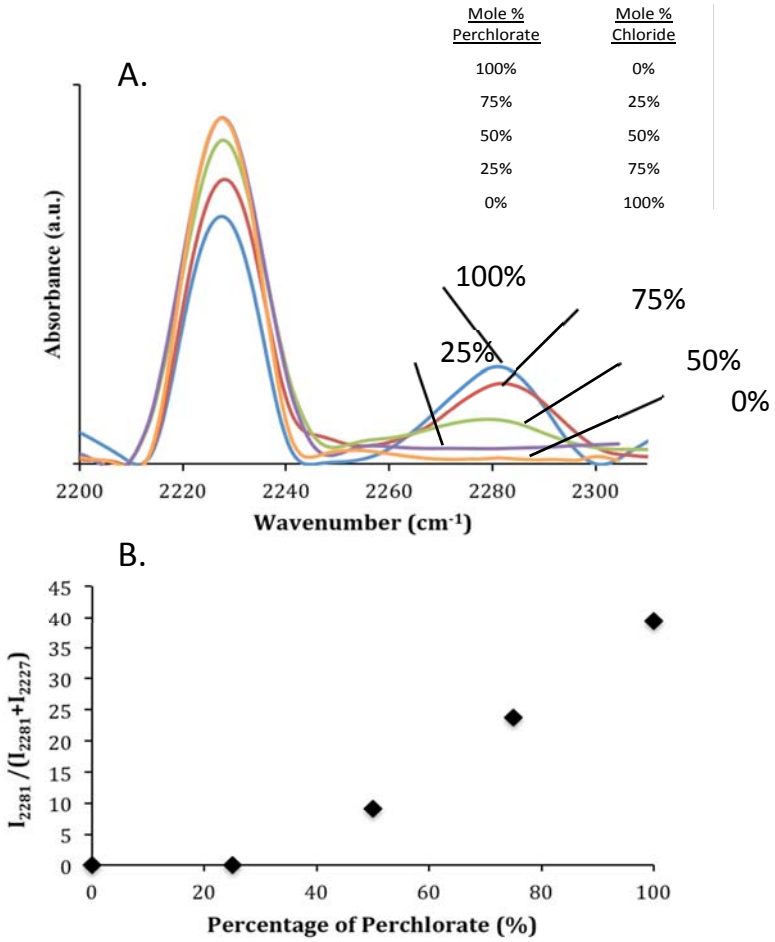

Figure 5.3. (A) PM-IRRAS spectra of 8CB films supported on copper (II) salts with mixed anions: blue (100% perchlorate), red (75% perchlorate and 25% chloride), green (50% perchlorate and 50% chloride), purple (25% perchlorate and 75% chloride), orange (100% chloride). (B) Ratio (expressed as a percentage) of the intensity of the coordinated nitrile peak at 2281 cm^{-1} to the sum of the intensity of the free nitrile peak at 2227 cm^{-1} and coordinated nitrile peak at 2281 cm^{-1}, plotted as a function of the perchlorate as the anion. See (A) for details.

In summary, to obtain a homeotropic alignment of the LC at the interface, we conclude that a threshold number density of coordination interactions (number per unit area of interface) between the LC and metal cation on the surface is required. The density of interactions can be engineered by controlling the ratio of weakly and strongly coordinating anions.

5.3.2 Effect of metal salt anions on the response of nematic 5CB to DMMP

This section expands upon the observations presented in the previous section by reporting how the anion composition impacts the response of an aligned LC system to the vapor analyte DMMP. As noted in the Introduction, past studies have shown that DMMP, when transported from the vapor phase to the metal salt interface, can displace the LC from the coordination complex with the metal salt. These changes in the molecular interactions occurring at the interface cause the LC to undergo an anchoring transition. In experiments described below, we tested the proposition that a lower number density of coordination interactions between the metal salt and LC, achieved by using mixed anions, would result in an alignment of the LC that is more easily disturbed by DMMP.

The optical response of a supported film of nematic 5CB to DMMP, plotted as a function of the composition of the anion of the aluminum salt, is shown in Figure 5.4. Figure 5.4a shows polarized light micrographs for situations in which the anion was 10% perchlorate and 90% nitrate, 50% perchlorate and 50% nitrate, or 100% perchlorate. Initially, the optical micrographs exhibit a dark appearance, consistent with homeotropic alignment of the 5CB at both the metal salt surface and air interface. In the presence of 1 ppm DMMP, the optical micrographs change to a bright appearance indicative of a change in the alignment of the LC at the metal salt surface from homeotropic to a planar or tilted alignment. As reported previously, this transition is a result of the disruption in the coordination complex formed between the metal salt and LC by DMMP.[8] Inspection of Figure 5.4a reveals that the time required for a measurable change in the LC film to be observed decreases as the amount of

perchlorate anion in the system is decreased. To quantify the effect of anion composition on the response, four central squares of each LC film were analyzed and the average intensity of light transmitted through cross polarizers was measured, as shown in Figure 5.4b (see Methods section). Figure 5.4b shows that the length of time required to measure an anchoring transition of the LC is influenced by the composition of the anion of the metal salt decorating the solid surface. Below we provide a quantitative analysis of the response shown in Figure 5.4b.

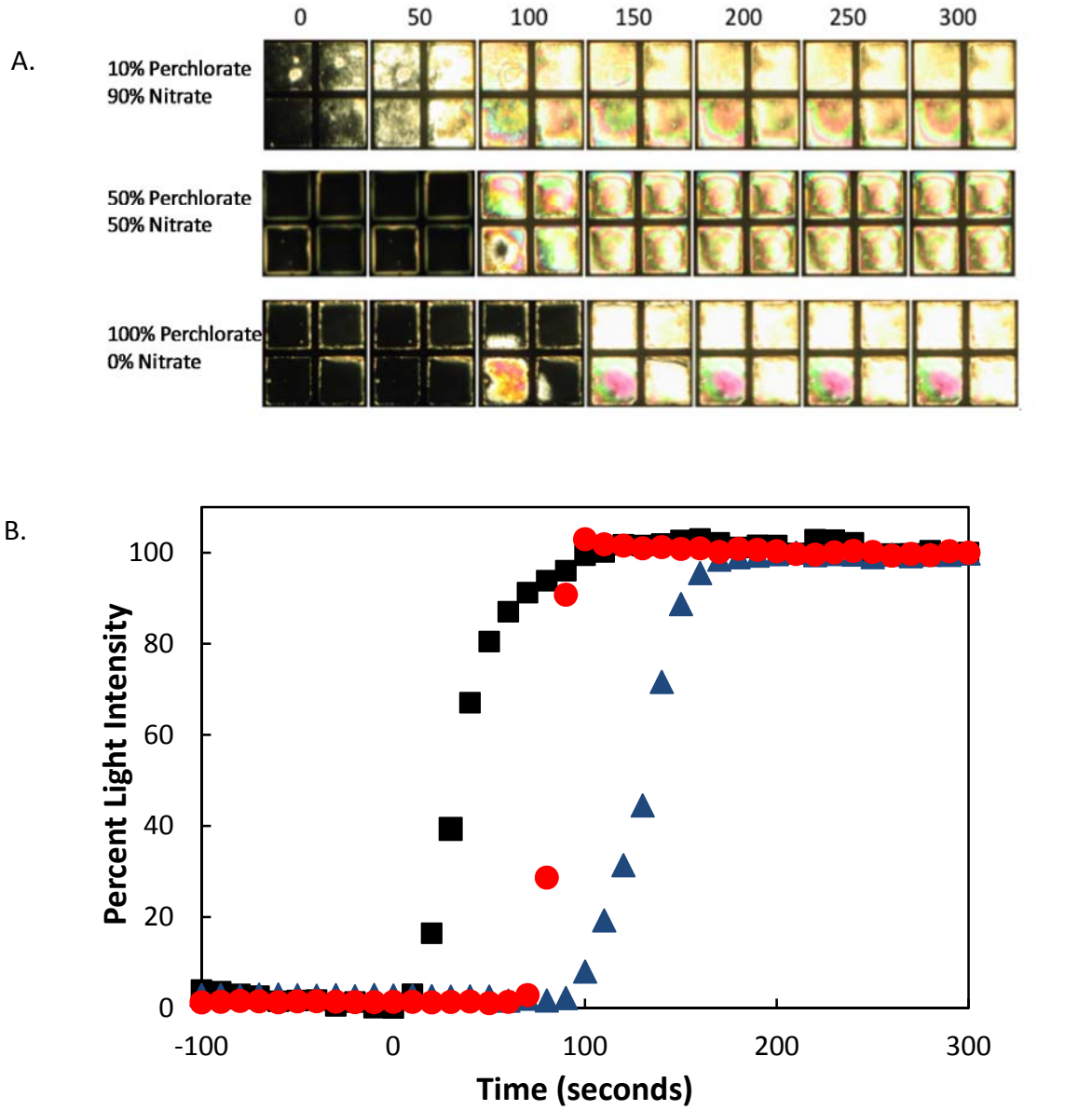

Figure 5.4. (A) Polarized light images of the response of LC films exposed to a vapor of 1 ppm DMMP at 0 seconds (prior to exposure each sample was exposed to air at 30% R.H.). The LC films were supported on surfaces coated with aluminum (III) salts (with the indicated anion composition). The flow rate of the gas over the sample was 1000 mL/min. The number above each image indicates the time (in seconds) of exposure to the DMMP. (B) Normalized light intensities for the images shown in (A). The black data points indicate aluminum (III) salt composed of a 10% perchlorate and 90% nitrate anion mixture, the red data points indicate aluminum (III) salt composed of a 50% perchlorate and 50% nitrate anion composition, and the blue data points indicate aluminum (III) salt composed of a 100% perchlorate anion.

Previously, we established that the LC anchoring on a metal salt surface is not changed by DMMP until a critical concentration of DMMP, $C_{min,LC}$, is accumulated within the LC film such that coordination of the LC and metal ion is disrupted.[15] The value of $C_{min,LC}$ is linearly related to the minimum concentration of DMMP in the vapor phase, C_{min}, based on Henry's Law. An estimate of C_{min} can be obtained by measuring the time of response, t_{on}, of the LC sensor system as a function of the concentration of DMMP in the vapor phase (C_∞) and analyzing the results using a simple mass transport model of the system. The relevant equation of the model that relates t_{on}, C_∞, and C_{min} is

$$t_{on} = \frac{\delta_{5CB}}{K_H \cdot k_{ov}} ln\left(\frac{C_\infty}{C_\infty - C_{min}}\right) \qquad (1)$$

where the thickness of the 5CB film is δ_{5CB}, the partitioning coefficient DMMP from air to LC is K_H, and the overall mass transfer coefficient is, k_{ov}. Based on our prior studies, these parameters are estimated as: k_{ov} = 0.24 cm/s, $K_H = 5.3 \times 10^{-5}$, and δ_{5CB} = 18 μm.[15]

By varying C_∞ and measuring the response time t_{on} (Figure 5.5a) we determined C_{min} for the LC films supported on metal salt films with three different mixed anion compositions (Figure 5.5a). The 100% perchlorate surface yielded a value of C_{min} of 250 ppb, whereas a 50% perchlorate/50% nitrate surface lead to a C_{min} of 110 ppb, and a 10% perchlorate/90% nitrate has the lowest C_{min} at 25 ppb, as shown in Figure 5.6. Overall, this result indicates that the sensitivity of the LC system can be substantially improved by using mixtures of weakly and strongly coordinating anions.

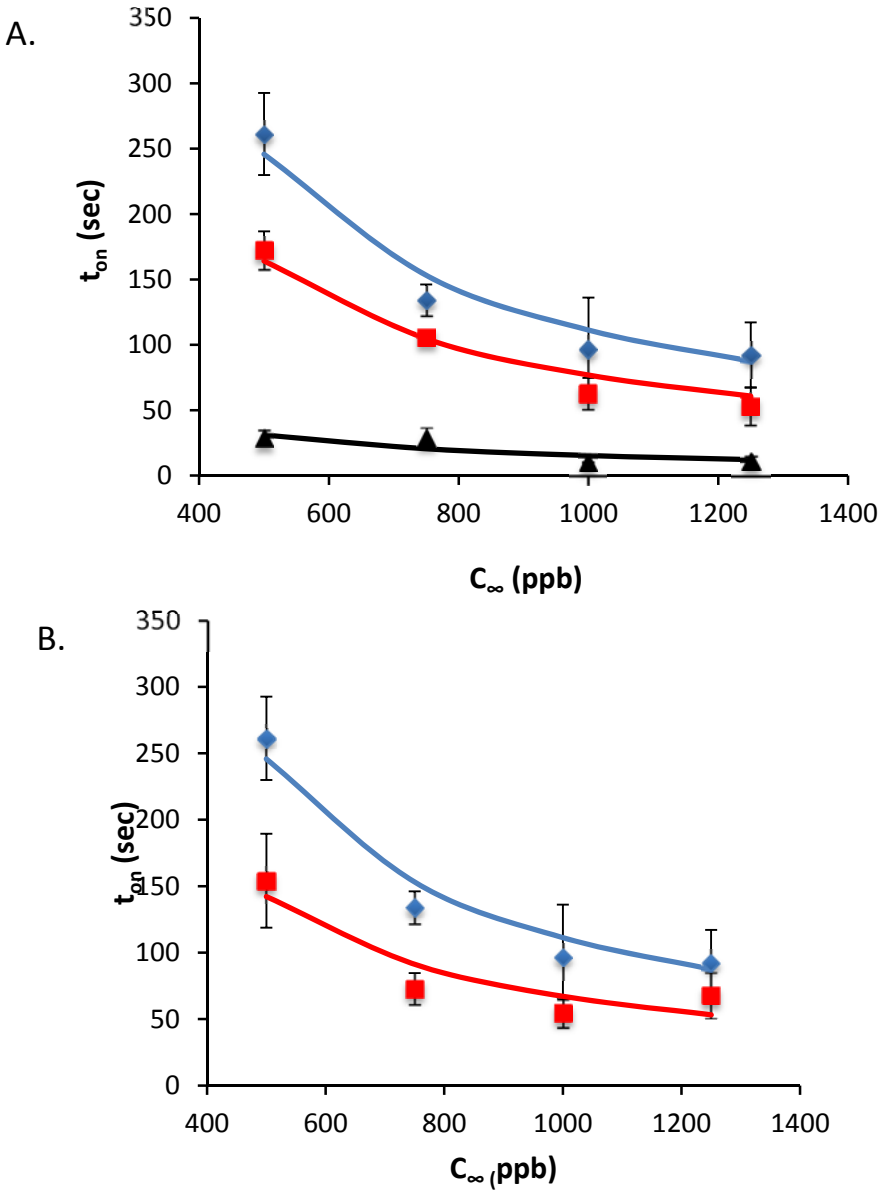

Figure 5.5. (A) The time of response (t_{on}) of LC films to DMMP as a function of DMMP concentration. The LC films were supported on surfaces that were coated with aluminum (III) salts with different anion compositions; blue (100% perchlorate), green (50%/ 50% nitrate/ perchlorate), black (90%/ 10% nitrate/perchlorate) (B) Comparison of t_{on} when using aluminum (III) salts with the anions being 100% perchlorate (blue) or 50%/ 50% perchlorate/ acetylacetonate (red).

To provide additional support for the above results, we measured the response of the LCs at the predicted sensitivities of the systems. The 100% perchlorate salt surfaces gave an

optical response when exposed to a 300 ppb environment of DMMP, but no optical response was seen at lower concentrations such as at 200 ppb. In contrast, a 10% perchlorate/ 90% nitrate mixture generated an optical response of the LC when the sample was exposed to 100 ppb of DMMP. These results provide general support for our conclusions regarding sensitivities that are based on measurements of t_{on}.

We also explored the extent to which the results above were seen in experiments performed with acetylacetonate. Figure 5.5b shows experimental results obtained with a mixture of 50% acetylacetonate and 50% perchlorate (by mole percent). From this data, C_{min} was calculated to be 100 ppb. This sensitivity is improved relative to that of the 100% perchlorate sample and similar to that of a 50%/ 50% perchlorate/ nitrate mixture suggesting that the bidentate anion also improves the sensitivity of the LC based system to DMMP. Overall, the results described above indicate that the sensitivity of the LC-based system increases as the anions of the metal salt are enriched in the more strongly coordinating anion (Figure 5.6).

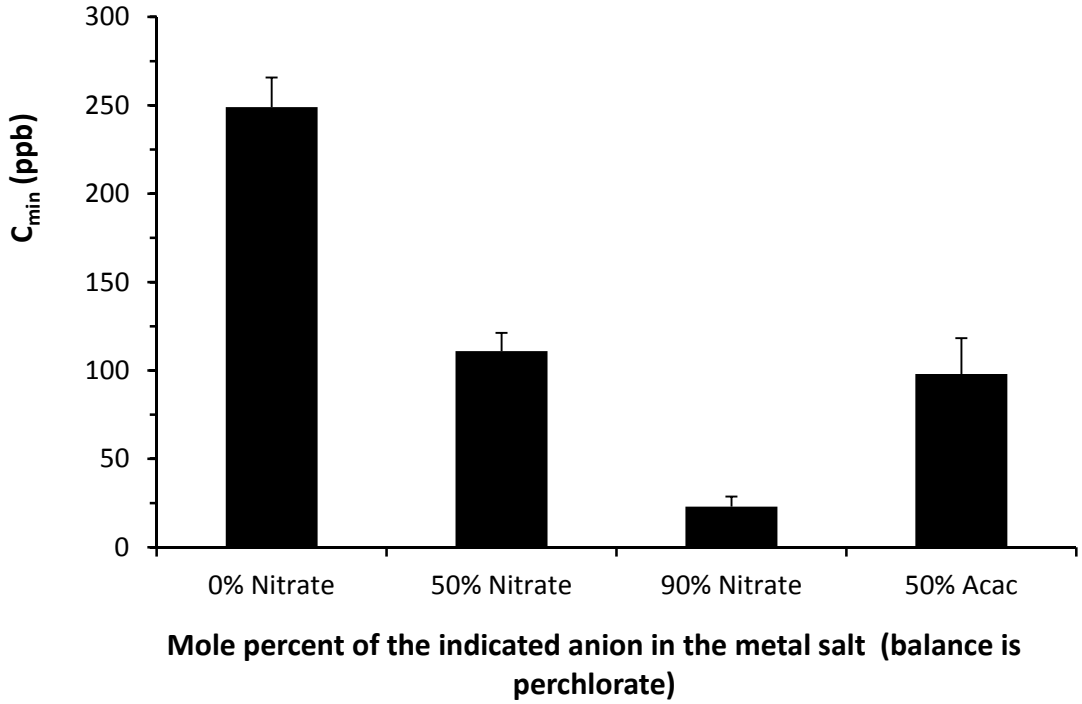

Figure 5.6. The influence of anion composition on the sensitivity of LC films to DMMP. The sensitivity (C_{min}) was determined using the model described in Equation 1 and the data shown in Figure 4. The error bars indicate the standard deviation of residuals from the fit in Figure 4.

The general observations reported above are consistent with a simple equilibrium model of the ligand exchange reaction occurring at the interface. In brief, we considered the ligand exchange reaction occurring at the surface as:

M-LC + DMMP → M-DMMP + LC (2)

where M-LC is the metal cation coordinated to the LC, DMMP is the concentration of free DMMP in the LC, M-DMMP is the metal cation coordinated to the DMMP molecules, and LC is the concentration of free mesogens within the system. We write the equilibrium constant for the ligand exchange as:

$$K = \frac{[M-DMMP][LC]}{[M-LC][DMMP]} \quad (3)$$

Because the ligand exchange reaction is occurring in the thin film of the salt, the number of binding sites remains constant and therefore the sum of [M-DMMP] and [M-LC] must be constant.

When the anchoring transition occurs in response to DMMP, we assume that binding of DMMP reduces the concentration of metal-LC interactions ([M-LC]) to a threshold level that we define as $[M\text{-}LC]_{crit}$. This threshold concentration of metal ion-LC interactions is given by the result shown in Figure 5.2. For mixtures of perchlorate and nitrate, the change in orientation of the LC occurred when using 10% perchlorate and 90% nitrate counter anion. Thus, we can write $[M\text{-}LC]_{crit}$ as $[M]x_{crit,}$ where [M] is the total metal binding sites in the salt film, and x_{crit} is the fraction of the total metal binding sites in the salt film that are accessible to the LC (i.e., x_{crit}=0.1 for perchlorate and nitrate). We calculate the number of [M-DMMP] interactions at the anchoring transition induced by DMMP as $[M]x_{perc}$ - $[M]x_{crit}$, where x_{perc} is the mole fraction perchlorate in the mixed anion in the experiment of interest (in general, $x_{perc} \neq x_{crit}$). The concentration of DMMP at which the anchoring transition takes place is defined above as C_{min} (calculated by equation 1). We assume that the concentration of the free LC, [LC], does not change significantly, and thus rewrite equation 3 as:

$$[C_{\min}] = \frac{[x_{perc} - x_{crit}]}{K[x_{crit}]} \qquad (4)$$

Equation 4 predicts that C_{min} plotted versus $(x_{perc} - x_{crit})/(x_{crit})$ is a straight line passing through the origin. Such a fit was obtained using the data in Figure 5.6 (see Figure 5.9 of supporting information). This agreement between the model and data is consistent with a ligand exchange reaction in which one mesogen is replaced by one DMMP molecule in the

coordination sphere of the aluminum (III). We end this discussion by noting that the above-described model is a very simple one that contains many assumptions, including that the equilibrium constant does not change as the mole fraction of perchlorate varies. Although simple, the model demonstrates the physical principles that underlie the dependence of the sensitivity of the LC films to DMMP on the total number of interactions between the surface and LC.

5.3.3 Influence of the metal salt anion on the effects of humidity

Whereas the studies described above were focused on the competitive interactions of DMMP and 5CB with aluminum (III) ions, the presence of other ligands that can potentially coordinate with aluminum (III) may influence the anchoring transitions induced by DMMP. For example, the coordination interactions of the nitrile moiety of acetonitrile with aluminum (III) perchlorate have been reported to be perturbed by high concentrations of water.[31-37] On the other hand, a past study of a metal salt-LC-DMMP system showed that ordering of the LC was not disrupted by concentrations of water up to 75% RH.[14] Below we expand upon these results by investigating the effects of humidity on the dynamics of DMMP-induced anchoring transitions (t_{on}), measured as a function of the composition of the anions in the aluminum (III) salt used to support the LC film.

Figure 5.7 shows t_{on} for the 100% perchlorate system and a 50% perchlorate/ 50% nitrate system when using 30% RH and 60% RH and a concentration of 500 ppb DMMP. Inspection of Figure 5.7 reveals the effect of a change in RH on the response of the LC to DMMP to be lower for the samples containing 50%/ 50% nitrate/ perchlorate as compared to 100%

perchlorate. We propose that this increased tolerance to water is due to the weaker interactions of water with the nitrate anion as compared to the perchlorate anion. Water is known to have weaker interactions with the nitrate anion because of the lower polarizability of the nitrate anion in comparison to the perchlorate anion.[38] We speculate that an accumulation of water around the aluminum (III) that is mediated by the perchlorate slows the ligand exchange process involving the DMMP, as is reflected in the dynamics of the anchoring transitions shown in Figure 5.7. Although the molecular-level details of the mechanism by which the substitution of nitrate for perchlorate changes the influence of water remain to be fully elucidated, the main conclusion of the experiment reported in this section is that changes in the composition of anions can be used to tailor the tolerance of LC-based sensors to potentially interfering compounds.

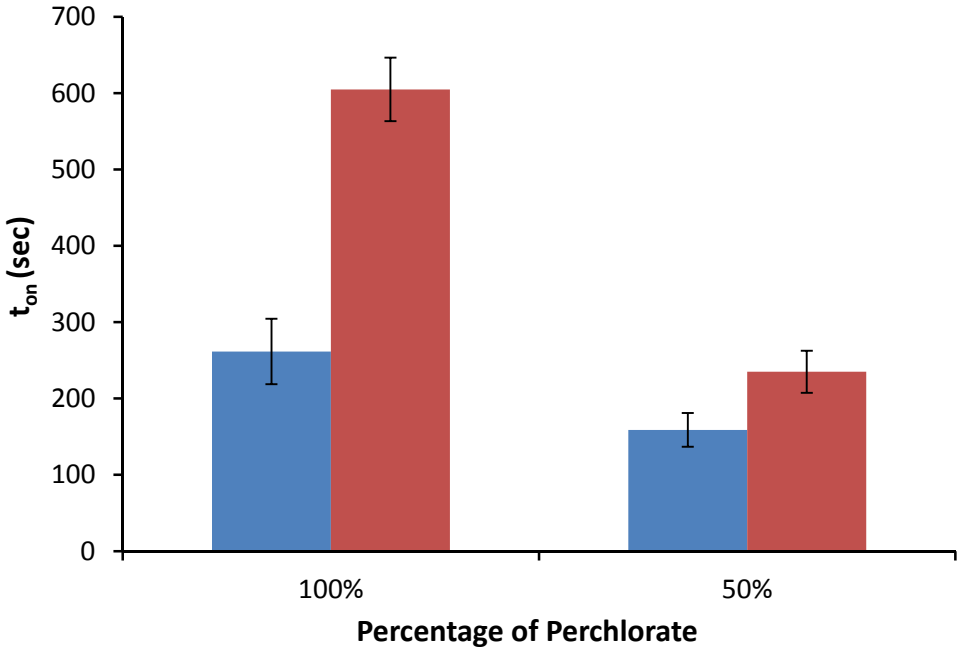

Figure 5.7. Measured values of t_{on} for a 100% perchlorate or a 50% perchlorate/ 50% nitrate salt surfaces (mole percent) under 30% humidity (blue) and 60% humidity (red) conditions at a concentration of 500 ppb DMMP.

5.4 Conclusions

The key result presented in this paper is that manipulation of the composition of mixed anions can be used to improve the sensitivity of adsorbate-induced anchoring transitions involving films of LCs supported on surfaces decorated with metal salts. Our results, which are supported by IR spectroscopic studies, suggest that the fraction of strongly coordinating anion within the salt can be used to regulate the number of coordination sites available to both the LC and DMMP. Furthermore, although the number of accessible coordinate sites on the metal cation on the surface does change with the choice of anion, our IR measurements suggest that the strength of the interactions is not substantially perturbed. Our results demonstrate that mixtures of anions can be used to improve the sensitivity of LCs to targeted adsorbates by at

least an order of magnitude. Furthermore, preliminary results also support the proposition that the anion composition can also be used to minimize the effects of potentially interfering compounds in designs of LC-based sensors. Overall, our results provide guidance for the design of responsive materials based on adsorbate-induced changes in the orientations of LCs.

5.5 Acknowledgements.

The authors thank Mr. John Cannon for help fabricating the metal plates and the flow cell. The study was funded primarily by the National Science Foundation (DMR-1121288, Materials Research Science and Engineering Center), with additional partial support from the Army Research Office (W911NF-11-1-0251 and W911NF-10-1-0181) and the National Institute of Health grant CA108467 and CA105730.

5.6 Supplementary Information.

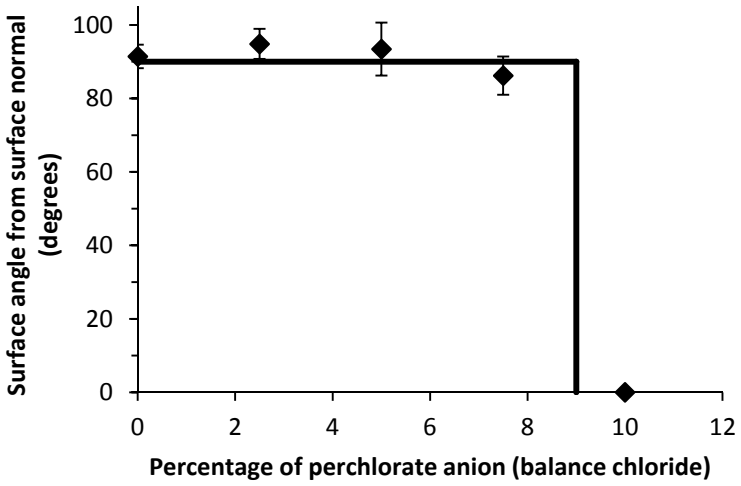

Figure 5.8. The measured tilt angle of 5CB at solid surfaces decorated with mixtures of copper (II) perchlorate and copper (II) chloride.

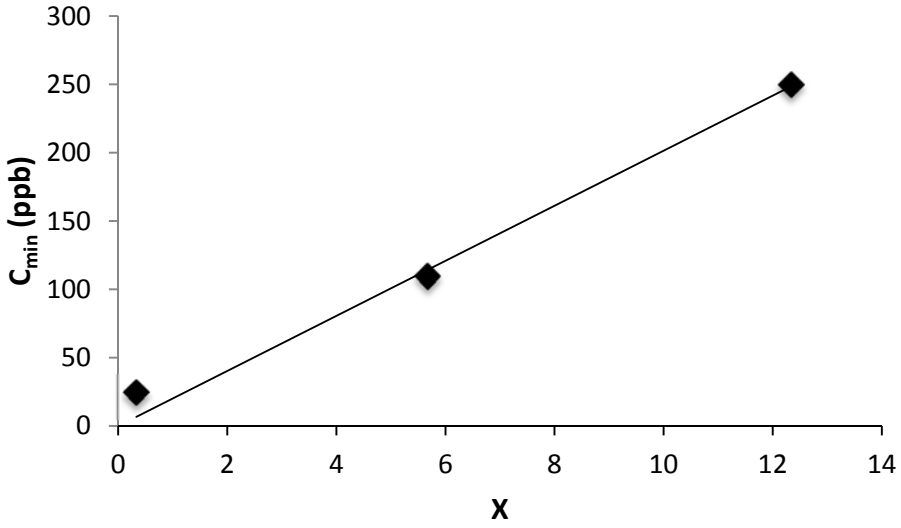

Figure 5.9. The sensitivity of the LC supported on aluminum (III) to DMMP (data from Figure 6) as it relates to X $(x_{perc} - x_{crit})/ x_{crit})$. The data is from the aluminum (III) perchlorate/ nitrate system. The line represents a best fit of a linear line that goes through the origin.

5.7 References

1. Shah, R. R.; Abbott, N. L. *Science* **2001,** *293*, 1296-1299.
2. Shah, R. R.; Abbott, N. L. *Langmuir* **2003,** *19*, 275-284.
3. Jerome, B. *Rep. Prog. Phys.* **1991,** *54*, 391-451.
4. Yokoyama, H. *Mol. Cryst. Liq. Cryst.* **1988,** *165*, 265-316.
5. Sanda, P. N.; Dove, D. B.; Ong, H. L.; Jansen, S. A.; Hoffmann, R. *Phys. Rev. A* **1989,** *39*, 2653.
6. Yang, K. L.; Cadwell, K.; Abbott, N. L. *J. Phys. Chem. B* **2004,** *108*, 20180-20186.
7. Sridharamurthy, S. S.; Cadwell, K. D.; Abbott, N. L.; Jiang, H. *Smart Mater. Struct.* **2008,** *17*, 4.
8. Cadwell, K. D.; Alf, M. E.; Abbott, N. L. *J. Phys. Chem. B* **2006,** *110*, 26081-26088.
9. Cadwell, K. D.; Lockwood, N. A.; Nellis, B. A.; Alf, M. E.; Willis, C. R.; Abbott, N. L. *Sens. Actuators, B* **2007,** *128*, 91-98.
10. Cheng, D. M.; Sridharamurthy, S. S.; Hunter, J. T.; Park, J. S.; Abbott, N. L.; Jiang, H. R. *J. Microelectromech. Syst.* **2009,** *18*, 973-982.
11. Hunter, J. T.; Abbott, N. L., Liquid Crystal-Based Chemical Sensors In *Liquid Crystals Beyond Displays: Chemistry, Physics, and Applications*, Li, Q., Ed.; Wiley: Hoboken, New Jersey, **2012**; pp 485-505.
12. Hunter, J. T.; Pal, S. K.; Abbott, N. L. *ACS Appl. Mater. Interfaces* **2010,** *2*, 1857-1865.
13. Pal, S. K.; Acevedo-Velez, C.; Hunter, J. T.; Abbott, N. L. *Chem. Mater.* **2010,** *22*, 5474-5482.

14. Yang, K. L.; Cadwell, K.; Abbott, N. L. *Sens. Actuators, B* **2005,** *104*, 50-56.

15. Hunter, J. T.; Abbott, N. L. *Sens. Actuators, B* **2013,** *183*, 71-80.

16. Wang, P.-H.; Yu, J.-H.; Zhao, Y.-B.; Li, Z.-J.; Li, G.-Q. *Sens. Actuators, B* **2011**.

17. VanTreeck, H. J.; Most, D. R.; Grinwald, B. A.; Kupcho, K. A.; Sen, A.; Bonds, M. D.; Acharya, B. R. *Sens. Actuators, B* **2011,** *158*, 104-110.

18. Namkung, J.; Zou, Y.; Abu-Abed, A.; Lindquist, R. G. *IEEE Sens. J.* **2010,** *10*, 1479-1485.

19. Stewart, C. E. *Weapons of mass casualties and terrorism response handbook*. Jones & Bartlett Learning: Sudbury, MA, **2006**.

20. Sen, A.; Acharya, B. R. *Liq. Cryst.* **2011,** *38*, 495 - 506.

21. Tatsuya Urabe, T. T. M. T. *J. Mass Spectrom.* **2009,** *44*, 193-202.

22. Edwards, J. O. *J. Am. Chem. Soc.* **1954,** *76*, 1540-1547.

23. Parr, R. G.; Pearson, R. G. *J. Am. Chem. Soc.* **1983,** *105*, 7512-7516.

24. Pearson, R. G. *J. Chem. Educ.* **1968,** *45*, 581-587.

25. Pearson, R. G. *J. Chem. Educ.* **1968,** *45*, 643-648.

26. Pearson, R. G. *Inorg. Chem.* **1988,** *27*, 734-740.

27. Pearson, R. G. *Chem. Br.* **1991,** *27*, 444-447.

28. Yamada, S.; Tanaka, M. *J. Inorg. Nucl. Chem.* **1975,** *37*, 587-589.

29. Acharya, A. S. B. R. *Liq. Cryst.* **2011,** *38*, 495-506.

30. Lockwood, N. A.; Gupta, J. K.; Abbott, N. L. *Surf. Sci. Rep.* **2008,** *63*, 255-293.

31. Jamroz, D.; Wojcik, M.; Lindgren, J.; Stangret, J. *J. Phys. Chem. B* **1997,** *101*, 6758-6762.

32. Jamroz, D.; Stangret, J.; Lindgren, J. *J. Am. Chem. Soc.* **1993,** *115*, 6165-6168.

33. Ruben, Y.; Reuben, J. *J. Phys. Chem.* **1976,** *80*, 2394-2400.

34. Supran, L. D.; Sheppard, N. *Chem. Commun. (London)* **1967**, 832-834.

35. Cho, H.-G.; Andrews, L. *J. Phys. Chem. A* **2010,** *114*, 5997-6006.

36. O'Brien, J. F.; Alei, M. *J. Phys. Chem.* **1970,** *74*, 743-746.

37. Richardson, D.; Alger, T. D. *J. Phys. Chem.* **1975,** *79*, 1733-1739.

38. Atkins, P.; De Paula, J. *Physical Chemistry*. 7 ed.; Oxford University Press: New York, **2006**.

Chapter 6: Analyte Induced Anchoring Transitions of Thin Films of Chiral Nematic Liquid Crystals Supported on Surfaces Decorated with Metal Perchlorate Salts

6.1 Introduction.

Thermotropic liquid crystals (LCs) exhibit a temperature dependent nematic phase in which the mesogens display long-range orientational order and can be sensitively oriented by physical or chemical interactions with confining interfaces.[1] These properties allow the ordering within the bulk LC material to be controlled by engineering the surfaces that confine the material, as the long-range order causes the preferred alignment at the surfaces to propagate tens of micrometers away from the interface. As the confining dimensions of the LC material are decreased, the bulk elastic properties of the LC become of greater importance relative to the surface anchoring. For example, there exists a bulk elastic energy due to strain or deformation of the LC confined within a micrometer-thick film in a so-called hybrid alignment of the LC (when one surface supporting the LC gives a homeotropic alignment while the other surface gives a planar alignment of the LC), and this energy (strain) increases in magnitude when the thickness of the LC film is decreased. If the film becomes thin enough, the bulk elastic energy of the LC film can disrupt the surface anchoring of the LC at the surface with the weaker surface anchoring (e.g., the alignment of the LC within the film follows the preferred alignment of LC at the surface with stronger anchoring).[2-3]

Past work has shown that intermolecular interactions such as coordination interactions occurring between solid interfaces decorated with high electron affinity metal salts (e.g. Al (III)

perchlorate) and nitrile containing LCs (e.g. 4-Cyano-4'-pentylbiphenyl, 5CB) result in a perpendicular (homeotropic) alignment of the LC at the interface (homeotropic). At an air-LC interface the ordering of the LC also adopts a homeotropic orientation.[4-5]

When a LC film supported by the metal salt decorated surface, initially exposed to air, is exposed to certain targeted vapor analytes, an ordering transition of the LC at the metal salt surface is observed where the surface anchoring of the LC changes from homeotropic to planar. This causes an optical change from a dark to bright appearance when the sample is viewed through crossed polarizing films due to the resulting hybrid alignment.[4-7] It has been determined that this ordering transition is due to the disruption of the coordination interactions between the LC and the metal salt by the vapor analyte.[7] In addition, the dynamics of the response are governed by the rate of accumulation of the vapor analyte in the LC film. Thus, the thickness of the LC film is observed to be an important parameter to minimize in order to decrease the accumulation time of the analyte into the LC film, and thereby decrease the time of response of the system.[8] A particularly interesting illustration of these principles is disruption of the coordination interaction between the Al (III) perchlorate metal salt and the 5CB by dimethyl methylphosphonate (DMMP), because this molecule contains an organophosphonate chemical moiety that is found in many toxic species such as certain nerve gases (e.g. sarin) and pesticides (e.g. parathion). It is important for health concerns to be able to detect these species at low vapor concentrations of parts-per-billion (ppb) or parts-per-million (ppm) in as little time periods as possible.[9] Therefore, we wish to utilize a system that minimizes the thickness of the LC film and alters the effects of the elastic energy in order to increase the responsiveness of the system.

In the present study, we study the effect that the elastic energy of the system has on the time of response of the LC sensor system as the thickness of the LC film becomes small. We hypothesize that the elastic energy penalty in going from a uniform homeotropic to a hybrid system upon introduction of the vapor analyte will influence the time of response for thin films of LC. The time of response is expected to decrease as the film thickness decreases from 20 µm to a critical value. However we propose that as the thickness of the LC film is further decreased, the time of response of the system should begin to increase due to the influence of the elastic penalty.

Furthermore, in this study, we investigate the introduction of chiral LCs in this system by adding a chiral dopant into 5CB in order to utilize the elastic energy of the LC to increase responsiveness of the system to DMMP. A chiral dopant introduced into a nematic LC causes the LC to organize into a helical structure with a pitch (p) on the order of micrometers thus forming a chiral LC. The pitch length is inversely proportional to the concentration of the chiral dopant (at low dopant concentrations). For chiral LCs to accommodate the anchoring conditions of the confining interfaces, the ordering of the LC adopts an orientation that is dependent on the pitch length of the LC (p), the thickness of the LC film (d), and the anchoring conditions at the solid surfaces.[10-12]

We explore the role of the chiral LCs on the elastic penalty for small values of the LC film thickness. We propose that the system will begin in a strained state with the chiral LCs supported on surfaces that give a homeotropic alignment, and the transitioning to a hybrid alignment of the LC can alleviate this strain. The ordering transition of the chiral LCs for this system is caused by a change in the surface anchoring of the chiral LC which has been not been

explored in the literature previously. In order to fully understand the influence of the chiral LCs, we use chiral LCs with pitch lengths greater than, equal to, and less than the thickness of the LC film.

The research explored in this study can be applied as guidance for the optimal design of vapor sensors based on anchoring transitions of LCs caused by the presence of vapor analytes. By the addition of the chiral doping agent into the LC, the anchoring transition to the hybrid anchoring conditions when exposed to DMMP may be optimized to achieve shorter response times through control of the film thickness and pitch length of the LC.

6.2 Experimental Methods

6.2.1 Materials

Al (III) perchlorate nonahydrate and trichloro(octydecyl)silane (OTS) were purchased from Sigma Aldrich (Milwaukee, WI). 5CB and ZLI-811 were purchased from EMD Chemicals (Gibbstown, NJ). Methanol and Fischer's Finest glass slides were purchased from Fischer Scientific (Pittsburgh, PA). Absolute ethanol (anhydrous, 200 proof) was purchased from Pharmco-AAPER (Brookfield, CT). The polyimide (PI 2556) was purchased from HD MicroSystems (Parlin, NJ). SU-8 2010 and SU-8 2050 photoresists and SU-8 solvent developer were purchased from MicroChem (Newton, MA). All chemicals and solvents were of analytical reagent grade and were used as received without any further purification. All deionized water used in the study possessed a resistivity of at least 18.2 MΩ cm.

6.2.2 Methods

6.2.2A Fabrication of the microwells.

Glass microscope slides were cleaned by rinsing in ethanol and then dried under a stream of nitrogen at least three times. Treatment with oxygen plasma was then carried for 10 minutes (250 W RF power, 50 cm^3/min oxygen gas flow) to remove any organics from the surface. Oxygen plasma used a PE-200 Benchtop System from Plasma Etch (Carson City, NV). SU-8 2010 or SU-8 2050 was spin-coated into substrates at different spin speeds to obtain films with thickness in the range of 2-20 μm. Photolithography was then carried out according to the specifications by the manufacturer. An emulsion photomask with a dot pattern (200 μm in diameter) was purchased from Advance Reproductions Corp. (Andover, MA). Photolithography was carried using a 365-nm UV cross-linker from Spectronics Corporation (Westbury, NY). (Tridecafluoro-1,1,2,2-tetrahydrooctyl)-trichlorosilane was purchased from Gelest (Morrisville, PA).

6.2.2B Creating the chiral doped LC:

This study focused on concentrations of the chiral agent (ZLI-811) doped into the LC (5CB) on the order of 0.0 – 3.0% (by weight). In order to create these concentrations, we dissolved the chiral dopant into toluene at a defined concentration. Then the stock solution was added into the 5CB at the defined amount in order to control the amount of the chiral doping agent in the 5CB. After adding the toluene solution to the LC, the mixture became isotropic. The toluene was removed from the sample by a combination of flowing dry nitrogen

over the mixture, heating up the solution to ~60 °C, and allowing the toluene to evaporate until the solution returned to the nematic phase.

6.2.2C Chemically functionalizing and filling the microwells.

After the microwells were fabricated, the wells were functionalized, filled, and exposed to DMMP within three hours. To begin, the wells were plasma oxidized using the procedure utilized previously. Next, a 5 mM ethanolic solution of Al (III) perchlorate salt was spin coated onto the microwell surface using a speed of 3000 rpm for 1 minute. The functionalized wells were filled with the desired LC by spin coating the LC solution at 3000 rpm for 1 minute.

6.2.2D Creating chemically functionalized wedge cells with differing boundary conditions.

In order to understand the change in the pitch of the chiral LC along with the anchoring of the LC under homeotropic, hybrid, and planar alignment conditions, wedge cells were fabricated such that we had well-defined anchoring at each interface. In order to create the homeotropic alignment, the glass slides were functionalized with an OTS coating (method from a previously published study). For a planar alignment, the glass surfaces were decorated with a thin layer of polyimide, PI (spin coating the polymer at 3000 rpm, and cross-linking the sample at temperatures greater than 200 °C). In order to test the interaction with DMMP, surfaces were also decorated with Al (III) perchlorate (in a manner similar to the functionalization of the microwells). The wedge cells were assembled with a spacer of a defined thickness (5 μm or 10 μm) at one end and no spacer at the other end such that the slides were in contact with each other. The LC was filled into the sandwich cell in the nematic phase. For the OTS-OTS wedge cell, the sample was brought into the isotropic phase for best filling.

6.2.2E Exposing the filled microwells to a vapor of DMMP

The microwells, prepared as described above, was exposed to a stream of air containing DMMP within a flow cell that was constructed to direct the flow of air across the LC samples while permitting simultaneous observation of the samples through a polarized light microscope (CH40, Olympus, Melville, NY). The stream of gas containing DMMP was generated using a certified cylinder containing 10 ppm DMMP in nitrogen (Matheson Tri-Gas Inc, Eagan, MN). The gas of DMMP was diluted by air at a specified relative humidity (RH). The RH of the air was controlled using a portable dew point generator (LI-610, LI-COR Biosciences, Lincoln, NE). The temperature of the gas fed to the flow cell was maintained at room temperature (25 °C) and the RH was controlled to 30% unless indicated otherwise. The flow system was plumbed using 1/16'' stainless steel Swagelok tubing (Badger Fluid System Technologies Milwaukee, WI). The flow rate of the gas through the exposure system was controlled using a series of rotameters (Aalborg Instruments & Controls, Inc., Orangeburg, NY). The concentration of DMMP used in the study reported in this paper ranges from 500 ppb to 1,000 ppb and the overall volumetric flow rate of the gas stream passed over the samples remained constant at 1000 mL/min.

The flow cell was fabricated by machining a rectangular prism of aluminum metal. Glass windows allowed transmission of polarized light through the flow cell. The intensity of light that was transmitted through the LC sample in the flow cell was recorded using an Olympus camera (Olympus C2040 Zoom, Melville, NY). The total volume of the flow cell was 10.5 cm^3 (6 cm x 3.5 cm x 0.5 cm), giving rise to a gas residence time of ~0.6 sec when the flow rate was

1000 mL/min. The Reynolds number was calculated to be 51 for airflow within the flow cell at 1000 mL/min, corresponding to laminar flow.

6.2.2F Analyzing the Fast Fourier Transform (FFT) of the cross-polarizer micrographs of the LC film

The cross polarizing micrographs were analyzed by transforming the image to the FFT using ImageJ. The FFT was analyzed by calculating the radial average of the FFT image. The radius of the FFT was converted to the characteristic length of the sample. From the raw data, the intensity at certain characteristic lengths was compared for the various images that were obtained from the exposure of the system at various times.

6.3 Results

6.3.1 Effect of elastic energies on the time of response of the system.

The first section of this study focuses on the effect of bulk elastic energies on the dynamics of the LC vapor-sensing system in the absence of a chiral dopant. Specifically, we investigate how the LC film thickness affects the time of response of the system as it is exposed to low concentrations of the vapor analyte DMMP. A previous study has shown that the time of response is a result of an accumulation of DMMP within the LC film, and therefore dependent on the thickness of the LC film. This behavior is shown in Equation 1.[8]

$$t_{on} = \frac{d}{K_H \cdot k_{ov}} ln\left(\frac{C_\infty}{C_\infty - C_{min}}\right) \qquad (1)$$

In Equation 1, the time of response is t_{on}, the thickness of the 5CB film is d, the partitioning coefficient of DMMP from air to LC is K_H, the overall mass transfer coefficient is k_{ov}, the vapor

concentration of DMMP is C_{∞}, and the minimum concentration of the sample is C_{min}. In order to test the validity of Equation 1 for the effect of LC film thickness, we measured the time of response of the LC sensor system as a function of the thickness of LC film by supporting the LC within microwells of various thicknesses as shown in Figure 1. Past work has shown that the thickness of the LC film is closely related to the thickness of the microwells. Figure 1a is comprised of crossed polarized micrographs of nine wells that are approximately 8 μm in thickness as they are exposed to 1 ppm DMMP vapor at 0 seconds. From the images in Figure 1a, we observed the wells to go from a uniform dark appearance to a bright appearance after 200 seconds when viewed through crossed polarizers, indicative of a transition of the LC at the metal salt surface from a homeotropic to a planar alignment of the LC. The wells reach a steady state in terms of the appearance of colors after 300 seconds. The average light intensity of each of the wells is measured as a function of the time and averaged to give the response shown in Figure 1b. The time of response is calculated by fitting the initial change in light intensity to a line and calculating the value at which the line crosses the x-axis.

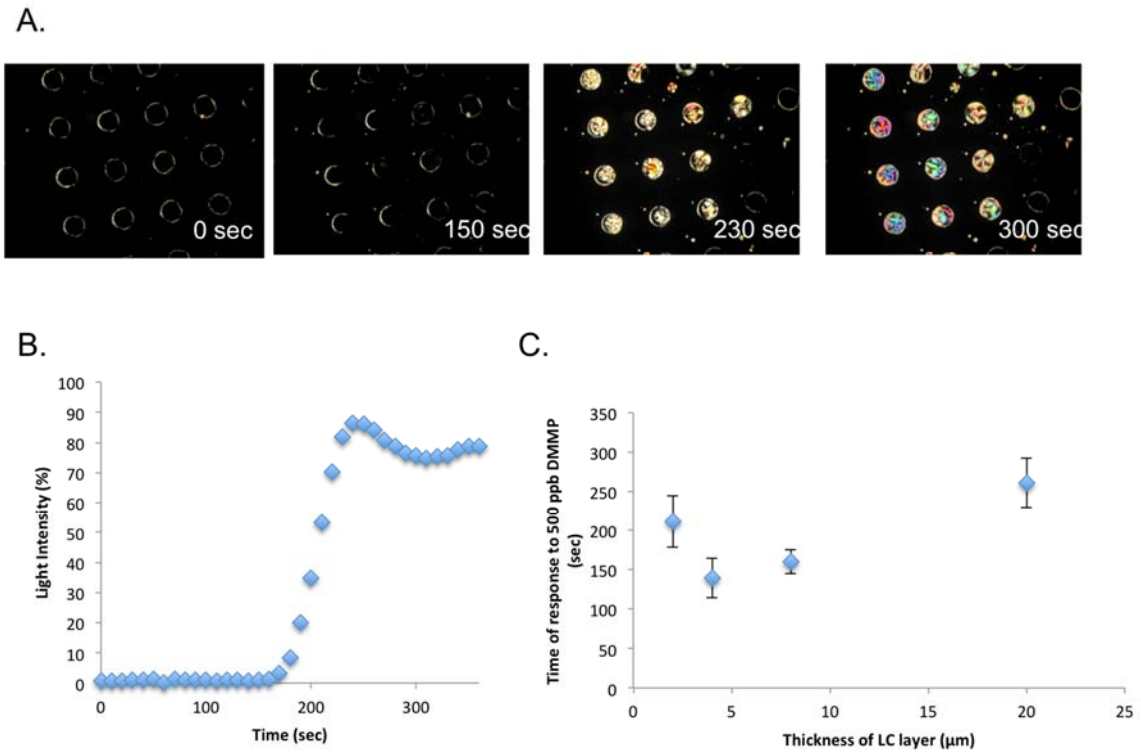

Figure 6.1. (A) shows polarized light micrographs of 8 µm thick LC films supported on Al (III) perchlorate decorated surfaces and exposed to 1 ppm DMMP at 0 seconds. The diameter of each microwell is 200 µm. (B) shows the average of the normalized light intensity of 9 microwells from the sample shown in (A) as it was exposed to the DMMP vapor. The time in which the light intensity increases is the time of response for the sample. (C) shows the average time of response for thin films of varying film thickness exposed to 500 ppb DMMP.

By varying the thickness of the microwell supporting the LC film, the effect of the LC film thickness on the time of response is investigated. The average of the time of response for three independent samples of nine wells of varying thicknesses exposed to 500 ppb DMMP is shown in Figure 1c. For thicknesses ranging from approximately 20 µm to 4 µm, the time of response decreased as the film thickness decreased as expected from Equation 1. However, as the film thickness decreased further to 2 µm, the time of response increased when compared to the 4 µm thick LC film. In order to explain this result, we hypothesize that the bulk elastic energies of the LC film affect the time of the response for the system for thin films of LCs. In these

experiments, the initial state of the homeotropic alignment of the LC film contains no bulk elastic strain. However when DMMP is introduced into the system, the alignment at the bottom surface changes to planar alignment. This change in the boundary conditions introduces strain into the system in order to accommodate both differing boundary conditions (hybrid alignment). This bulk elastic strain has been investigated in previous studies and has been shown for systems with hybrid anchoring conditions to follow Equation 2 (with various assumptions discussed in the past studies[1]).

$$F_{el} = \frac{K\pi^2}{8d} \qquad (2)$$

In Equation 2, F_{el} is the bulk elastic energy, K is the one constant approximation of the elastic constant of the LC, and d is the thickness of the LC. Equation 2 demonstrates that the bulk elastic strain of a hybrid-aligned system is inversely proportional to the thickness of the LC film. Therefore, we expect that this elastic strain becomes more important for very thin films of LC. We attribute the increase in the time of response for LC vapor sensors at small thicknesses to the increase in the elastic energy of the system as indicated by Equation 2.

In order to test the proposed hypothesis, we used wedge cells, which confine a LC film between two solid surfaces, in order to study the effect of thickness under different boundary conditions. By using surfaces with known boundary conditions, specifically, surfaces decorated with either Al (III) perchlorate (initially homeotropic, responsive to DMMP), OTS (homeotropic), or PI (planar), we are able to control whether or not there is strain in the initial (and final) state of the LC system. By measuring the length of the bright region or change in interference colors of the LC film, we aim to determine the penetration of DMMP into the wedge cell, and the

effect of the thickness under the different anchoring conditions. The wedge cell was fabricated by separating one end of the cell with a 5 μm spacer and allowing the glass substrates to be in contact at the other end of the wedge cell. The wedge cell was then filled with the LC in the nematic phase.

The first case that we tested consisted of a wedge cell with both of the surfaces decorated with Al (III) perchlorate. We expect that both surfaces give an initial homeotropic alignment when the wedge cell is in air and that when the LC film is exposed to DMMP for a sufficient duration of time both of the surfaces would transition to a planar alignment. The penetration of DMMP into the edges of the wedge cell triggers an anchoring transition that is shown by the bright stripe in Figure 2a. We see that the width of the bright region is related to the square root of the time of exposure, consistent with diffusion of DMMP into the edges of the wedge cell (shown in the supporting information). In this case, the interference colors of the film are consistent with a transition to planar anchoring at both surfaces when the sample is exposed to DMMP. From this figure, we see that the penetration of the bright region of the LC film after 2 hours of DMMP exposure is constant as the thickness of the LC film goes from 5 μm to 0 μm as quantified in the blue data of Figure 2d. The data points of Figure 2d represent the results of two independent wedge cells with both surfaces decorated with Al (III) perchlorate.

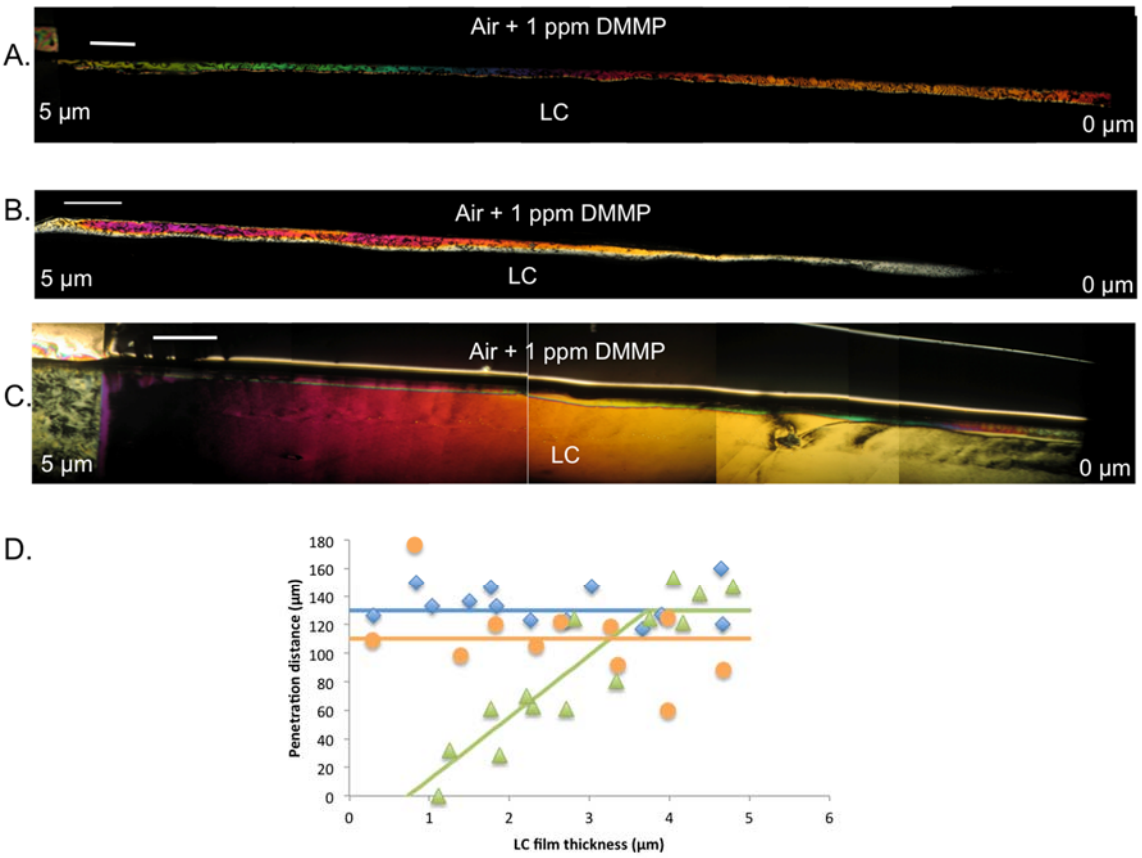

Figure 6.2. (A-C) are polarized light micrographs of 5CB wedge cells (one end 5 µm and the other in contact) fabricated with varying surfaces and then exposed to 1 ppm DMMP. A wedge cell with both surfaces decorated with Al (III) perchlorate and filled with 5CB is shown in (A), a wedge cell with one surface OTS coated and one surface Al (III) perchlorate decorated and filled with 5CB is shown in (B), and a wedge cell with one surface PI coated and one surface decorated with Al (III) perchlorate and filled with 5CB is shown in Figure C. (D) quantifies the penetration length of the bright regions as a function of the thickness of the LC film. The blue diamonds represent symmetric Al (III) perchlorate wedges as in (A), the green triangles represent OTS/Al (III) perchlorate wedges as in (B), and the orange circles represent PI/Al (III) perchlorate wedges as in (C). The scale bars for each image represent 500 µm.

Next, we studied a system that goes from a symmetric homeotropic alignment to a hybrid alignment when the system is exposed to DMMP. In this case, we use one surface decorated with the Al (III) perchlorate and one surface decorated with OTS that remains homeotropic even when it is exposed to DMMP. In this system upon penetration of DMMP into the LC film,

the bright region of the LC contains lower-order interference colors (relative to Figure 2a, which has symmetric planar boundary conditions) consistent with the transition to a hybrid alignment of the LC as shown in Figure 2b. We calculated the width of the bright region to indicate the penetration of the anchoring transition due to DMMP after 2 hours of exposure in the LC film for two independent samples shown in the green data points in Figure 2d. We see that the thickness of the bright region decreases as the LC film thickness decreases. This result is consistent with our hypothesis presented above that the hybrid boundary conditions can inhibit the anchoring transition of the thin LC films when exposed to DMMP due to the bulk elastic strain.

Finally, we studied a system where we initially start in a hybrid anchoring alignment, and upon introduction of DMMP we transition to a uniform planar anchoring. According to our hypothesis, this geometry should enhance the anchoring transition, especially for thin films of the LC, by releasing the strain upon the system upon the anchoring transition. In order to accomplish this, we decorated one surface with a PI coating and the other surface is decorated with Al (III) perchlorate. Under these conditions, we expect hybrid anchoring conditions initially. The results of this case are shown in Figure 2c and quantified for two independent samples as the orange data in Figure 2d. An example of this system is shown in Figure 2c. From this image, we see the appearance of the LC film in terms of the lower interference colors suggesting hybrid anchoring conditions. However, the observation of the diffusion front of DMMP at which the sample responds to DMMP is not as clear when compared to the two systems discussed above. For thick portions of the wedge, we observe a front where the LC anchoring changed, but the color that the LC exhibits post-transitions is very similar to the

initial retardance colors. This was an unexpected observation. One hypothesis to explain this observation was that the DMMP was also interacting with the PI film to cause a weak homeotropic anchoring. In this case we have a reversal of the hybrid anchoring of the sample but the end result is the same and the retardance colors do not change significantly. The observation of the front would just be an indication that the DMMP interacts with one surface more favorably when compared to the other surface. In the case of thin surfaces, we see a penetration of the LC that increases the retardance of the LC relative to the initial state of the film. In this case, we assume that the DMMP interacting with the PI surface and gives a very weak homeotropic alignment. Therefore at the small LC film thicknesses, the anchoring at the salt surface dominates and the sample transitions to a uniform planar LC alignment based on the stronger anchoring surface. From these studies, it is clear that future experiments are needed to explain the result of this case and to understand the effect of this system on the anchoring transition of the LC.

In this section of the study, we have demonstrated that the generation of bulk elastic strain imposed on the system during hybrid anchoring conditions can inhibit the anchoring transition of the LC vapor sensor to DMMP for LC film thicknesses that are less than 4 μm. The remainder of this study will focus on ways of utilizing this strain by using LCs that are doped with a chiral dopant.

6.3.2 Properties of adding a chiral dopant into a nematic LC

This section of the study will focus on the introduction of the chiral dopant ZLI-811 into nematic 5CB and the resulting alignment of the chiral LC on surfaces with defined anchoring

conditions. By performing these experiments, we sought to confirm what has been reported in the literature previously and guide us in our observations of the change in the alignment of the chiral LC sensor system when DMMP is introduced into the system.

Past studies have shown that the addition of a chiral dopant into a nematic LC causes the mesogens of the LC to arrange to give the LC a twist on the order of micrometers. The distance of the LC that is required for the LC to make a complete 360 degree rotation is called the pitch (p) of the chiral LC. The pitch of the chiral nematic LC is inversely proportional to the concentration of the chiral dopant introduced into the LC as shown in Equation 3.[10]

$$\frac{1}{p} = \beta c r \qquad (3)$$

In Equation 3, β is the helical twisting power of the chiral dopant, *c* is the concentration of the chiral dopant, and *r* is the enantiomeric excess of the chiral dopant.

First, we study the alignment of the chiral LC of varying chiral dopant concentrations on surfaces that give a defined homeotropic orientation, i.e. sandwiched between two glass slides functionalized with OTS, for varying thicknesses of the LC film. Past studies have indicated that there are three regions of interest for the alignment of the chiral LC on homeotropic surfaces. For film thicknesses that are larger than the pitch length, a bright appearance throughout the sample is observed through crossed polarizers that is formed from the overlapping of the so-called fingerprint patterns, referred to as a translationally invariant configuration (TIC).[13] This behavior is seen in Figure 3a for a 2% chiral LC that is approximately 7 μm thick. Likewise, Figure 3d shows a similar behavior for a 1% chiral LC for a film that is 10 μm thick. A diagram of the LC alignment for Figure 3a and d is sketched in Figure 3g for this TIC.

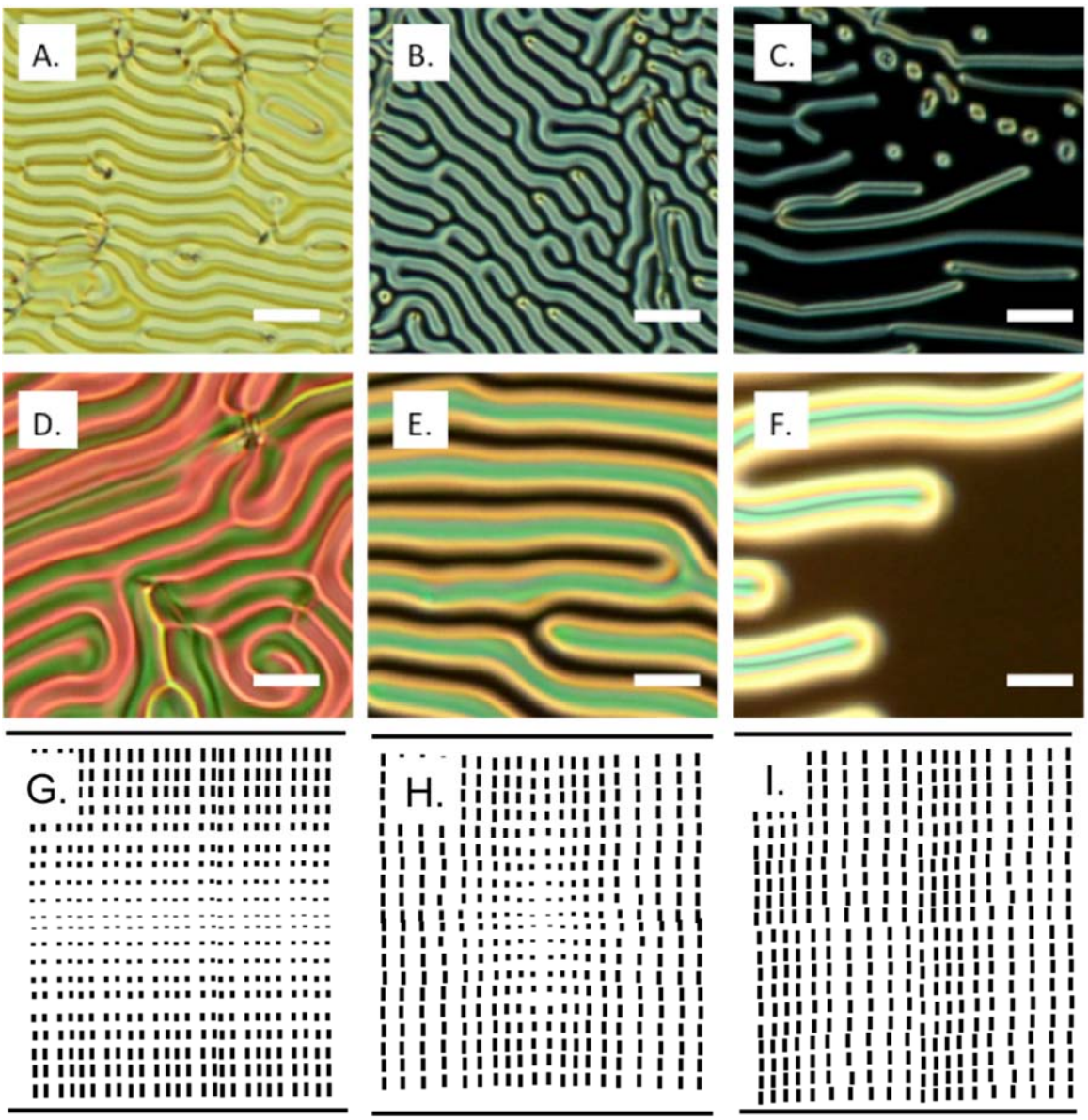

Figure 6.3. Crossed-polarized light micrographs of chiral doped LCs filled within a wedge cell with homeotropic alignment at both surfaces. (A-C) is the 2% chiral doped LC. (A) has a large thickness close to 7 µm, (B) is an intermediate thickness of around 2 µm, and (C) is a thin LC film at around 1 µm. Likewise (D-F) is the 1% chiral doped LC. (D) has a thickness close to 10 µm, (E) has a thickness close to 4 µm, and (F) has a thickness close to 2 µm. The scale bars represent 25 µm. (G) is a schematic of the alignment of the LC in (A) and (D). (H) is a schematic of the alignment of the LC in (B) and (E). (I) is a schematic of the dark regions in the LC film for (C) and (F).

For chiral LC films that are of the same thickness as the pitch length and supported on homeotropic aligning surface, a fingerprint pattern is observed. In this case, there is a modulation of a dark appearance and bright regions consistent with a nematic homeotropic alignment (dark regions) that alleviates the chiral strain found in the bright regions.[13] This is shown in Figure 3b for a 2% chiral LC that is 2 μm thick and 3e for a 1% chiral LC that is 4 μm thick. This result is consistent with what is expected from the literature and the alignment is diagrammed in Figure 3h. The periodicity was measured by analysis of the change in light intensity. The distance between the dark regions was calculated to be 8.2 ± 0.4 μm for the 2% chiral LC to be 23.9 ± 1.0 μm for the 1% chiral LC. This periodicity of the samples is directly related to the pitch length for the particular LC. We estimate this periodicity to be roughly the twice the pitch length of the chiral LC. These measurements are consistent with the trend defined in Equation 3.

Finally, for thin films of LC in which the film thickness is less than the pitch of the LC, the LC adopts a nematic homeotropic alignment.[13] In this case, the initial alignment of the LC adopts is perpendicular to the surfaces throughout the entire film in a manner similar to that in the first section (pure 5CB). Figure 3c shows the change from the fingerprint region (shown in Figure 3b) to the nematic homeotropic alignment for the 2% chiral LC at thickness around 1 μm. This behavior is also seen for the 1% chiral LC at thicknesses around 2 μm as shown in 3f. The alignment of LCs within the homeotropic regions is diagrammed in Figure 3i.

Next, we looked at the 2% chiral LC in a system that is composed of hybrid anchoring conditions with one surface giving homeotropic alignment and one surface giving planar alignment at varying thicknesses. A cross-polarized micrograph for a thin LC

film (around 1 μm) is shown in Figure 4a, a thicker LC film (around 4 μm) is shown in Figure 4b, and a schematic of the LC film is shown in Figure 4c. For the case of chiral LCs in hybrid anchoring conditions, past studies observed that the alignment of the LC occurs in two regions dependent on the distance from each of the surfaces. The first region is a purely planar alignment where the LC adopts the chiral helix perpendicular to the solid surface. The second region (the elastic region), occurs at a thickness of p/2 from the homeotropic surface and it is seen that a tilt of the LC from planar to homeotropic occurs in this region. The LC adopts an arch texture when viewed through cross polarizers and the periodicity of the modulation is close to double the pitch length. This is observed when the LC film is much greater than the pitch length of the LC. At thin films of LCs ($d < p/2$) there is a modulation of the LC film but very small amplitude of the modulation.[14-15] This behavior is also shown in Figure 4a-b. In the thin LC films seen in Figure 4a, the modulation was still observed, but there was smaller amplitude in the periodicity. In a thicker film, the periodicity is much clearer, as shown in Figure 4b. We measured the periodicity of the film to be 10.2 ± 0.7 μm. From past studies, this periodicity is equal to approximately twice the pitch length, depending on the film thickness. From our measurements, we estimate the pitch length of the 2% chiral LC from this experiment to be on the order of 5 μm.

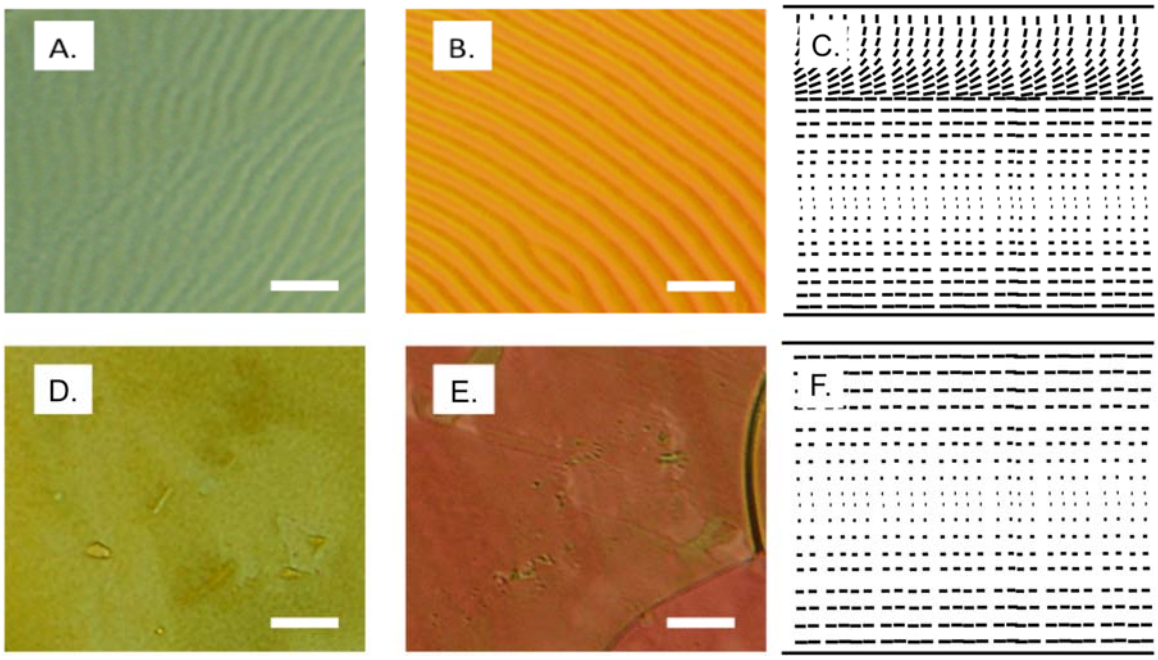

Figure 6.4. Alignment of the 2% chiral doped LC in a wedge cell of various anchoring conditions. For (A-B) the wedge cell had one side give a homeotropic alignment (OTS) and the other giving planar alignment (PI). (C) is the schematic of the LC films in (A) and (B). The thickness of the cell on (A) is around 1 µm and the thickness in (B) is around 4 µm. For (D-E), both confining surfaces give planar alignment (PI) at the confining surfaces. The thickness of the cell in (D) is around 1 µm and the thickness in (E) is around 6 µm. (F) is the schematic of the LC films in (D) and (E). The scale bars represent 25 µm.

Finally, we looked at the alignment of the LC when it is confined in a cell with both surfaces giving a planar alignment of varying LC film thicknesses shown in Figure 4d-e and diagrammed in Figure 4f. From these images, there is no texture on the order of micrometers, and variation in the thickness of the LC film only changes the retardance colors of the films.

From these results, we have shown the alignment of the chiral LCs under varying controlled surface anchoring conditions. These experiments are consistent with the results that have been shown in the literature. In addition, we can estimate the period of the

chiral-doped LCs. From these experiments, we see that the pitch length of the LC ranges range from 5 μm - 13 μm for chiral dopant calculations of 2% -3%.

6.3.3 Anchoring transitions of the LC vapor system to DMMP

In this section of the study, we study the change in alignment of thin films of chiral LCs supported on Al (III) perchlorate surfaces to 1 ppm DMMP. The samples were supported within 4 μm microwells, and an example of the anchoring transitions of the LC for varying concentrations of chiral dopant in 5CB is shown in Figure 5. For comparison sake we studied the anchoring transition of plain 5CB and it is shown in Figure 5a. We see the sample go from a dark appearance to a bright appearance after an average of 2.67 minutes for 3 independent samples. Close analysis of the retardance colors of the bright microwells upon exposure to the DMMP indicate that the filling is not completely uniform, but instead there is a gradient in thickness with the thickness increasing as you move closer to the center of the microwell. Upon removing the DMMP from the system, the LC film returns to the initial homeotropic alignment.

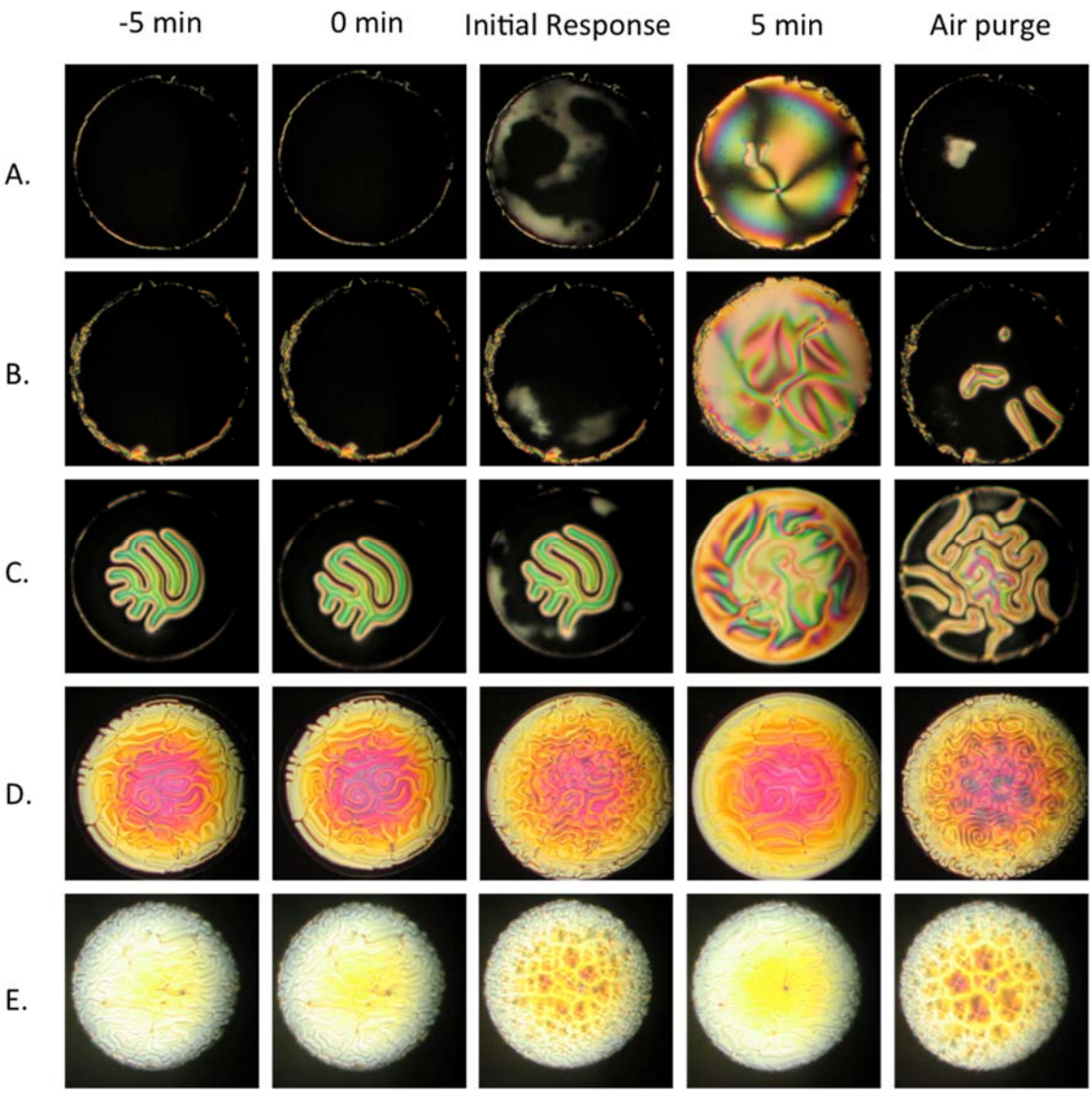

Figure 6.5. Cross-polarized light micrographs of chiral doped LC supported on Al (III) perchlorate decorated surfaces as it is exposed to 1 ppm DMMP at 0 seconds. The concentration of the chiral doped in the LC is for (A) 0.0%, (B) 0.5%, (C) 1.0%, (D) 2.0%, and (E) 3.0%. The pictures in the initial response correspond to the first change in the light micrographs as it is exposed to DMMP. The final response is taken after 5 minutes of exposure to DMMP and represents the final state of the LC film as it no longer changes from this state. The air purge is the appearance after the film has been purged with air for greater than 10 minutes and the images no longer appear to be changing. The diameter of each well is 200 µm.

If we add a small amount of the chiral dopant into the LC (0.5 %), the initial alignment of the LC is homeotropic and the alignment of the LC is the same nematic homeotropic alignment. This appears as a dark film when viewed through cross polarizers. Upon introduction of the DMMP into the system, the alignment of the LC changes and the film gives a bright appearance after 2.2 minutes near the edges of the microwells for 3 independent samples. This value is not significantly different than that for the pure 5CB systems. The change in the colors of the microwell is very different for the 0.5% chiral LC when compared to the anchoring transition of the pure 5CB. In general, there are bright green domains that arrange around the center of the microwell in a sort of a pinwheel pattern. The alignment of the LC in this pattern is not entirely clear, but the appearance of these patterns could be because the pitch length is on the order of one tenth of the diameter of the microwell and the chiral axis aligns with the diameter of the well. Upon removing the DMMP from the environment, the sample returns to the initial homeotropic alignment.

By further increasing the chiral dopant concentration to 1.0%, we see the initial alignment of the LC in air to be the fingerprint region texture in the central parts of the microwells shown in Figure 5c. This pattern is similar to that seen in Figure 3b. Closer to the edges of the microwell, the appearance of the LC film shows an alignment similar to a nematic LC or the 0.5% chiral dopant. Upon introduction of DMMP, the alignment of the LC changes, and the outer edges of the microwells changed in optical intensity at 2.5 minutes. After further exposure to DMMP, the entire microwell transitioned to a texture very similar to that of the alignment of the 0.5% chiral LC in DMMP. Upon purging the system with air, the sample

returned to the alignment similar to the initial state, but the fingerprint region of the microwell expanded suggesting some change in the LC film thicknesses.

By increasing the concentration of the chiral dopant even further to 2.0% or 3.0% the initial alignment is in a TIC in air and is shown in Figure 5d-e. The texture of the texture is consistent with Equation 3. Analysis of the retardance colors of the microwells for these systems again suggest that the thickness close to the center of the well is greater than the edges of the microwell. For both of these cases, upon introduction of DMMP into the system an initial transition state is seen where the intensity of the defect structure increases. Upon further exposure to DMMP, the defect structure of the chiral LC films relaxes to a structure with a less defined defect structure. This final structure of the LC film when exposed to DMMP is more consistent with the anchoring seen for hybrid aligned systems as shown in Figure 4a-b. After purging the system with air, the defect structure of the sample increases to be greater than the initial state or the transition state. The reason that this system does not go back to the alignment seen in the initial state is not clear at this point and we hope to further study this in the future.

We analyzed the defect structure of the 2.0% chiral LC system as it is exposed to 1 ppm DMMP using Fourier transform analysis of the images and analyzing the radial average shown in Figure 6. By examining these results, we see an interesting relationship of the intensity of the radial average that is occurring at a characteristic length of 1.5 μm that can be used to measure the intensity of the defect structure for these samples. We see upon the initial exposure of the sample to air, this value does not change much, but upon introduction of DMMP to the system this value begins to change. At first the value increases indicating the observed transition state

of the LC film, but then decreases to a value less than the initial state suggesting that the defects have relaxed (consistent with the images). Upon purging the system with air, the value begins to increase until is higher than the initial state. We have not been able to return the sample to the initial state. These results suggest that we can use Fourier analysis of the images to be able to monitor the change in the defect structure as it is exposed to DMMP.

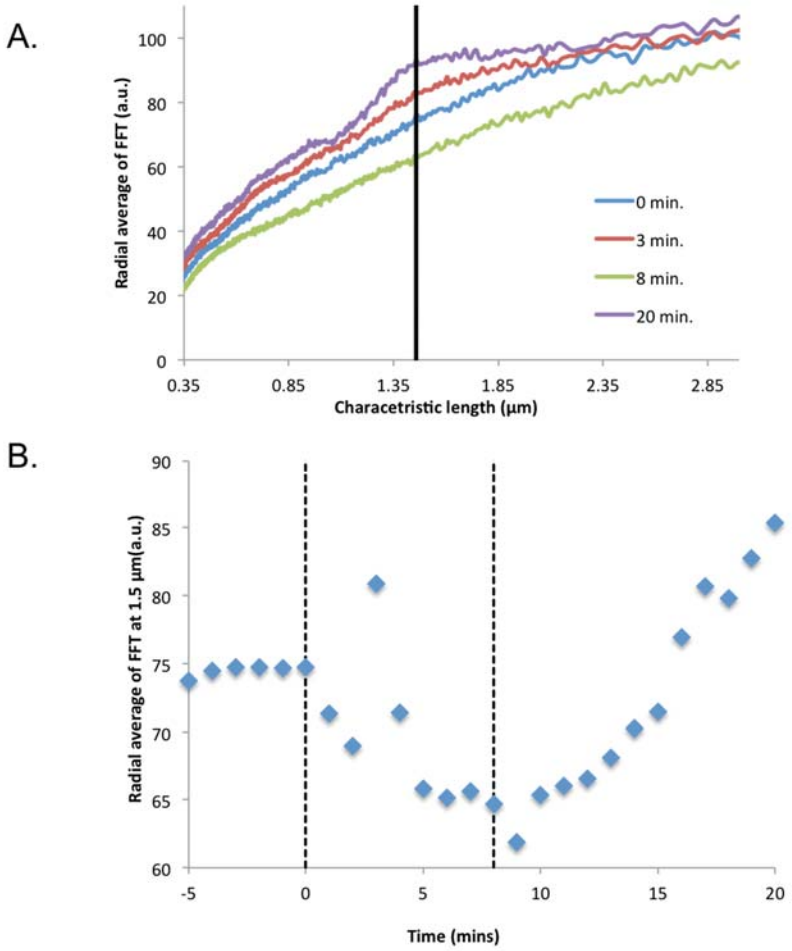

Figure 6.6. The FFT analysis of the 2% chiral LC film. (A) is the radial average of the FFT of the respective images shown in Figure 5D. The characteristic length of the radial average is shown on the x-axis. (B) shows the average intensity of the intensity of the peak at a characteristic length of 1.45 µm for 2 independent samples.

We end this section with analysis of the wedge cell system containing the chiral LC similar to that described in Figure 2. In this case, we create a wedge cell in the same manner as in Figure 2a by functionalizing both surfaces with Al (III) perchlorate and filling the wedge cell with the 2% chiral LC. We then exposed the system to a vapor containing 1 ppm DMMP and compared the penetration distance to a similar system using pure 5CB (same data as Figure 2a). These results are shown in Figure 7 and show that the penetration distance when viewed

through cross polarizers is very similar for the nematic LC (Figure 2a/7a) and chiral LC (Figure 7b) for films between 2 μm – 5 μm. However, as the thickness of the LC film decreases to a critical value close to 1 μm, the penetration distance decreases rapidly for the chiral LC. This could be because of the elastic strain of the chiral LC for the films that have a small LC film thickness compared to the pitch length of the LC. This is in contrast to the nematic LC. The penetration distance as a function of the LC film is quantified in Figure 7c. This suggests that the chiral LC system with thicknesses that are much lower than the pitch length might not be favorable for the anchoring transitions of the LC when exposed to DMMP. However, further studies need to be conducted with this system including using different anchoring conditions at the surfaces and different pitch lengths of the LC.

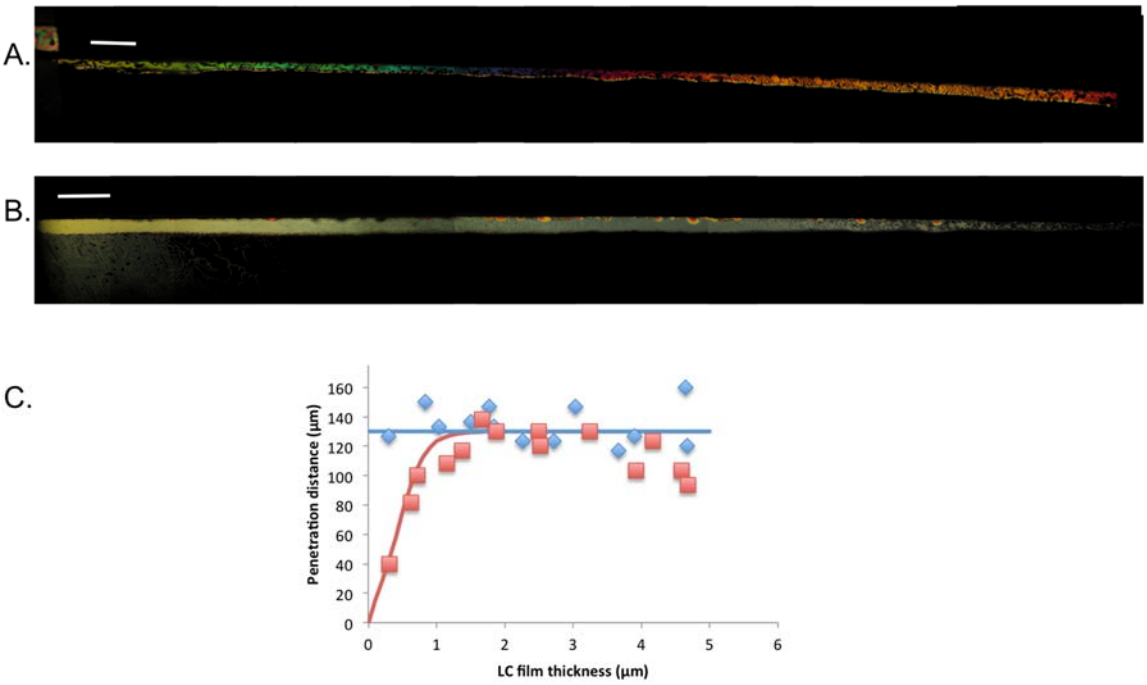

Figure 6.7. (A-B) are polarized light micrographs of wedge cells (one end 5 µm and the other in contact) fabricated with varying surfaces and LC. A wedge cell with both surfaces decorated with Al (III) perchlorate and filled with 5CB is shown in (A) (repeat of data shown in Figure 2a) while the same wedge filled with 2% chiral 5CB is shown in (B). (C) quantifies the penetration length of the bright regions for two independent samples as a function of the thickness of the LC film the blue diamonds represent the 5CB sample like in (A) and the red squares represent the sample filled with the chiral LC like in (B). The scale bars for each image represent 500 µm.

This section of the study has investigated the surface induced anchoring conditions for chiral LCs. This was done by exposing the chiral LCs supported on Al (III) perchlorate decorated surfaces to 1 ppm DMMP and observing the change in alignment of the LC film. The anchoring transition that we observed in this system is not clearly understood and gave interesting optical patterns that suggest a change in the alignment of the LC that does not simply go from homeotropic to planar. In addition, we have studied the change in the defect structure of the LC films using Fourier transform analysis and can observe a clear change in the pattern as the system is exposed to DMMP. We have also calculated the penetration of the bright regions in

wedge cells decorated with Al (III) perchlorate and filled with the chiral LC to suggest that the penetration is greatest for values of the LC that are equal to or greater than the pitch length of the LC.

6.4 Conclusions

In this study, we have shown the role of the elastic energies on the anchoring transitions of the LCs for nematic LCs in going from a uniform homeotropic alignment to a hybrid alignment. This change in the alignment plays a critical function in the development of the LC vapor sensor system described in this study. We see that, at low thicknesses of the LC film, the strain induced on this system begins to adversely impact the time of response. We propose a solution to this problem by introducing a chiral dopant into the LC. We are able to see an anchoring transition of the chiral LC sensor system when exposed to DMMP, but the exact changes in the alignment of the chiral LCs has not been clearly determined. Our preliminary results suggest that to get any benefit from the addition of the chiral dopant to the LC, a system where the pitch length of the chiral LC is less than or equal to the thickness of the LC film must be used.

6.5 References

1. Lockwood, N. A.; Gupta, J. K.; Abbott, N. L. *Surf. Sci. Rep.* **2008,** *63*, 255-293.
2. P.-G. de Gennes, J. P. *The Physics of Liquid Crystals*. 2nd ed.; Oxford University Press: New York, **1993**.
3. Jerome, B. *Rep. Prog. Phys.* **1991,** *54*, 391-451.
4. Shah, R. R.; Abbott, N. L. *Science* **2001,** *293*, 1296-1299.
5. Yang, K. L.; Cadwell, K.; Abbott, N. L. *J. Phys. Chem. B* **2004,** *108*, 20180-20186.
6. Hunter, J. T.; Pal, S. K.; Abbott, N. L. *ACS Appl. Mater. Interfaces* **2010,** *2*, 1857-1865.
7. Cadwell, K. D.; Alf, M. E.; Abbott, N. L. *J. Phys. Chem. B* **2006,** *110*, 26081-26088.
8. Hunter, J. T.; Abbott, N. L. *Sens. Actuators, B* **2013,** *183*, 71-80.
9. Stewart, C. E. *Weapons of mass casualties and terrorism response handbook*. Jones & Bartlett Learning: Sudbury, MA, **2006**.
10. Eelkema, R.; Feringa, B. L. *Org. Biomol. Chem.* **2006,** *4*, 3729-3745.
11. Ferrarini, A.; Moro, G. J.; Nordio, P. L. *Physical Review E* **1996,** *53*, 681-688.
12. Solladié, G.; Zimmermann, R. G. *Angewandte Chemie International Edition in English* **1984,** *23*, 348-362.
13. Kitzerow, H.; Bahr, C. *Chirality in Liquid Crystals*. Springer: **2001**.
14. Baudry, J.; Brazovskaia, M.; Lejcek, L.; Oswald, P.; Pirkl, S. *Liq. Cryst.* **1996,** *21*, 893-901.
15. Bosco, A.; Jongejan, M. G. M.; Eelkema, R.; Katsonis, N.; Lacaze, E.; Ferrarini, A.; Feringa, B. L. *J. Am. Chem. Soc.* **2008,** *130*, 14615-14624.

Chapter 7: Closing Statements

7.1 Conclusions

The research in this thesis advances our understanding of interfacial phenomena underlying adsorbate-induced anchoring transitions of LCs supported on chemically functionalized surfaces that are exposed to targeted vapor analytes. First, we examined time-dependent processes occurring at LC-metal salt interfaces and quantified dissolution of the metal salts decorating the surface into the LC. The dissolution of the metal salts change the properties of the system by (a) changing the interfacial interactions between the surface and the LC and thus the initial alignment of the LC or (b) creating an electrical double layer that aligns the LC parallel to the electric field. Secondly, we have analyzed the dynamics of the anchoring transitions to reveal key processes that control the LC anchoring transitions. From this analysis, we were able to identify the role of mass transport in determining the dynamic response of the LC and we were able to establish a methodology that permitted the sensitivity of the system to the targeted analyte to be estimated based on the dynamic response of the system. Finally, we have explored ways to either improve the sensitivity of the system or the time of response of the system. First, we optimized the coordination interactions between the solid surface and the LC in order to increase the sensitivity of the system to the targeted analyte. Second, we minimized the thickness of the LC film to investigate the role of the elastic energy of the LC on the dynamic response.

7.2 Future Directions

The results presented in this thesis suggest a number of future possible directions that have the potential to improve the sensitivity and responsiveness of LC films to a targeted analyte. In this section, I describe three research directions that offer the potential to tune the response of LC films to targeted vapors.

The first topic of potential future study addresses changes in the thickness of the metal salt layer that comprises the chemically functionalized surface. Specifically, we hypothesize that the anchoring energy of the LC at the metal salt decorate interface may be influenced by the substrate that supports the metal salt. In past studies, this type of physical situation has been described as a double layer alignment layer (DLAF).[1-2] We predict that a substrate that promotes planar anchoring of the LC may lead to metal-salt decorated interfaces that support LC films that are easily perturbed from the homeotropic alignment induced by coordination with the metal cations.

In addition, we propose that metal cations other than those that have been the focus of past studies may permit an increased sensitivity or speed of response of the LC systems to targeted analytes. The interactions of ligands with metal cations is a complicated phenomena that is dependent on the solvent in which the ligand exchange is happening, the electron affinity of the cation, the chemical potential of the ligand, and the overlap of the orbitals of the molecules. Preliminary data has characterized the initial alignment of the 5CB supported on the metal salt surfaces based on the electron affinity of the metal cation of the metal salt.[3] However, the ligand exchange reaction and the influence of other species in the system such as

the anion and water are not yet fully understood. We predict the choice of metal cation to impact the dynamics of the anchoring transitions of the LCs. For example, we hypothesize that iron (III) perchlorate might be more sensitive to DMMP than the 5CB when compared to aluminum (III) perchlorate. This idea can be expanded upon by tailoring mesogens to contain chemical moieties that interact specifically with metal salt functionalized surfaces.

Finally, we can engineer systems to accomplishing the goal of increasing the sensitivity of the system to the targeted analyte by controlling the elastic energies of the system to favor the responsiveness to the targeted analyte. By engineering elastic strain into the initial state of the LC film, the strain can be used to help promote an anchoring transition in the presence of an analyte. One method to do this would be to create an interface that gives the LC a planar alignment that would not impede the mass transport of the DMMP into the LC film that can be paired with a metal salt decorated surface. In this set-up, the initial strain induced by the hybrid anchoring conditions will be relieved when the functionalized surface goes planar at both interfaces. This would be more favorable when the film thickness is low, thus allowing the time of response to be short.

7.3 References

1. Zhang, K.; Liu, N.; Twieg, R. J.; Auman, B. C.; Bos, P. J. *Liq. Cryst.* **2008,** *35*, 1191-1197.

2. Zhang, K.; Liu, N.; Twieg, R. J.; Bos, P. J. *Liq. Cryst.* **2009,** *36*, 1031-1035.

3. Yang, K. L.; Cadwell, K.; Abbott, N. L. *J. Phys. Chem. B* **2004,** *108*, 20180-20186.